STATUS OF THESIS

Title of thesis | **CRUDE OIL FOULING ON HEAT TRANSFER SURFACES**

I **UMESH B. DESHANNAVAR**

hereby allow my thesis to be placed at the Information Resource Centre (IRC) of Universiti Teknologi PETRONAS (UTP) with the following conditions:

1. The thesis becomes the property of UTP
2. The IRC of UTP may make copies of the thesis for academic purposes only.
3. This thesis is classified as

[√] Confidential

[ ] Non-confidential

If this thesis is confidential, please state the reason:

The present study is part of a major funded research project which is governed by the confidentiality agreement with the funding body.

The contents of the thesis will remain confidential for 5 years.

Remarks on disclosure:

_____
_____
_____

Endorsed by

_____ _____

Signature of Author | Signature of Supervisor

Permanent address
S/o B.R. Deshannavar
Vidyanagar, 1st cross, Badami – 587201
Karnataka, India

Name of Supervisor
Assoc. Prof. Dr. M. Ramasamy

Date : _____ Date : _____

UNIVERSITI TEKNOLOGI PETRONAS

CRUDE OIL FOULING ON HEAT TRANSFER SURFACES

by

UMESH B. DESHANNAVAR

The undersigned certify that they have read, and recommend to the Postgraduate Studies Programme for acceptance of this thesis for the fulfilment of the requirements for the degree stated.

Signature: _____

Main Supervisor: Assoc. Prof. Dr. M. Ramasamy

Signature: _____

Co-Supervisor: Prof. Dr. Duvvuri Subbarao

Signature: _____

Head of Department: Assoc. Prof. Dr. Shuhaimi Mahadzir

Date: _____

CRUDE OIL FOULING ON HEAT TRANSFER SURFACES

by

UMESH B. DESHANNAVAR

A Thesis
Submitted to the Postgraduate Studies Programme
as a Requirement for the Degree of

DOCTOR OF PHILOSOPHY

CHEMICAL ENGINEERING DEPARTMENT

UNIVERSITI TEKNOLOGI PETRONAS

BANDAR SERI ISKANDAR,

PERAK

JANUARY 2011

DECLARATION OF THESIS

Title of thesis | **CRUDE OIL FOULING ON HEAT TRANSFER SURFACES**

I, **UMESH B. DESHANNAVAR**

hereby declare that this thesis is based on my original work except for quotations and citations which have been duly acknowledged. I also declare that it has not been previously or concurrently submitted for any other degree at Universiti Teknologi PETRONAS or other institutions.

Witnessed by

_____ _____

Signature of Author | Signature of Supervisor

Permanent address
S/o B.R. Deshannavar
Vidyanagar, 1st cross, Badami – 587201
Karnataka, INDIA

Name of Supervisor
Assoc. Prof. Dr. M. Ramasamy

Date:_____ Date:_____

ACKNOWLEDGEMENTS

I would like to express my sincere thanks to my research supervisor Associate Professor Dr. M. Ramasamy for his beneficial guidance, utmost patience, helpful suggestions and support throughout the duration of this research work. I am also very much thankful for his crucial comments and guidance in shaping and improving this dissertation.

I express my sincere gratitude to my research co-supervisor Professor Dr. Duvvuri Subbarao for his valuable guidance and support throughout my research work.

I am very grateful to Universiti Teknologi PETRONAS for offering me the graduate assistantship and providing the facilities for this research work.

I extend my sincere thanks to Dr. S.C. Pilli, Principal, K.L.E. Society's college of Engineering and Technology, Belgaum, my colleagues and friends for their encouragement and support to pursue my Ph.D.

I am indebted to Symazari B Rafeen, Totok R. Biyanto, Mohanad Osman, Nor Husna, Zamidi Ahmad, Dr. Lemma Tufa, Naveen Chandran, Desta, Aamir Amanat Ali Khan, Saqib Khan, Rafi Raza Malik and Chane Taye for their support and kind assistance.

Finally, special thanks are due to my wife Savitri Deshannavar and loving daughter Shreya Deshannavar for all of the extended hours I spent in the lab instead of being with them, and to my parents, brother and sister for their encouragement and support.

ABSTRACT

Hydrocarbon fouling in a petroleum refinery crude preheat train has been identified as a critical issue affecting the economy of the plant very badly. Fouling undergoes different mechanisms at different stages of heating the crude oil in the preheat train. Understanding the fouling mechanisms is essential in formulating appropriate fouling mitigation strategies.

The present research focuses on the study of fouling characteristics of four different Malaysian crude oils through experiments in a pilot-scale, high-pressure and high-temperature recirculation flow loop fitted with two identical fouling probes. The procedures reported in the open literature employ very high surface temperatures. It has been identified in this study that there is a maximum surface temperature/heat flux beyond which the forced convective heat transfer regime changes to boiling regime. As the industrial preheat exchangers operate at forced convective heat transfer regime, it is therefore, necessary to carry out the experiments in the same heat transfer regime. In this study, an improved method has been developed for calibrating the surface temperature using the heater temperature measurement by the Wilson plot technique. This method enables identification of the heat transfer regimes more accurately. Maximum heat flux under the forced convective heat transfer regime was determined for each crude oil at the corresponding operating conditions. A model to determine the maximum heat flux has also been proposed in terms of the crude oil true boiling point data.

A series of experiments were planned and carried out to study the fouling characteristics of different crude oils at different initial surface temperatures, bulk temperatures and flow velocities at a pressure of 50 bar. Data from each experiment were collected, processed and the resistance due to fouling was determined. The induction periods and the initial fouling rates were estimated from the fouling resistance profiles. It was observed that the induction period decreased with an increase in initial surface temperature; increased with an increase in the bulk

temperature and flow velocity. It was also observed that the initial fouling rates increased with increase in initial surface temperature; decreased with increase in bulk temperature and flow velocity for all the crude oils.

The experimental data were analyzed using the existing threshold fouling model. This model assumes the rate of fouling is the net effect of fouling precursor formation through chemical reaction and deposition, and removal by the wall shear. The apparent activation energy values were estimated for the crude oils at different bulk temperatures and flow velocities. It was observed that the variations in the apparent activation energy values for flow velocities of 0.4 and 0.5 m/s are insignificant and that it increased linearly with increase in the bulk temperature. The existing threshold fouling models predict an increase in the initial fouling rates with an increase in the film temperatures. Although the existing models predict the fouling rates well for increase in film temperature due to increased surface temperature at constant bulk temperature, they fail to predict the fouling rates for an increase in film temperature due to the increase in bulk temperature at constant surface temperature. A new threshold fouling model was developed to account for the effect of bulk temperature on fouling by considering the apparent activation energy as a function of bulk temperature. The new threshold fouling models for the crude oils tested were proposed. The proposed threshold fouling model has been found to be in good agreement with the experimental data.

ABSTRAK

Penempelan bendasing bagi hidrokarbon di dalam rangkaian penukar haba bagi kilang penapisan minyak telah dikenalpasti sebagai masalah yang kritikal yang menjejaskan factor ekonomi sesebuah loji dengan begitu teruk. Penempelan bendasing boleh berlaku melalui mekanisme yang berbeza yang berkait rapat dengan peringkat pemanasan yang berbeza di dalam rangkaian penukar haba. Pemahaman terhadap mekanisme penempelan bendasing adalah elemen yang begitu penting bagi mencari formula yang sesuai untuk mengatasi penempelan bendasing.

Kajian yang dijalankan ini memfokuskan penyelidikan terhadap karakteristik penempelan bendasing bagi empat minyak mentah Malaysia melalui eksperimen yang dijalankan menggunakan loji berskala kecil, bertekanan tinggi dan bersuhu tinggi yang dilengkapi dengan dua rod penempelan bendasing yang serupa. Prosedur yang diterbitkan bagi rujukan umum melaporkan kajian dijalankan pada suhu yang amat tinggi. Ia telah dikenal pasti di dalam kajian ini bahawa terdapat suhu permukaan/aliran haba yang maksimum, jika dilangkaui menyebabkan kawasan aliran haba melalui perolakan paksa bertukar menjadi kawasan aliran haba melalui pendidihan. Oleh kerana penukar haba di dalam industri beroperasi didalam kawasan aliran haba melalui perolakan paksa, jadi adalah perlu untuk menjalankan eksperimen didalam kawasan aliran haba yang sama. Di dalam penyelidikan ini, kaedah yang diperbaharui telah diperkenalkan untuk mengkalibrasi suhu permukaan menggunakan suhu pemanas haba yang diperolehi melalui teknik plot Wilson. Kaedah ini membolehkan penentuan kawasan aliran haba dengan lebih tepat. Aliran haba yang maksimum didalam kawasan aliran haba melalui perolakan paksa ditentukan bagi setiap minyak mentah berpandukan keadaan operasi yang tertentu. Satu model bagi menentukan aliran haba maksimum telah dicadangkan dengan berpandukan kepada data takat didih benar bagi minyak mentah.

Satu siri eksperimen telah dirancang dan dijalankan bagi mengkaji karakteristik penempelan bendasing bagi minyak mentah berlainan pada suhu permukaan awal,

suhu umum dan halaju yang berbeza pada tekanan 50 bar. Data yang diperolehi bagi setiap eksperimen dikumpul, diproses dan rintangan disebabkan penempelan bendasing ditentukan. Tempoh masa induksi dan kadar awal penempelan dianggarkan berpandukan profil rintangan penempelan. Pemerhatian menunjukkan bahawa tempoh masa induksi berkurangan dengan peningkatan suhu permukaan awal; bertambah dengan peningkatan suhu umum dan halaju. Ia juga dapat diperhatikan bahawa kadar awal penempelan bertambah dengan peningkatan suhu awal permukaan; berkurangan dengan peningkatan suhu umum dan halaju untuk semua minyak mentah.

Data daripada eksperimen dianalisa menggunakan model penempelan 'threshold' yang sedia ada. Model ini menganggap kadar penempelan terhasil daripada pembentukan zarah-zarah penempelan melalui tindak balas kimia dan endapan, dan penyingkiran yang disebabkan oleh kesan ricih bendalir pada permukaan. Tenaga pengaktifan nyata dianggarkan bagi minyak mentah pada suhu umum dan halaju yang berbeza. Ia dapat diperhatikan bahawa variasi bagi tenaga pengaktifan nyata bagi halaju 0.4 dan 0.5 m/s adalah terlalu kecil dan ianya meningkat secara linear dengan peningkatan suhu umum. Model penempelan 'threshold' yang sedia ada meramalkan peningkatan pada kadar awal penempelan dengan peningkatan suhu permukaan. Walaupun model ini meramalkan kadar penempelan dengan begitu baik bagi peningkatan suhu filem disebabkan oleh peningkatan suhu permukaan pada suhu umum yang tetap, ianya gagal untuk meramalkan kadar penempelan bagi peningkatan suhu filem disebabkan oleh peningkatan suhu umum pada suhu permukaan yang tetap. Model penempelan 'threshold' yang baru telah diperkenalkan untuk mengambil kira kesan suhu umum terhadap penempelan bendasing dengan menganggap tenaga pengaktifan nyata adalah berkait dengan suhu umum. Dengan itu, model penempelan 'threshold' yang baru telah dicadangkan. Model penempelan ini dilihat dapat meramal data eksperimen dengan baik.

COPYRIGHT

In compliance with the terms of the Copyright Act 1987 and the IP Policy of the university, the copyright of this thesis has been reassigned by the author to the legal entity of the university,

Institute of Technology PETRONAS Sdn Bhd.

Due acknowledgement shall always be made of the use of any material contained in, or derived from, this thesis.

© Umesh B. Deshannavar, January 2011
Institute of Technology PETRONAS Sdn Bhd
All rights reserved.

TABLE OF CONTENTS

ACKNOWLEDGEMENTS v
ABSTRACT vi
COPYRIGHT x
LIST OF TABLES xv
LIST OF FIGURES xvii
LIST OF PLATES xxii
NOMENCLATURE xxiii

Chapter

1. INTRODUCTION 1
    1.1 Fouling 1
    1.2 Fouling Mitigation 2
    1.3 Fouling Models 3
    1.4 Problem Statement 3
    1.5 Research objectives 6
    1.6 Research methodology 6
    1.7 Organization of the thesis 8

2. LITERATURE REVIEW 9
    2.1 Introduction 9
    2.2 Fouling experimental units 10
    2.3 Fouling mechanisms 15
        2.3.1 Chemical reaction fouling 15
            2.3.1.1 Initiation 16
            2.3.1.2 Transport 17
            2.3.1.3 Deposition / Attachment 17
            2.3.1.4 Removal 18
            2.3.1.5 Ageing 18
    2.4 Factors influencing fouling 19
        2.4.1 Effect of surface temperature 19

2.4.2 Effect of flow velocity 20
2.4.3 Effect of bulk temperature 20
2.4.4 Effect of crude type 21
2.4.5 Effect of crude blending 22
2.5 Modelling of crude oil fouling 22
2.5.1 Transport-adhesion Models 23
2.5.2 Transport-reaction Models 25
2.5.3 Threshold fouling Models 29
2.6 Summary 35

3. EXPERIMENTAL 37
3.1 Introduction 37
3.2 Experimental unit 38
3.2.1 Feed tank 41
3.2.2 Pump 42
3.2.3 Annular test sections 43
3.2.4 Double pipe heat exchanger 44
3.2.5 Instrumentation 45
3.2.6 Data acquisition and control system 48
3.3 Determination of surface temperature 50
3.4 Crude oils and their properties 53
3.4.1 Crude collection, storage and preparation 53
3.4.2 Properties of crude oils 53
3.5 Determination of maximum heat flux under the forced convective heat transfer regime 56
3.6 Experimental procedure for determining fouling rates 59
3.7 Experimental plan 60
3.8 Estimation of initial fouling rates and induction periods 62
3.9 Summary 64

4. MAXIMUM HEAT FLUX UNDER FORCED CONVECTIVE HEAT TRANSFER REGIME 65
4.1 Introduction 65
4.2 Maximum heat flux under the forced convective heat transfer regime 65

4.2.1 Crude oil A 66
4.2.2 Crude oil B 67
4.2.3 Crude oil C 70
4.2.4 Crude oil D 73
4.2.5 Discussion on the maximum heat flux for all crude oils .. 76
4.3 A model for the estimation of maximum heat flux 82
4.4 Summary 84

5. RESULTS AND DISCUSSIONS 85
5.1 Introduction 85
5.2 Fouling characteristics of crude oils 85
5.2.1 Effect of initial surface temperature on fouling characteristics 89
5.2.1.1 Crude oil A 89
5.2.1.2 Crude oil B 91
5.2.1.3 Crude oil C 93
5.2.1.4 Crude oil D 96
5.2.1.5 Discussion on the effect of initial surface temperature on fouling characteristics 98
5.2.2 Effect of bulk temperature on fouling characteristics 98
5.2.2.1 Crude oil B 98
5.2.2.2 Crude oil C 100
5.2.2.3 Crude oil D 102
5.2.2.4 Discussion on the effect of bulk temperature on fouling characteristics 104
5.2.3 Effect of flow velocity on fouling characteristics 104
5.2.3.1 Crude oil B 104
5.2.3.2 Crude oil C 106
5.2.3.3 Crude oil D 109
5.2.3.4 Discussion on the effect of flow velocity on fouling characteristics 111
5.3 Evaluation of the data in the light of the model of Panchal et al. . 111
5.3.1 Estimation of the model parameters 111
5.3.1.1 Crude oil A 112
5.3.1.2 Crude oil B 113
5.3.1.3 Crude oil C 113
5.3.1.4 Crude oil D 117

5.4 Development of a new threshold fouling model 120
5.5 Induction period and initial fouling rate..... 124
5.6 Fouling mechanism..... 125
5.7 Summary 131

6 CONCLUSIONS AND RECOMMENDATIONS 133
6.1 Conclusions 133
6.2 Recommendations..... 134

References 135

Publications..... 143

LIST OF TABLES

Table 2.1:	Summary of various fouling experimental units	11
Table 3.1:	Design details of feed tank	42
Table 3.2:	Dimensions of heat exchanger fouling probes	43
Table 3.3:	Instrumentation in AFFRU	45
Table 3.4:	Controllers and their tuning parameters	49
Table 3.5:	Values of constants *a* and *b* for thermocouples embedded in fouling probes	52
Table 3.6:	Assay of Malaysian crude oils used in this study	54
Table 3.7:	Values of constants for the crude oils	55
Table 3.8:	Summary of the operating conditions for the experiments	61
Table 4.1:	Maximum heat flux, heat transfer coefficients under forced convective heat transfer and physical properties of crude oils at the respective operating conditions	81
Table 5.1:	Induction periods and the initial fouling rates of the crude oils	86
Table 5.2:	Initial fouling rates and induction periods of crude oil A (T_b = 120^{o}C, v = 0.5 m/s)	89
Table 5.3:	Initial fouling rates and induction periods of crude oil B (T_b = 120^{o}C, v = 0.5 m/s)	91
Table 5.4:	Initial fouling rates and induction periods of crude oil C	94
Table 5.5:	Initial fouling rates and induction periods of crude oil D	96
Table 5.6:	Initial fouling rates and induction periods of crude oil B at different bulk temperatures and flow velocities	99
Table 5.7:	Initial fouling rates and induction periods of crude oil C at different bulk temperatures	100

Table 5.8: Initial fouling rates and induction periods of crude oil D at different bulk temperatures 102

Table 5.9: Initial fouling rates and the induction periods of crude oil B at different velocities 105

Table 5.10: Initial fouling rates and the induction periods of crude oil C at different velocities 107

Table 5.11: Initial fouling rates and the induction periods of crude oil D at different velocities 109

Table 5.12: Apparent activation energy values for crude oil C at different bulk temperatures 115

Table 5.13: Apparent activation energy values for crude oil D at different bulk temperatures 119

Table 5.14: Constants for apparent activation energy determination for crude oils C and D..... 120

Table 5.15: Fouling model parameters for crude oil C 121

Table 5.16: Relative percentage error between the experimental and the predicted values of crude oil C..... 122

Table 5.17: Fouling model parameters for crude oil D 123

Table 5.18: Relative percentage error between the experimental and the predicted values of crude oil D 124

Table 5.19: Summary of the effect of parameters on the induction period and the initial fouling rate..... 125

LIST OF FIGURES

Fig. 2.1: Two-step chemical reaction fouling mechanism 16

Fig. 2.2: Threshold film temperature as a function of wall shear stress 31

Fig. 3.1: Schematic diagram of re-circulation flow loop (AFFRU) 41

Fig. 3.2: Schematic diagram of fouling probe with annular flow geometry. (a) cross sectional view in the axial direction and (b) cross sectional view across A-A 44

Fig. 3.3: Piping and Instrumentation diagram of AFFRU 47

Fig. 3.4: Typical Wilson plot ($1/h_{eff}$ versus $v^{-0.8}$) for HEFP1 with thermocouples TT104 and TT105..... 51

Fig. 3.5: The thermal wall resistance vs. the heater temperature for the two thermocouples in HEFP1..... 52

Fig. 3.6: True boiling point curves for the crude oils..... 56

Fig. 3.7: The temperature difference, (T_s-T_b), vs. the heat flux, q, for crude oil C at T_b = 120^{o}C, v = 0.5 m/s, P = 50 bar 57

Fig. 3.8: The heat transfer coefficient, h, vs. the temperature difference (T_s-T_b) for crude oil C at T_b = 120^{o}C, v = 0.5 m/s, P = 50 bar..... 58

Fig. 3.9: The thermal fouling resistance, R_f, vs. time for crude oil A at T_b = 120^{o}C, v = 0.5 m/s, T_{so} = 223^{o}C (Run 3)..... 63

Fig. 3.10: The thermal fouling resistance, R_f, vs. time for crude oil C at T_b = 80^{o}C, v = 0.4 m/s, T_{so} = 201^{o}C (Run 14)..... 63

Fig. 4.1: The temperature difference, (T_s-T_b), vs. the heat flux, q, for crude oil A at T_b = 120^{o}C, v = 0.5 m/s, P = 50 bar..... 66

Fig. 4.2: The heat transfer coefficient, h, vs. the temperature difference, (T_s-T_b), for crude oil A at T_b = 120^{o}C, v = 0.5 m/s, P = 50 bar..... 67

Fig. 4.3: The temperature difference, (T_s-T_b), vs. the heat flux, q, for crude oil B at v = 0.5 m/s, P = 50 bar for various bulk temperatures 68

Fig. 4.4: The heat transfer coefficient, h, vs. the temperature difference, (T_s-T_b), for crude oil B at v = 0.5 m/s, P = 50 bar for various bulk temperatures 68

Fig. 4.5: The temperature difference, (T_s-T_b), vs. the heat flux, q, for crude oil B at v = 0.4 m/s, P = 50 bar, bulk temperatures of 90 and 105^{o}C 69

Fig. 4.6: The heat transfer coefficient, h, vs. the temperature difference, (T_s-T_b), for crude oil B at v = 0.4 m/s, P = 50 bar, bulk temperatures of 90 and 105^{o}C 70

Fig. 4.7: The temperature difference, (T_s-T_b), vs. the heat flux, q, for crude oil C at v = 0.5 m/s, P = 50 bar for various bulk temperatures 71

Fig. 4.8: The heat transfer coefficient, h, vs. the temperature difference, (T_s-T_b), for crude oil C at v = 0.5 m/s, P = 50 bar for various bulk temperatures 71

Fig. 4.9: The temperature difference, (T_s-T_b), vs. the heat flux, q, for crude oil C at v = 0.4 m/s, P = 50 bar, bulk temperatures of 80 and 100^{o}C 72

Fig. 4.10: The heat transfer coefficient, h, vs. the temperature difference, (T_s-T_b), for crude oil C at v = 0.4 m/s, P = 50 bar, bulk temperatures of 80 and 100^{o}C 72

Fig. 4.11: The temperature difference, (T_s-T_b), vs. the heat flux, q, for crude oil D at v = 0.5 m/s, P = 50 bar, bulk temperatures of 80 and 100^{o}C 73

Fig. 4.12: The heat transfer coefficient, h, vs. the temperature difference, (T_s-T_b), for crude oil D at v = 0.5 m/s, P = 50 bar, bulk temperatures of 80 and 100^{o}C 74

Fig. 4.13: The temperature difference, (T_s-T_b), vs. the heat flux, q, for crude oil D at v = 0.4 m/s, P = 50 bar, bulk temperatures of 80 and 100^{o}C 75

Fig. 4.14: The heat transfer coefficient, h, vs. the temperature difference, (T_s-T_b), for crude oil D at v = 0.4 m/s, P = 50 bar, bulk temperatures of 80 and 100^{o}C 75

Fig. 4.15: Maximum temperature difference, $(T_s\text{-}T_b)_{max}$, vs. bulk temperature at different velocities 77

Fig. 4.16: Maximum temperature difference, $(T_s\text{-}T_b)_{max}$, vs. flow velocity .. 78

Fig. 4.17: Maximum heat flux, q_{max} vs. bulk temperature, T_b, for the crude oils at different velocities..... 78

Fig. 4.18: Maximum heat flux, q_{max} vs. flow velocity, v, for the crude oils at different bulk temperatures 79

Fig. 4.19: Maximum heat transfer coefficient, h_{max} vs. bulk temperature, T_b, for the crude oils at different velocities 80

Fig. 4.20: Maximum heat transfer coefficient, h_{max} vs. flow velocity, v, for the crude oils at different bulk temperatures 80

Fig. 4.21: $(h_{max}D\text{Pr}^{-1/3}/0.023k)$ vs. $\text{Re}^{0.8}$ 83

Fig. 4.22: Comparison of the calculated maximum heat flux with the experimental values for different crude oils 84

Fig. 5.1: Induction period vs. initial surface temperature of crude oil A at $T_b = 120^oC$, $v = 0.5$ m/s..... 90

Fig. 5.2: Initial fouling rate vs. initial surface temperature of crude oil A at $T_b = 120^oC$, $v = 0.5$ m/s..... 91

Fig. 5.3: Induction period vs. initial surface temperature of crude oil B at $T_b = 120^oC$, $v = 0.5$ m/s..... 92

Fig. 5.4: Initial fouling rate vs. initial surface temperature of crude oil B at $T_b = 120^oC$, $v = 0.5$ m/s..... 93

Fig. 5.5: Induction periods vs. initial surface temperatures at different bulk temperatures and flow velocities of crude oil C 95

Fig. 5.6: Initial fouling rates vs. initial surface temperatures at different bulk temperatures and flow velocities of crude oil C..... 95

Fig. 5.7: Induction period vs. initial surface temperature at different bulk temperatures and flow velocities of crude oil D 97

Fig. 5.8: Initial fouling rate vs. initial surface temperature at different bulk temperatures and flow velocities of crude oil D 97

Fig. 5.9: Initial fouling rates vs. bulk temperature for different velocities of crude oil B (T_{so} = 214±2^{o}C) 99

Fig. 5.10: Induction period vs. bulk temperature at different initial surface temperatures and flow velocities of crude oil C 101

Fig. 5.11: Initial fouling rate vs. bulk temperature at different initial surface temperatures and flow velocities of crude oil C 101

Fig. 5.12: Induction period vs. bulk temperature at different velocities and initial surface temperatures of crude oil D 103

Fig. 5.13: Initial fouling rate vs. bulk temperature at different velocities and initial surface temperatures of crude oil D 103

Fig. 5.14: Induction period vs. flow velocity at different bulk temperatures of crude oil B 105

Fig. 5.15: Initial fouling rate vs. flow velocity at different bulk temperatures of crude oil B 106

Fig. 5.16: Induction period vs. flow velocity at different bulk and initial surface temperatures of crude oil C 108

Fig. 5.17: Initial fouling rate vs. flow velocity at different bulk and initial surface temperatures of crude oil C 108

Fig. 5.18: Induction period vs. flow velocity at different bulk and initial surface temperatures of crude oil D 110

Fig. 5.19: Initial fouling rate vs. flow velocity at different bulk and initial surface temperatures of crude oil D 110

Fig. 5.20: Arrhenius plot for crude oil A 112

Fig. 5.21: Arrhenius plot for crude oil B 113

Fig. 5.22: Arrhenius plot for crude oil C at different velocities (T_b = 80^{o}C) .. 114

Fig. 5.23: Arrhenius plot for crude oil C at different velocities (T_b = 100^{o}C) 114

Fig. 5.24: Arrhenius plot for crude oil C (T_b = 120^{o}C) 115

Fig. 5.25: Apparent activation energy, E, vs. bulk temperature, T_b, for crude oil C 117

Fig. 5.26: Arrhenius plot for crude oil D at different velocities ($T_b = 80^oC$) . 118

Fig. 5.27: Arrhenius plot for crude oil D at different velocities ($T_b = 100^oC$) 118

Fig. 5.28: Apparent activation energy, E, vs. bulk temperature, T_b, for crude oil D 120

Fig. 5.29: Comparison of the model predicted values vs. the experimental values of crude oil C 122

Fig. 5.30: Comparison of the model predicted values vs. the experimental values of crude oil D 123

Fig. 5.31: Concentrations of A, R and S vs. $k_{eff}t$ 126

Fig. 5.32 Concentration of S vs. $k_{eff}t$ 127

Fig. 5.33: The initial fouling rate vs. $DaT_b v/\Delta TL$ for the crude oils 130

Fig. 5.34: The initial fouling rate vs. the induction period for the crude oils. 130

LIST OF PLATES

Plate 3.1: Photograph of AFFRU 39

NOMENCLATURE

Variable	Description	Units
a	Constant in Eq. (2.16)	(-)
A	Pre-exponential factor in Eq. (2.4)	s^{-1}
A_o	Cross sectional area in Eq. (2.19)	m^2
A_o	Power law constant in Eq. (2.16)	(-)
A	Parameter in Eq. (2.15)	m^2K/kJ
B	Parameter in Eq. (2.15)	(-)
b	constant	(-)
C	Parameter in Eq. (2.15)	varies
C	Concentration of precursor	kg/m^3
C_1 & C_2	Proportionality constant in Eq. (2.19)	(-)
C_3 & C_4	Constants in Eq. (2.19)	(-)
C_f	Fanning friction factor in Eq. (2.15)	(-)
C'	Concentration of foulant in Eq. (2.7)	kg/m^3
d	Tube diameter	m
D	Equivalent diameter in Eq. (4.2)	m
D	Diffusion coefficient	m^2/s
E	Activation energy	kJ/mol
f	Fanning friction factor	(-)
G	Mass flow rate	kg/s
k_a	Reaction rate constant in Eq. (2.11)	varies
k_t	Mass transfer coefficient	m/s
k_r	Reaction rate constant	varies
k_f	Thermal conductivity of foulant	W/mK
k', k''	constants	(-)
K_1& K_2	constants	(-)
m	Mass per unit surface area in Eq. (2.3)	kg/m^2
M	Mass flow rate in Eq. (2.7)	kg/s

$\dot{m}_d$	Rate of deposition	kg/m^{2}s
$\dot{m}_r$	Rate of removal	kg/m^{2}s
n	Order of the reaction in Eq. (2.2) and Eq. (2.14)	(-)
P	Pressure	bar
Pr	Prandtl number	(-)
q	Heat flux	kW/m^2
R	Universal gas constant	kJ/mol.K
Re	Reynolds number	(-)
R_f	Thermal fouling resistance	m^{2}K/kWh
R_b	Deposition bond resistance	(-)
r	Reaction order in Eq. (2.19)	(-)
Sc	Schmidt number	(-)
S	Sticking probability	(-)
T	Temperature	K
u	Fluid velocity	m/s
V	Volume	m^3
W	Flow rate	LPM
x	Thickness	m
dR_f/dt	Fouling rate	m^{2}K/kWh
Greek Letters	**Description**	**Unit**
α	Deposition constant	m^{2}K/kWh
β	Constant	(-)
γ	Removal constant	m^{2}K/kWh/Pa
ρ	Density	kg/m^3
μ	Fluid viscosity	Pa-s
ϕ	Deposition mass flux	kg/m^{2}s
τ	Shear stress	N/m^2
λ	Thermal conductivity	W/mK
Λ_1	Function of surface roughness in Eq. (2.12)	(-)
η	Fluid viscosity in Eq. (2.12)	Pa-s
ψ	Deposit strength in Eq. (2.3)	(-)

Subscripts

b	bulk
f	film, foulant, deposit, fluid
o	initial
s	surface
w	Wall
t	At time “t”
TB	Thermal boundary layer
∞	At infinite time, asymptotic
r	Reactant
D	Deposit
Di	Deposit at interface
rb	Reactant/precursor in bulk fluid

CHAPTER 1

INTRODUCTION

1.1 Fouling

In process industries, heat recovery from the product streams into the process streams is generally practiced to improve the energy efficiency of the plant. In petroleum refineries, a crude preheat train (CPT) is used in the crude distillation unit to recover heat from the product and pumparound streams by exchanging heat with the crude oil stream. Generally, multi-pass shell and tube heat exchangers are used as heat recovery units. Due to the complex nature of crude oil, the heat exchangers are prone to fouling. Fouling, in general, refers to the deposition of solid particles on the heat transfer surfaces which increases the thermal resistance to heat transfer and results in loss of thermal efficiency of the equipment [1]. The consequential effects of fouling are: (i) need for additional fossil fuels, (ii) increase in pressure drop across the heat exchangers, (iii) the necessity of frequent cleaning of heat exchangers and (iv) the environmental problems arising due to the disposal of the deposits containing sulphur, nitrogen and metals. The costs associated with fouling are mainly due to (i) additional capital costs for larger heat exchangers, (ii) additional fuel costs to meet the heat duty requirements, (iii) costs associated with cleaning of heat exchangers and

(iv) loss in production due to reduced throughputs [2]. Taking into account all these factors, Nostrand et al. [3] estimated an overall loss of about USD 10 million per year for a hypothetical 100000 barrels per day petroleum refinery. Panchal et al. [4] estimated USD 40000 to 50000 per annum as the cost for cleaning a fouled industrial heat exchanger. Hence, minimizing the foulant formation is a key step in process industries to reduce the plant economic loss [5].

1.2 Fouling Mitigation

Various approaches have been employed to minimize the effect of fouling. Traditionally, the heat exchangers are designed with allowable fouling resistances as recommended by Tubular Exchanger Manufacturers Association (TEMA). The use of fixed fouling resistances specified by TEMA imposes a static condition to the dynamic nature of fouling and results in over-design of heat exchangers. Most of the fouling resistance values recommended by TEMA are limited to fluids such as water and hydrocarbons. Moreover, the TEMA tables do not provide any information about the effect of operating parameters such as flow velocity, fluid temperature, heat flux and fluid composition on fouling rate even though these parameters have significant effect [1, 6].

Fouling in heat exchangers is reduced by the use of chemical additives as anti-foulants. The general function of anti-foulants is to prevent the physical or chemical processes leading to the formation of foulant or where the foulants are already present to prevent their attachment on hot surfaces. Large quantities of added chemicals may require removal at a later stage in the process. High concentrations of residual additives require treatment before discharge to the environment. The treatment operations to meet the discharge requirements are very expensive and may not be acceptable. Online monitoring and assessing the performance of anti-foulants is also a difficult task.

A number of techniques are available for reducing the effects of fouling by chemical or physical means but the prime considerations will be that of the cost associated with cleaning, treatment operations, associated equipment requirement and modifications to the existing units. The physical methods of fouling mitigation include the use of inside and outside tube mitigation devices [7]. The inside tube mitigation devices include wire matrix inserts, twisted tubes and displaced enhancement devices. These devices are usually placed in the process streams. The vibrations and the turbulences created by these devices enhance the heat transfer and hence the heat transfer coefficient, thus decreasing the surface temperature and hence fouling. The outside tube mitigation devices include helical flow baffles, rod baffles and twisted tubes and equivalent devices.

1.3 Fouling Models

It has been recognized by many researchers that there exists a threshold fouling condition at which the net rate of fouling is zero. In other words, operating a heat exchanger below the threshold conditions would mean nil or very low fouling rates. Ebert and Panchal [8] in 1995 proposed a semi-empirical fouling model for determining threshold conditions of film temperature and flow velocity. The fouling model proposed by Ebert and Panchal is given by:

$$\frac{dR_f}{dt} = \alpha \,\mathrm{Re}^{-\beta} \exp\left(-E/RT_f\right) - \gamma\tau_w \tag{1.1}$$

This model was originally developed using the Exxon crude-oil-slip stream coking data obtained by Scarborough et al. [9]. The Ebert and Panchal model has been further modified by Panchal et al. [10], Polley et al. [11] and Nasr and Givi [12] with simple modifications. The threshold fouling conditions show regimes in which the chosen operating conditions lead to fouling or no-fouling. The threshold fouling regimes are established by setting the fouling rate to zero and solving for film temperatures for a wide range of wall shear stresses or flow velocities. Establishing such a threshold fouling regime permits the operation of heat exchangers at the highest economically possible rate of heat transfer without the danger of fouling [13].

Several researchers have attempted to model fouling characteristics of crude oils through experimental studies using different types of experimental units which include: stirred batch cells [14, 15], hot liquid process simulator [16, 17], recycle flow loop with a tubular cross section [18] and recycle flow loop with annular cross section [19, 20].

1.4 Problem Statement

Laboratory units are designed and operated to achieve accelerated fouling. High surface temperatures or heat fluxes and low velocities are generally used to accelerate the fouling. A summary of the experimental units and the operating conditions reported are tabulated in Table 2.1. In most of the reported studies on hydrocarbon

fouling, reference to boiling was rarely made although the operating conditions used suggest that it was indeed often present [21]. The fouling characteristics determined at these operating conditions will be influenced by boiling and are not applicable to crude preheat exchangers. Generally, the crude preheat exchangers operate in the forced convective heat transfer regime and it is only appropriate that the heat transfer in the laboratory experimental units is also in the same heat transfer regime to study the fouling in the preheat exchangers. The heat transfer regime is mainly determined by the heat flux. Thus, there is a maximum heat flux beyond which the heat transfer regime changes to sub-cooled, nucleate or film boiling conditions.

> "The maximum heat flux at which the heat transfer regime changes from forced convection to boiling needed to be determined for all the test crude oils at desired bulk temperature and flow velocity to carry out the fouling characterization studies under the forced convective heat transfer regime".

In view of this the heat transfer experiments will be carried out for all the test crude oils at desired bulk temperatures and flow velocities to determine the surface temperatures as a function of heat flux. The temperature difference between the surface and the bulk *i.e.* (T_s-T_b) will be plotted against the corresponding heat flux, q. With this information, the boiling curve represented by the heat transfer coefficient, h, vs. (T_s-T_b) will be plotted. The maximum temperature difference beyond which the boiling occurs and the corresponding maximum heat flux shall be determined from h vs. (T_s-T_b) and (T_s-T_b) vs. q plots, respectively.

Experimental units employing annular flow geometry are generally equipped with fouling probes which are heated from inside using cartridge heaters. Direct measurement of surface temperature is not feasible. Usually, one to four thermocouples are embedded in the heater close to the sheath to measure the heater temperature. Surface temperature is estimated through a calibration following Wilson plot technique. In this technique, the thermal wall resistance between the thermocouple inside the heater and the fouling probe outside surface is determined. Accurate determination of thermal wall resistance plays an important role in establishing the heat transfer regimes. The wall resistance is assumed to be a constant in most of the studies on fouling [13, 20, 22-24]. But, theoretically, the wall

resistance is expected to change with heater/source temperature due to the changes in the thermal conductivity of the materials between the thermocouple location and the heater surface. Hence, the use of a constant wall resistance leads to an incorrect estimation of surface temperature and changes in the heat transfer regimes cannot be identified.

> "The surface temperature is to be estimated by using the thermal wall resistance between the thermocouple location in the heater and the heat transfer surface as a function of heater temperature".

Calibration experiments will be carried out using non-fouling heat transfer oil and the thermal wall resistance will be determined using the Wilson plot technique at different heater temperatures. It is known that the thermal wall resistance changes with heater temperature. An appropriate relationship between the thermal wall resistance and heater temperatures will be established for a given range of operating conditions.

The determination of fouling characteristics of crude oils help in the effective management and scheduling of cleaning of heat exchangers. The information about the fouling propensities of crude oils with respect to the operating conditions will also help in increasing the run time between the cleanings.

> "The effect of operating conditions such as surface temperature, flow velocity and bulk temperature on the fouling characteristics of crude oils are to be determined experimentally".

Fouling experiments will be carried out in an annular flow fouling test rig at different surface temperatures, flow velocities and bulk temperatures to establish the fouling characteristics of some Malaysian crude oils.

The decrease/increase in fouling rates with an increase in bulk temperature has been reported in the literature [14, 22-27]. It has also been reported in the literature that the solubility of the fouling precursors increases with an increase in the bulk temperature up to certain value of bulk temperature [28] leading to reduced fouling rates at higher bulk temperatures. This effect is expected to be reflected in the

apparent activation energy values. The decrease in fouling rate with an increase in the bulk temperature has not been explained by the existing threshold fouling models, as they predict increase in fouling rates with an increase in the film temperature as a consequence of increase in the bulk temperature.

> "A generalized threshold fouling model needed to be developed to account for the effect of bulk temperature on fouling".

Using the experimental data on the fouling characteristics of crude oils, the apparent activation energy values will be determined at different bulk temperatures. An appropriate relationship between the apparent activation energy and the bulk temperature will be established and will be used in developing a generalized fouling model that accounts the effect of both bulk and surface temperatures.

1.5 Research objectives

The objectives of the present investigation include the followings:

1. To develop an improved method for the surface temperature estimation;
2. To develop a systematic procedure for the selection of appropriate operating conditions for the thermal fouling experiments in the forced convective heat transfer regime;
3. To investigate the effects of surface temperatures, bulk temperatures and flow velocities on the fouling characteristics of Malaysian crude oils; and
4. To develop a new threshold fouling model to incorporate the effect of bulk temperature on fouling.

1.6 Research methodology

The research problems mentioned above are investigated based on the following methodology.

1. Fabrication of a pilot-scale fouling unit: A pilot-scale high pressure, high temperature, re-circulation flow-loop is designed and fabricated to study the fouling characteristics of crude oils.

2. Calibration of surface temperature as a function of heater temperature: In this study, calibration is carried out with non-fouling heat transfer oil as per the procedure proposed by Wilson [29]. The thermal wall resistance between the thermocouple location and the fouling probe surface is determined for different heater temperatures and an accurate relationship is established between the wall resistance and the heater temperature.

3. Determination of maximum heat flux under forced convective heat transfer regime: Experiments are carried out using the test crude oils at a constant pressure, flow velocity and bulk temperature. In this method, the power to the fouling probe heater is increased gradually and the heater temperatures measured for each power level. With this information, the surface temperature and the heat transfer coefficient is estimated. From the plot of heat transfer coefficient versus the temperature difference between surface and bulk temperatures, the maximum heat flux under the forced convective heat transfer regime is determined.

4. Determination of fouling characteristics of crude oils at different bulk and surface temperatures and flow velocities using the pilot-scale fouling test unit and development of new threshold fouling model: Experiments are carried out in the pilot-scale fouling unit using fresh batch of crude oils to study the effect of surface temperature, flow velocity and bulk temperature on fouling. The thermal fouling profiles are plotted and the initial fouling rates are estimated for each fouling experiment. Based on the experimental observations, a new threshold fouling model to account for the effect of bulk temperature on fouling is developed.

1.7 Organization of the thesis

This thesis is divided into 6 chapters. The general background on fouling, the problem statements, objectives and research methodology are covered in Chapter 1. Chapter 2 presents the literature review which mainly focuses on the general fouling mechanisms, sequential events of fouling, factors influencing fouling and general fouling prediction models. The experimental investigations were performed in a pilot-scale fouling test unit. The detailed description of the experimental unit and the experimental procedures are explained in Chapter 3. Chapter 4 presents the experimental results for the estimation of the maximum heat flux under the forced convective heat transfer regime for each crude oil. Chapter 5 describes the analysis of the experimental results for the effect of operating conditions such as initial surface temperature, bulk temperature and flow velocity on fouling characteristics of the crude oils. Based on the experimental observations, a new threshold fouling model was developed and presented. Finally, the conclusions drawn from the experimental results and recommendations for future study are discussed in Chapter 6.

CHAPTER 2

LITERATURE REVIEW

2.1 Introduction

Fouling of heat exchangers greatly affects the energy efficiency and the economy of the plant in process industries in general and particularly in petroleum refineries. Fouling in the crude preheat train in the refineries is a very complex phenomenon owing to the complex nature of the crude oil being processed. The presence of various components in the crude oil such as basic sediment, water, salt, corrosion products, suspended particles and reactive constituents contribute to the fouling in the heat exchangers of the preheat train at various stages of heating through a multitude of mechanisms [30].

Understanding the fouling mechanisms is essential for effective management and control of fouling. It is known that different mechanisms such as particulate fouling, corrosion fouling, chemical reaction fouling and crystallisation fouling prevail in the heat exchangers of the preheat train. Fouling due to the presence of reactive hydrocarbons in the crude oil predominates the other fouling mechanisms in crude preheat train especially in the heat exchangers after the desalter unit. Crude oils contain hydrocarbons with very complex molecular structure and wide range of molecular weights which differs from crude to crude. This fact excludes the possibility of developing first-principle models for the chemical reaction fouling for petroleum crude oils [1].

In general, the chemical reaction fouling mechanism is deduced from experimental studies in laboratory scale fouling units. Several types of fouling units have been reported in the literature to characterize crude oil fouling. The crude oil fouling characterization involves a detailed investigation of the effect of several factors such as surface temperature, flow velocity, bulk temperature, crude type and

crude blending. Based on the experimental observations, a number of semi-empirical fouling models have been reported in the literature [7].

This chapter is intended to provide a general background on fouling experimental units, factors influencing fouling and the fouling mechanisms. The various fouling models used by several researchers are also discussed.

2.2 Fouling experimental units

Several types of fouling units are reported to be used to establish the fouling characteristics of crude oils and other petroleum mixtures at different operating conditions. Fouling experimental units are generally classified based on (i) the flow geometry of the test sections (fouling probes) and (ii) the source of heating the test fluid [31]. Test sections with tubular or annular flow geometries with the test fluid being heated electrically are most common in the experimental units. It is reported that the fouling characterization studies were also carried out in the operational heat exchangers [32]. Table 2.1 summarizes the various fouling experimental units and their operating conditions used for characterizing fouling of crude oils and other petroleum mixtures. Table 2.1 is an extended version of the summary of experimental fouling units by ESDU [7] and Watkinson and Wilson [33].

Table 2.1: Summary of various fouling experimental units

Reference	Experimental unit type	Mode of operation	Operating conditions					Remarks
			T_b	T_{so}	v	q	P	
			^oC	^oC	m/s	kW/m^2	bar	
Weiland et al. [34]	Preheat train	Once through	N/A	max 310	N/A	N/A	N/A	Crude/residues
NACE report [35]	Preheat train	Once through	N/A	max 400	N/A	N/A	N/A	Crude/residues
Scarborough et al. [9]	Field fouling unit	Once through	345 - 370	376 – 467	1.2 – 2.5	N/A	41.5	Coking experiments
Latos and Franke [36]	Hot wire probe	Recirculation	90	175 – 400	N/A	N/A	N/A	Crude oil, kerosene, shale oils
Lambourn and Durrieu [25]	Preheat train	Once through	N/A	max 374	N/A	N/A	N/A	Crude/residues
Eaton and Lux [14]	Heated probe	Batch	71-287	287	N/A	N/A	20	Crude oil refinery cuts with pitch, resin
Dickakian and Seay [37]	Single heated tube	Recirculation	232 – 266	N/A	N/A	N/A	N/A	Crude oil

Reference	Experimental unit type	Mode of operation	Operating conditions					Remarks
			T_b	T_{so}	v	q	P	
			^oC	^oC	m/s	kW/m^2	bar	
Dickakian [38]	Annular thermal fouling test unit	Recirculation	275	N/A	N/A	N/A	N/A	Crude oil
Dickakian [39]	Annular thermal fouling test unit	Recirculation	350 – 380	510 – 593	N/A	N/A	N/A	FCC streams, oils, asphaltenes
Crittenden et al. [32]	Refinery preheat train	Once through	Up to 250	165-260	1.1 – 2.1	N/A	N/A	Crude oil
Crittenden et al. [40]	Tubular heater	Recirculation	140	197 – 218	0.5	N/A	15	Crude oil, residue and styrene
Oufer and Knudsen [41, 42]	Annular flow geometry	Recirculation	87 - 100	151 – 190	0.9 -2.4	N/A	10	Styrene / heptane
Haquet et al. [43]	Refinery exchangers and inserts	Once through	230 - 270	N/A	N/A	N/A	N/A	Crude / residue
Bach et al. [44]	Coupon in quench stream (mass deposition)	Recirculation	350 - 500	N/A	N/A	N/A	1	Isobutene in N_2

Reference	Experimental unit type	Mode of operation	Operating conditions					Remarks
			T_b	T_{so}	v	q	P	
			^oC	^oC	m/s	kW/m^2	bar	
Knudsen et al. [13]	Annular flow geometry	Recirculation	149 - 204	177 - 329	0.91 – 3.1	N/A	3 - 11.7	Alaskan Crude oil
Asomaning et al. [28]	High pressure autoclave unit	Recirculation	237 - 310	265 - 400	1.0 - 3.1	N/A	20	Crude oil
	Field fouling unit	Once through	215 - 230	236 - 302	0.91 – 1.2	29 - 172	23 - 30	Crude oil
Asomaning et al. [45]	Annular flow geometry	Recirculation	85	160 - 240	0.75	N/A	4.1	10% wt Cold Lake heavy oil + 90% fuel oil cut from a refinery
Watkinson [17]	Hot liquid process simulator (HLPS)	Recirculation	120 - 193	225 - 380	0.003	10	42	Cold Lake crude oil, Light Sour blend crude oil, Midale crude oil
Srinivasan and Watkinson [24]	Portable fouling unit with annular flow geometry	Recirculation	200 - 285	300 - 380	0.75	265-485	10 - 13	Canadian Crude Oils

Reference	Experimental unit type	Mode of operation	Operating conditions					Remarks
			T_b	T_{so}	v	q	P	
			^oC	^oC	m/s	kW/m^2	bar	
Saleh et al. [23]	Portable fouling unit with annular flow geometry	Recirculation	80 - 120	180 - 260	0.25 – 0.65	400	3.79	Australian light crude oil
Bennett et al. [46]	Annular flow, high temperature unit	Recirculation	200 - 260	260 - 320	1 - 3	N/A	20 - 70	Industry recommended procedure
Bennett et al. [20]	High temperature, annular flow	Recirculation	315 - 319	360 - 426	1.65 - 2.16	N/A	69	Crude oils
Crittenden et al. [18]	Tubular flow, twin column unit	Recirculation	150	250 - 280	0.5 – 4.0	max 282	15	Maya crude oil
Young et al. [15]	Stirred vessel	Batch	240 - 280	345 - 420	N/A	85 - 122	24 - 28	Crude oils
Wilson and Watkinson [47]	Annular flow geometry	Recirculation	80	180-240	Re = 3000-12000	N/A		Indene in different solvents

Fouling is a very slow phenomenon in process industries and thus experimental fouling units are designed and operated to achieve accelerated fouling rates in order to reduce the time scale during experiments. High surface temperatures or heat fluxes and low velocities are generally used to accelerate the fouling rates. It is observed from Table 2.1 that the initial surface temperature, T_{so}, is in the range of 165 to 467^{o}C, flow velocity, v, from 0.003 to 3 m/s and bulk temperature, T_b, from 80 to 370^{o}C specifically for crude oil characterisation studies.

2.3 Fouling mechanisms

Fouling mechanisms have been classified into five major categories, namely: particulate fouling, corrosion fouling, chemical reaction fouling, crystallization fouling and biological fouling [48]. For the hydrocarbon fouling, the presence of particulate matter, inorganic salts, corrosion products and the reactive hydrocarbons affect the deposition process, but the chemical reaction of reactive hydrocarbons is the predominant fouling mechanism. Hence the chemical reaction fouling mechanism predominates over the other fouling mechanisms [1].

2.3.1 Chemical reaction fouling

Chemical reaction fouling takes place when the deposits are formed on the heat transfer surface as a result of a chemical reaction which involves the following two-step process [33]:

$$\underset{\text{(Reactants, Soluble)}}{A} \longrightarrow \underset{\text{(Precursors, Sparingly soluble)}}{B} \longrightarrow \underset{\text{(Foulant, Insoluble)}}{C}$$

The various possible steps in chemical reaction fouling mechanism are shown in Figure 2.1 [33].

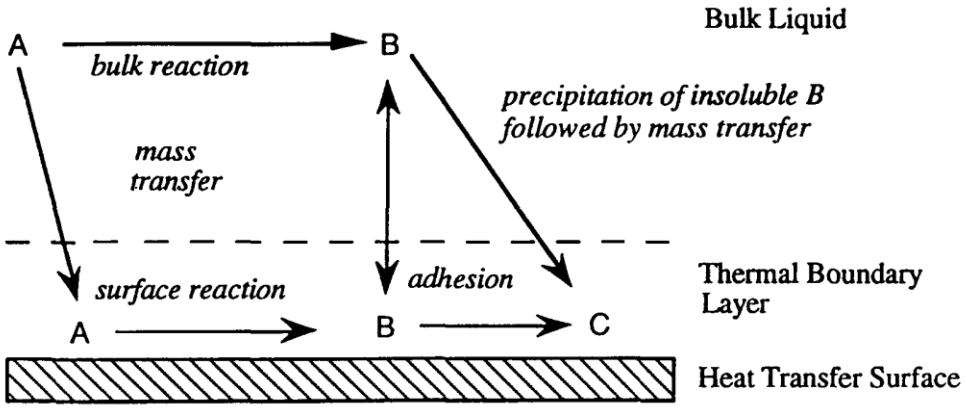

Fig. 2.1: Two-step chemical reaction fouling mechanism [33]

The soluble precursor A in the bulk fluid gets transported to the heat transfer surface and forms the deposit by chemical reaction on the wall. Alternatively, the precursor A may undergo chemical reaction in the bulk fluid or in the thermal boundary layer to form the foulant B and get transported and adhered to the heat transfer surface. The chemical reaction may involve three general classes of reactions such as autoxidation, polymerization, and thermal decomposition. During the reaction, the metal surface does not involve as a reactant but in many situations it may act as a catalyst. The foulant B may undergo ageing on the heat transfer surface to produce the deposit C. The fouling process generally occurs in a series of steps as outlined below [49].

2.3.1.1 Initiation

This step is associated with an induction period before any measurable fouling occurs. When a new or clean heat exchanger is commissioned, initially the heat transfer coefficient remains unchanged for a certain period of time before it starts to decline due to fouling. This induction period may last anytime from few seconds to several days. The duration of this phase depends upon factors such as type of fouling, surface temperature and surface conditioning. For instance, the initiation step is absent for particulate fouling while the induction period is much longer for chemical reaction fouling [6].

2.3.1.2 Transport

The fouling precursors must be transported from the bulk fluid to the heat transfer surface where its concentration decreases as the fouling process occurs. The precursors that are responsible for the deposit formation on the surface are originally either suspended or dissolved in the bulk fluid and they are transported from the bulk fluid to the heat transfer surface through diffusion. The driving force for the transport is the difference between the concentrations of precursor in the bulk fluid and at the surface [49]. The rate of transportation of these species can be described by:

$$\frac{dm}{dt} = k_t \left(C_b - C_s \right) \tag{2.1}$$

where C_b and C_s are the concentrations of precursor in the bulk and at the surface, respectively, and k_t is mass transfer coefficient that can be determined from mass transfer correlations for the given flow conditions and geometry.

2.3.1.3 Deposition / Attachment

When the fouling precursors reach the heat transfer surface, they either stick to the surface, leave the surface or react to form substances that finally stick to the surface. Deposition can either be controlled by mass transfer or chemical reaction. Under the conditions where the deposition is controlled by mass transfer, the precursor diffusivity plays an important role. If the deposition process is controlled by chemical reactions, and later attachment mechanism, the rate of reaction increases exponentially with surface temperature [6].

The rate at which precursor (reactant) is converted to foulant (product) by chemical reaction and attached to the heat transfer surface is given by:

$$\frac{dm}{dt} = k_r C_s^n \tag{2.2}$$

where k_r is the reaction rate constant, C_s is the concentration of precursor on the surface and n is the order of the reaction.

2.3.1.4 Removal

As the deposit layer starts building up on the heat transfer surface, some part of it may be removed by the action of fluid shear and mass transfer. The amount of the deposit removed depends upon the strength of the deposit layer and the mass of the deposit per unit surface area [50] as given by:

$$\dot{m}_r = \frac{b\tau_w m_f}{\psi} \tag{2.3}$$

where τ_w is wall shear stress, m_f is mass of deposit per unit surface area, Ψ is deposit strength and b is a constant.

2.3.1.5 Ageing

Every deposit layer on the surface is subjected to ageing with time. Ageing may increase the strength of the deposit by polymerization, re-crystallization, etc. Ageing is the least investigated and understood step and is usually ignored in modeling attempts. A fresh crude oil foulant generally consists of asphaltene with no coke. During heating and fouling process the foulant deposits or attaches on the heat transfer surface and undergoes ageing reaction to produce coke. The rate of conversion of asphaltene into coke may explain the ageing process. Dickakian [38] studied the crude oil deposit ageing process and observed that the fraction of coke in the crude oil deposit increased over time, whereas the asphaltene fraction decreased. In his study, he observed that a deposit containing 30% asphaltene with no coke, when subjected to three hour of heating and further fouling, resulted in 60% coke and about 14% asphaltene. The ageing process resulted in the conversion of asphaltene into coke in the crude oil deposit. This ageing process should be thoroughly studied if the fouling mechanisms are to be deduced from the deposits taken from the industrial heat exchangers that may have been on stream for many months. Ishiyama et al. [51] studied impact of deposit ageing on thermal fouling and proposed a lumped parameter model that demonstrate that ageing can have a substantial influence on the rate of heat transfer and hence on the surface temperature and rate of fouling. They also concluded that deposit ageing dynamics should be considered alongside

deposition rate dynamics when interpreting experimental fouling data and when modeling fouling behavior in support of heat exchanger design or operation. Coletti et al. [52] proposed a kinetic model to describe the effects of ageing on deposit thermal conductivity and the thermal performance of a shell-and-tube heat exchanger undergoing crude oil fouling. The results demonstrated the substantial effects over time of ageing and roughness on heat transfer and pressure drop.

2.4 Factors influencing fouling

It is generally known that surface temperature, flow velocity, bulk temperature, crude type and crude blending influence the rate of fouling. The factors such as nature and type of surface, equipment design, fluctuations in operating conditions, properties of the deposit and so on also have some effect on the fouling rates as compared with surface temperature, flow velocity, bulk temperature, crude type and crude blending but are usually neglected [7].

2.4.1 Effect of surface temperature

The rate of fouling increases exponentially with increasing surface temperature for almost all fouling mechanisms [53, 54]. The effect of surface temperature on the fouling rate is generally expressed by an Arrhenius-type equation.

$$\frac{dR_f}{dt} = A\exp\left(-E/RT\right) \tag{2.4}$$

Activation energy, E, and the pre-exponential factor, A, in Equation (2.4) are determined from the experimental data at different initial surface temperatures and constant velocity, fluid composition and geometry. There are also attempts to use the film temperature, T_f, instead of surface temperature, T_s [8, 23, 24]. The use of surface temperature or the film temperature in the Arrhenius equation depends upon the location of occurrence of the chemical reaction. If the chemical reaction occurs in the thermal boundary layer close to the heat transfer surface, the film temperature is

used. On the other hand, if the chemical reaction occurs on the heat transfer surface, the surface temperature is used.

2.4.2 Effect of flow velocity

It is reported that the fouling rate increases for some crude oils while it decreases for other crude oils with an increase in the flow velocity. For a case, where the fouling rate decreases with an increase in flow velocity, the fouling mechanism is said to be reaction controlled. In this case, the increase in flow velocity at constant bulk temperature and heat flux increases the heat transfer coefficient and thus reduces the surface and film temperature. The increase in flow velocity also increases the wall shear stress which may give rise to erosion of the foulant layer and that offsets the deposition. On the other hand, if the fouling rate increases with increase in flow velocity, the fouling mechanism is said to be mass transfer controlled. In such a case, the increase in flow velocity increases the mass transfer coefficient from the bulk fluid to the heat transfer surface leading to an increase in the fouling rate [7].

Watkinson and Epstein [53] developed a model for gas oil fouling and found that the initial fouling rate is inversely proportional to mass flow rate. A similar dependence of initial fouling rate on flow velocity was observed by other researchers [9, 18, 22, 23, 55, 56] and hence the fouling mechanism is said to be reaction controlled.

2.4.3 Effect of bulk temperature

The effect of bulk temperature on deposit formation was studied by a few researchers and contradicting conclusions were reported. Some researchers have observed that the fouling rate increased with a decrease in bulk temperature [14, 22, 25-27]. The decrease in bulk temperature at a constant velocity and surface temperature results in an increase in the thermal driving force and hence an increase in the fouling rate. An increase in the fouling rate with an increase in the bulk temperature has also been reported in the literature [23, 24]. The increase in bulk temperature increases the film temperature and thus the fouling rate.

The solubility of asphaltene plays an important role in crude oil fouling. Generally, the solubility of asphaltene in crude oil increases with increase in temperature [26]. A complex relationship between asphaltene solubility and temperature has been reported by Lambourn and Durrieu [25] in which the solubility of asphaltene increased to a maximum at 140^{o}C and then decreased at higher temperatures. At high bulk temperatures (>150^{o}C), the asphaltene is in the form of solution in crude oil, and the fouling rate is low; whereas at low bulk temperatures (below 150^{o}C), asphaltene precipitates out from crude oil and the fouling rate is high.

The bulk temperature effects are also strongly interrelated with the Reynolds number. Increase in bulk temperature decreases the viscosity and hence increases the Reynolds number. At high Reynolds numbers, the thickness of the thermal boundary layer becomes smaller and the rate of formation of fouling precursors decreases due to the reduction in the volume for the chemical reaction [22].

2.4.4 Effect of crude type

The crude oil is a mixture of a large number of hydrocarbons. The most commonly found molecules are paraffins, naphthenes, aromatic hydrocarbons and asphaltenes. The crude oils can be classified as light, medium or heavy according to its measured API gravity. Heavy oils contain much higher proportions of asphaltenes and sulfur than medium or light oils and they tend to foul at a faster rate as compared with light and medium crude oils. Dickakian and Kengwood [57] separated crude oils quantitatively into three specific components such as (i) a hydrocarbon saturate fraction, (ii) a neutral hydrocarbon aromatic fraction and (iii) polar aromatic fractions containing sulfur, nitrogen and oxygen by using high performance liquid chromatography techniques and observed that crude oils containing high saturate hydrocarbon fraction (more than 75% by weight of the total crude oil) and lower neutral hydrocarbons and polar aromatics (less than 25% by weight of the total crude oil) showed higher fouling tendency in refinery heat exchangers.

2.4.5 Effect of crude blending

Another important factor which influences the fouling is crude blending. Blending of crudes can cause unstable mixes which precipitate species such as asphaltene and result in rapid fouling [58]. The crude oil incompatibility and the precipitation of asphaltene on blending of crude oils can cause significant fouling and coking in crude preheat train. For this reason, the crude oil compatibility model and tests were developed to predict proportions and order of blending of oils that would avoid incompatibility [59]. Saleh et al. [60] studied the effect of mixing and blending of four Australian crude oils at certain operating conditions with the intention of using the results to guide a fouling mitigation strategy. They reported that the effect of blending on fouling rate is non-linear.

2.5 Modeling of crude oil fouling

A number of models for crude oil fouling have been developed and reported in the literature. The models describing fouling, usually, are based on the well-known concept of Kern and Seaton [61] where the net fouling rate is the difference between the rates of deposition and removal.

Fouling rate = rate of deposition – rate of removal

$$\frac{dm}{dt} = \dot{m}_d - \dot{m}_r \tag{2.5}$$

where $\dot{m}_d$ is deposition rate of foulant and $\dot{m}_r$ is removal rate of foulant.

The basic differences between various models reported in literature are in the description of the deposition and removal terms. The rate of deposition is described by either transport-adhesion models or transport-reaction models while the rate of removal is described by either shear-related or mass-transfer related expressions.

2.5.1 Transport-adhesion Models

Kern and Seaton [61] developed an equation to describe the fouling rate with the following assumptions:

1. No chemical reaction is involved
2. Fouling removal is directly proportional to deposit thickness and
3. Rate of deposition is independent of mass of deposit.

The Kern and Seaton equation is given by:

$$R_{ft} = R_{f\infty}\left(1 - e^{-\beta t}\right) \tag{2.6}$$

It is an idealized model and the values of $R_{f\infty}$ and β were determined from the experimental data. The actual values of these constants depend upon the fouling mechanism and the operating conditions.

Kern and Seaton proposed a mathematical restatement of Equation (2.6) as [1]:

$$\frac{dx_f}{dt} = K_1 C' M - K_2 \tau_w x_f \tag{2.7}$$

where the first term on the RHS represents 1st order reaction which is a function of concentration of the foulant, C', and mass flow rate of fluid, M; and the second term represents the rate of removal which is a function of deposit thickness, x_f, and wall shear stress, τ_w.

Integrating Equation (2.7) by assuming constant C' and M gives

$$x_f = \frac{K_1 C' M}{K_2 \tau_w}\left(1 - e^{-K_2 \tau_w t}\right) \tag{2.8}$$

Equation (2.8) is similar to Equation (2.6)

In 1962, Atkins [62] observed two distinct layers in fired heater tubes, a hard layer next to the tube surface and an outer porous soft layer. These two layers coexist together and heat transfer occurs first through the hard deposit formed by coke and

then through the soft tarry layer which is formed due to the decomposition process. The overall fouling resistance on the tube side is

$$R_{f\,(overall)} = R_{f\,(hard\ layer)} + R_{f\,(soft\ layer)} \tag{2.9}$$

where $R_{f\,(hard\ layer)}$ and $R_{f\,(soft\ layer)}$ are the thermal resistances due to coke and porous soft layers, respectively.

Nijsing [63] assumed that fouling from an organic coolant in a nuclear reactor was caused by the instantaneous reaction of precursor to a product in the zone close to the surface which crystallized rapidly when compared with its diffusion to the deposition surface. Assuming that the physical properties were not temperature dependent and the diffusivities of precursors and products were equal, the average rate of deposition was given by:

$$\text{Average rate of deposition} \propto \frac{C_b D \,\mathrm{Re}^{0.875}\,\mathrm{Sc}^{0.33}}{d} \tag{2.10}$$

It is clear from Equation (2.10) that the deposition is mass transfer controlled and increased with an increase in flow velocity.

Watkinson and Epstein [53] proposed a transport-adhesion-release model based on the experimental observations of both gas oils and sand-water slurries. They assumed that deposition was mainly caused by mass transfer of suspended particles to the surface and followed by adhesion and the removal is first order function of deposit thickness as proposed by Kern and Seaton.

Jackman and Aris [64], Fernandez-Baujin and Solomon [65] and Sundaram and Froment [66] proposed models without considering the removal term in the case of vapor phase pyrolysis. This is reasonable since the deposit formed at high temperatures in a pyrolyzer is not easily removed from the surfaces.

Jackman and Aris [64] proposed a model for coke deposition by two reactions: A first order reaction which explains the dissociation of reactant in to the product, coke and a zero order reaction that describes the deposition of coke on to the tube walls. But this model was not tested for any laboratory or plant data.

Fernandez-Baujin and Solomon [65] developed a two-step, mass transfer and kinetics model to account for the formation of coke in steam cracking furnaces. The overall rate of coke formation was given by:

$$\frac{dR_f}{dt} = \frac{1}{\rho_f k_f}\left[\frac{C_b}{\frac{1}{k_m}+\frac{1}{k_a}}\right] \tag{2.11}$$

where k_m and k_a are the mass transfer coefficient and the reaction rate constant, respectively. Fernandez-Baujin and Solomon claimed that condensation of coke precursors contained in the fuel oil accounts for fouling and they assumed that the mass transfer of coke precursors from the bulk of the gas to the heat transfer surface was controlling the rate of deposition. Fernandez-Baujin and Solomon model showed good agreement with the plant data.

Sundaram and Froment [66] presented a model for cracking of propane in to coke and this reaction was assumed to be controlled by kinetics *i.e*, diffusion problems were not considered as the reaction was carried out in a mixed flow reactor. The model showed a good agreement between industrial and numerically simulated data.

2.5.2 Transport-reaction Models

In 1979, Crittenden and Kolaczkowski [67] carried out a systematic investigation on chemical reaction fouling and proposed a general model that considers the transport of fouling precursors and also chemical reaction. Crittenden and Kolaczkowski [68] also proposed a modified fouling model to determine the polystyrene deposition from the dilute solution of styrene in kerosene as:

$$\frac{dR_f}{dt} = \frac{1}{\rho_f k_f}\left[\frac{C_{rb}}{\frac{\rho d_p^{1.8} c_r^{0.67}}{1.213\lambda_1\eta^{0.2}G^{0.8}}+\frac{1}{Ae^{\frac{-E}{RT}}}} - \frac{1.213\lambda_1\eta^{0.2}G^{0.8}C_{Di}}{\rho d_p^{1.8} c_D^{0.67}}\right] \tag{2.12}$$

where C_{Di} is the foulant/deposit concentration at the solid-liquid interface. Equation (2.12) is an extremely complex and difficult to use in design or in the analysis of an operating system due to too many unknowns. This model also contains foulant back diffusion term (2nd term in RHS of Equation 2.12) which is a function of foulant/deposit concentration at solid-liquid interface which is very difficult to determine practically. Epstein [69] observed that at time zero, it is fundamentally difficult to justify the finite concentration of foulant at the surface which would be required for back diffusion to occur. Epstein developed a model for the initial chemical reaction fouling rates at the surface in which the surface attachment is proportional to residence time of the fluid at the surface. The greater the residence time, the greater would be the opportunity for the chemical reaction to occur. The relationship between the initial fouling rate and the mass flux is given as:

$$\left[\frac{dR_f}{dt}\right]_{t=0} = \frac{m\phi}{k_f \rho_f} \tag{2.13}$$

The driving force for the mass transfer from the bulk fluid to the heater surface of foulant precursor was expressed as the difference between its bulk and surface concentrations, C_b and C_s, respectively. The deposition mass flux is given by:

$$\phi = \frac{C_b}{\frac{1}{k_m} + \frac{1}{k_r C_s^{n-1}}} \tag{2.14}$$

where

$$k_m = \frac{v\left(f/2\right)}{k' \mathrm{Sc}^{2/3}} \text{ and}$$

$$k_r = \frac{\mu \exp\left(-E/RT_{so}\right)}{k'' \rho v^2 f}$$

The first term in the denominator of Equation (2.14) represents the mass transfer of foulant or precursor to the heated surface and the second term represents the reaction and attachment aspects. Epstein's model showed an excellent fit to Crittenden's data for initial fouling rates of polymerization of styrene. It was also

able to explain the effects of temperature and velocity. This model could not be used for describing the crude oil fouling mainly due to the following reasons:

1. The order of the reaction plus attachment term, *n*, and Schmidt number is unknown for crude oil fouling, and

2. Petroleum crude oil has complex compositions that make it difficult to isolate the key precursors to fouling and hence it is impossible to determine the concentration of foulant precursor in the bulk fluid.

Yeap et al. [70] reduced the Epstein's model to in terms of dimensional parameters *A*, *B* and *C* for turbulent flow conditions with mean velocity *v*, with a mass transfer related removal term as:

$$\frac{dR_f}{dt} = \frac{AC_f v T_s^{2/3} \rho^{2/3} \mu^{-4/3}}{1 + Bv^3 C_f^{\,2} \rho^{-1/3} \mu^{-1/3} T_s^{2/3} \exp\left(E / RT_s\right)} - Cv^{0.8} \tag{2.15}$$

They estimated the parameters of the above model using plant data from a UK refinery that processes mainly light to medium North Sea crude oils. The form of the denominator in the above equation enables this model to describe data sets where mass transfer predominate the fouling process and fouling increases with increasing flow rate which is encountered in a small number of data sets.

Saleh et al. [23] proposed a model to predict fouling without considering the effect of fluid velocity on the foulant removal and is given as:

$$\frac{dR_f}{dt} = A_o P^m v^n \exp\left(\frac{-E}{RT_f}\right) \tag{2.16}$$

Saleh et al. carried out the experiments to study the fouling caused by heating the Gipsland crude oil at moderate temperatures in a recirculation flow-loop equipped with an annular electrically heated probe.

Srinivasan and Watkinson [24] developed a correlation using a modified film temperature weighted more heavily on the surface temperature. The correlation is given by:

$$\frac{dR_f}{dt} = a\, v^{-0.35} \exp\left(\frac{-E}{RT_f^{'}}\right) \tag{2.17}$$

where v is flow velocity and $T_f^{'}$ is the modified film temperature which is determined as:

$$T_f^{'} = 0.3T_b + 0.7T_{so} \tag{2.18}$$

The correlation developed was found to fit the fouling rate data obtained using Canadian crude oils within ±8%. Srinivasan and Watkinson conducted the fouling experiments using Canadian crude oils in a recirculation fouling loop equipped with an annular electrically heated fouling probe.

Kovo [71] developed a mathematical model to predict the fouling rates of refinery naphtha and is given by:

$$\frac{dR_f}{dt} = C_1 C_2 \exp\left(E/RT_s\right) C_r^r - \frac{C_3 C_4}{\rho_f R_b}\left(\frac{W}{A_o}\right)^2 \tag{2.19}$$

Fan et al. [72] investigated the fouling mechanisms of a light conventional crude oil by characterizing the crude oil, performing fouling tests using a bench-scale Alcor hot liquid process simulator unit. They developed a mathematical fouling model under laminar flow regime following Epstein's methodology. It was concluded that under the laminar flow conditions, the unstable asphaltenes transport to the heat transfer surface and formed fouling deposits through chemical reactions. It was also reported that the mass transfer of entrained suspended particles in the crude oil also contributed to fouling although it is not the main cause of fouling as compared with chemical reactions. However, the fouling mechanisms established using hot liquid process simulator under laminar flow conditions is not applicable to turbulent flow conditions, such as those that prevail in industrial operations. The repeatability and reproducibility of fouling experiments are also believed to be poor in hot liquid process simulator.

Polley [73] proposed a new crude oil fouling model as:

$$\frac{dR_f}{dt} = \frac{A}{\alpha}\exp\left(-E/RT_f\right)P \tag{2.20}$$

where P is sticking factor which is a function of shear stress, having a value between 0 and 1. The model parameter α was estimated using plant data.

Although the transport-reaction models are based on fundamental principles, they cannot be used successfully in describing the fouling process as there are many parameters such as mass transfer coefficients, Schmidt number, diffusivity, concentration of reactants and order of the reaction which cannot be determined. Due to these limitations, researchers have resorted to semi-theoretical models with less dependency on the above constants [1].

2.5.3 Threshold fouling models

Considerable interest has been expressed in recent years in the concept of threshold fouling conditions for crude oils using less rigorous semi-empirical models. The threshold fouling concept for crude oil was introduced by Ebert and Panchal in 1995 at the Engineering Foundation conference on fouling in San Luis Obispo [74]. This approach provides a semi theoretical basis for quantitative interpretation of fouling data in terms of deposition and suppression mechanisms.

They developed a simplified correlation for predicting threshold fouling conditions based on the following assumptions:

1. The net deposition is given by formation minus removal of foulant from the thermal boundary layer.

2. Foulant is formed in the boundary layer by reactions which can be grouped as one-step reaction.

3. Concentration gradients of reactants in the boundary layer are negligible.

4. Foulant is transported back by diffusion and turbulence eddies from the boundary layer to the bulk flow.

5. Temperature profile in the boundary layer is linear.

6. An integrated reaction term can be expressed by the film temperature in the boundary layer.

The proposed correlation for predicting the linear rate of fouling or threshold conditions in terms of film temperature and fluid velocity is given by:

$$\frac{dR_f}{dt} = \alpha \,\mathrm{Re}^{-\beta} \exp\left(-E/RT_f\right) - \gamma\tau_w \qquad (1.1)$$

where α, β, E and γ are constants to be determined from the experimental data. This model was originally developed using the Exxon crude-oil-slip stream coking data obtained by Scarborough et al. [9] in a joint research project with US Department of Energy and verified by field and laboratory observations.

Ebert and Panchal reported the following values for their model parameters.

$\alpha = 30.2\times10^{6}$ (m^2K/kW)/hr

$\beta = 0.88$

$E = 68$ kJ/mol

$\gamma = 1.45\times10^{-4}$ m^2/N (m^2K/kW)/hr

This model allowed users to estimate operating conditions where the fouling rate would be close to zero which is termed as the threshold fouling conditions. A threshold fouling curve can be determined by setting Equation (1.1) to zero and calculating the film temperatures for a wide range of wall shear stresses. The threshold fouling curve is mainly a plot of film temperature versus the wall shear stress that represents the regions of fouling and no-fouling as shown in Figure 2.2. The importance of this model is that it demonstrates that fouling can be avoided by appropriate selection of operating conditions. Fouling deposition can be kept at negligible level by designing and operating heat transfer equipment inside the region

of favorable conditions. The proposed fouling threshold concept has been verified by field and laboratory observations [10, 13].

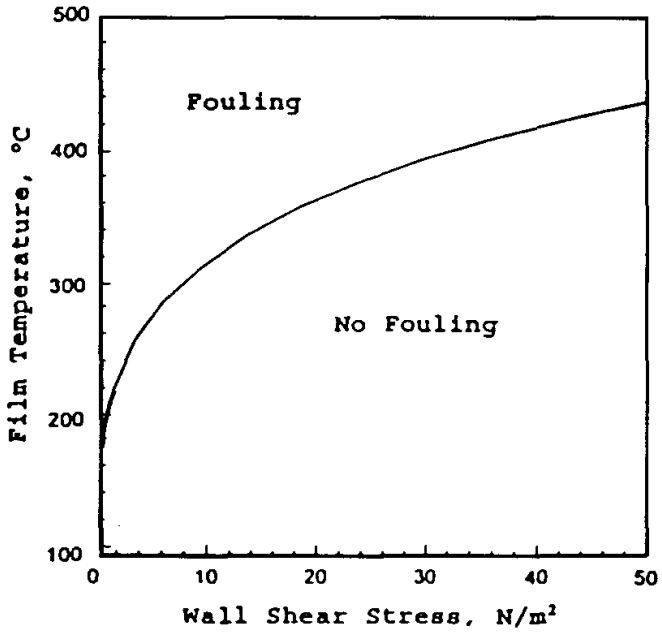

Fig. 2.2: Threshold film temperature as a function of wall shear stress [8]

Saleh et al. [23] fitted the experimental results obtained using Australian light crude oil to the Ebert-Panchal model. They observed that the predicted values closely match with the experimental data. Some researchers fixed the value for β as 0.66 or 0.8 based on the heat transfer correlations and determined the values of the other parameters from the experimental data. Saleh et al. determined the value of β together with the other model parameters α and γ. The values of the model parameters obtained for Australian light crude oil are:

$\alpha = 3.3 \times 10^{6}$ m^{2}K/kJ

$\beta = 0.3$

$E = 42.01$ kJ/mol

$\gamma = 1.45 \times 10^{-8}$ m^2/N (m^{2}K/kJ)

Ebert and Panchal model ignored the effect of crude oil thermal conductivity and specific heat and only considered the effect of crude oil density and viscosity through

Reynolds number. Panchal and coworkers in 1997 [10] modified the Ebert and Panchal model by incorporating the Prandtl number. The revised model is given as

$$\frac{dR_f}{dt} = \alpha \,\mathrm{Re}^{-0.66}\,\mathrm{Pr}^{-0.33} \exp\left(-E/RT_f\right) - \gamma\tau_w \qquad (2.21)$$

Panchal and co-workers considered data sets obtained from pilot plant tests and experimental data from a high pressure autoclave fouling unit under various operating conditions. Asomaning et al. [28] used this model to determine the threshold fouling conditions for crude oil fouling in the laboratory and field fouling units. The values of the model parameters were determined using the laboratory data and are given as:

$\alpha = 5.03\times10^{4}$ (m^2K/kW)/hr

$E = 48$ kJ/mol

$\gamma = 1.45\times10^{-4}$ m^2/N (m^2K/kW)/hr

They observed that the model developed with the experimental data predicted the threshold fouling conditions in the field unit with mixed results. Panchal and Huang-Fu [4] used the model proposed by Panchal et al. to calculate the fouling resistance as a function of time for each of the heat exchanger groups. The model parameters estimated based on the experimental data were used for the determination of fouling resistance. Bories and Patureaux [75] used Panchal et al. model to assess the fouling tendency of the exchangers of an industrial crude distillation unit preheat train. The model parameters are generally adjustable values and would be expected to vary from crude to crude. But, they used the values of the parameters of Ebert and Panchal [8]. They found that the ranking obtained through monitoring the performances of the different exchangers matched quite well with the predictions of the Panchal et al. model. Coletti and Macchietto [76] used Panchal et al. model as a building block to develop a simulation model of the whole hot end of a typical refinery preheat train. They estimated the model parameters from the actual plant data for one of the heat exchangers and used for all other units. At the tube level, the interactions between the operating conditions and the fouling were captured through this model and this

allowed the authors to calculate the thickness of the fouling layer along the tubes in each heat exchanger.

Polley et al. [11] observed that

1. For turbulent flow through circular tubes, the exponent of the Reynolds number of 0.8 is more appropriate than 0.66;

2. The use of wall temperature in the Arrhenius term is more appropriate than the film temperature; and

3. The removal mechanism is by mass transfer prior to the formation of a deposit; a simplistic approach to introduce mass transfer dependence is to use Reynolds number to a power of 0.8, in the same way that the convective mass transfer coefficient varies with velocity.

Based on these observations Polley et al. [11] made simple modifications to the Ebert and Panchal model as:

$$\frac{dR_f}{dt} = \alpha \,\mathrm{Re}^{-\beta}\,\mathrm{Pr}^{-0.33}\exp\left(E/RT_s\right)\gamma\,\mathrm{Re}^{0.8} \qquad (2.22)$$

Polley et al. verified their model using Knudsen's experimental data [13] and the following parameters are reported.

α = 1,000,000 (m^2K/kW)/hr

β = 0.8

E = 48 kJ/mol

$\gamma = 1.5\times10^{-9}$ (m^2K/kW)/hr

The Polley et al. model showed good predictions of the threshold temperature, particularly when the errors associated with the experimental measurements are considered. They reported that this model showed good agreement for a number of pilot plant and field fouling data sets reported by Asomaning et al. [28].

Polley et al. also compared their model with Shell Wood River and Shell Westhollow refinery crude oils. The Polley et al. model under-predicted fouling rates for Shell Wood River data when E = 48 kJ/mol. However, the model showed good agreement when the activation energy value was reduced to 44 kJ/mol. Polley et al. have compared their model with Westhollow refinery crude oil which is a mixed Mayan crude oil appeared in three sets (Set I-III). They determined the fouling rates at different activation energy values ranging from 48 to 58 kJ/mol and compared with the experimental observations. They found that for Westhollow refinery mixed Mayan crude set (I), the model predicted well only at highest value of E. For set (II) a good correlation was achieved for E = 50 kJ/mol, whereas for E = 58 kJ/mol the predicted fouling rates were much lower than the measured rates. For set (III) crude oils no firm conclusion was drawn.

Nesta and Bennett [30] suggested recommendations for the heat exchanger design and operation for minimizing fouling. The key points of the design method presented are to maximize shear stress and control wall temperature regardless of service. They also claimed that the application of the field-proven design methodology will significantly lower the capital costs and substantially increase run time between cleanings.

Nasr and Givi [12] proposed a threshold fouling model which is independent of Prandtl number as:

$$\frac{dR_f}{dt} = \alpha \,\mathrm{Re}^{-\beta} \exp\left(-E/RT_f\right) - \gamma \,\mathrm{Re}^{0.4} \tag{2.23}$$

The model was verified with the experimental data from Saleh et al. [23] for Australian crude oil. In this model, the value of β was determined together with the other model parameters α and γ. A value of -1.547 for β was reported for the Australian light crude oil. The authors have claimed that their model describes the data better than the earlier models. It may be noted that Nasr and Givi model has become more empirical than the earlier models since a value of -1.547 for β has no physical significance as compared to the other models. The disadvantage of this model may be that it cannot be used for extrapolation at other operating conditions.

2.6 Summary

The fouling units including the experimental test rigs, field fouling units and operational heat exchangers used for the characterization studies of crude oils and other petroleum products are summarized and presented. The factors influencing fouling, fouling mechanisms and series of steps involved in fouling processes are discussed in detail. Finally, the general fouling models (transport-adhesion, transport-reaction) and threshold fouling models associated with crude oil characterization studies are presented in this chapter. Due to the presence of many unknown parameters in the first-principle based models, the semi-empirical models have gained considerable importance in the recent studies. The models proposed by Ebert and Panchal, Panchal et al. and Nasr and Givi predict the increase in the initial fouling rate with an increase in the film temperature. But for a case, where the fouling rate decreases with an increase in the bulk temperature, the increase in the film temperature (by increasing the bulk temperature at a constant surface temperature) decreases the fouling rate. This phenomenon is not explained by any of these models. The model proposed by Polley et al. predicts the increase in initial fouling rate with an increase in the surface temperature. The effect of the bulk temperature on fouling is not considered.

CHAPTER 3

EXPERIMENTAL

3.1 Introduction

The fouling characteristics of crude oils are generally established through experiments in the laboratory experimental units which are designed and operated to achieve accelerated fouling rates. High surface temperatures or heat fluxes and low velocities are generally used to accelerate the fouling rates.

Several types of laboratory units have been reported to be used in the study of crude oil fouling characteristics. Stirred batch cells [14, 15], recycle flow loop with a tubular cross section [18] and recycle flow loop with annular cross section [19, 20] have been used to characterize crude oil fouling. Once-through flow fouling units have been reported to be used as field fouling units in the refineries [77]. The disadvantage of field fouling units is that the crude oil properties do not remain constant as the crude to the refinery changes very frequently. Recycle flow loop with annular flow geometry has been predominantly used due to their advantages such as visual observation of the fouling deposits, easier to collect foulant samples and to clean the surface for reuse, etc.

In this chapter, a detailed description of the pilot-scale recycle flow loop is presented in Section 3.2. Section 3.3 describes the method adopted for the determination of surface temperature. Further, the crude oil preparation and their properties are presented in Section 3.4. Section 3.5 describes the experimental procedure for the determination of maximum heat flux, q_{max}, under the forced convective heat transfer regime. The experimental procedure for determining the thermal fouling rates are explained in detail in Section 3.6. Section 3.7 and 3.8 provide the experimental plan designed for establishing the fouling characteristics of

different crude oils and the method adopted for the estimation of the initial fouling rates and induction periods, respectively.

3.2 Experimental Unit

In this study, a pilot-scale re-circulation flow loop with annular flow geometry, referred to as annular flow fouling research unit (AFFRU), is designed and fabricated to study the fouling characteristics of crude oils. Plate 3.1 shows the photograph of AFFRU and Figure 3.1 shows the schematic diagram of AFFRU. The experimental flow loop consists of a feed tank (V-100), a high pressure feed pump (P-100), two identical annular test sections (K-200, K-201), and a double pipe heat exchanger (E-401). The unit is equipped with necessary instrumentation, data acquisition and control system. The flow loop is designed to withstand a design temperature of 300^{o}C and a pressure of 50 bar. To prevent heat loss, the whole system is insulated with glass wool and then wrapped with aluminum sheet to keep the insulation intact. The individual components of the flow loop are explained in detail in the following sections.

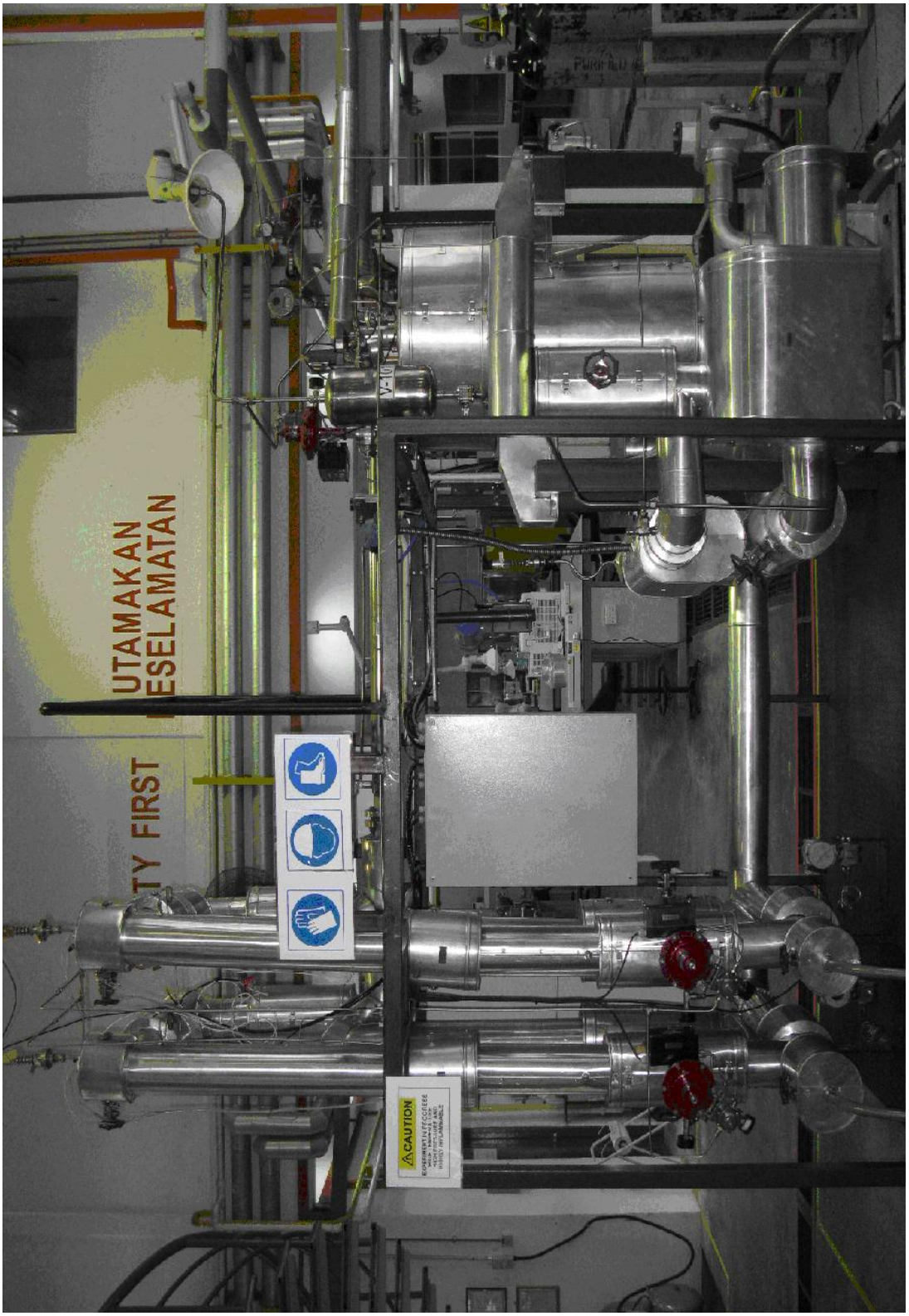

Plate 3.1: Photograph of AFFRU

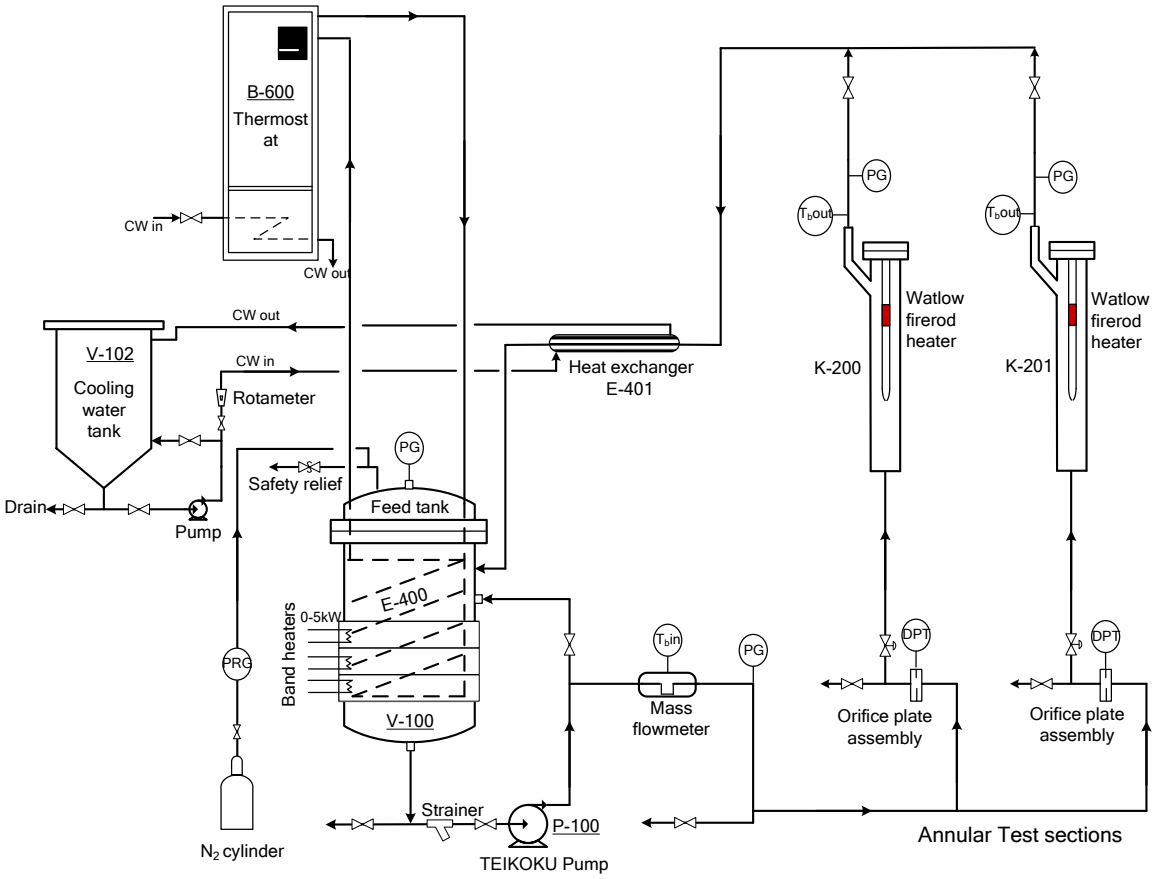

Fig. 3.1: Schematic diagram of re-circulation flow loop (AFFRU)

3.2.1 Feed tank

A cylindrical tank with tori-spherical top and bottom of 72 liter capacity is used as the crude feed tank (reservoir, V-100). This tank is equipped with three external band heaters of 5 kW power each to heat the fresh crude charge to the required bulk temperature quickly and a stainless steel internal coil for circulating hot thermal oil to maintain the bulk temperature during the experiment. It is fitted with a safety relief valve and nitrogen gas inlet at the top cover. It is also provided with a crude oil inlet at the top and an outlet at the bottom. Since the flow loop is a closed system, the crude oil leaving the test sections returns to the feed tank. An inlet nearer to the top of the feed tank is provided for this purpose. The design details of the feed tank are summarized in Table 3.1. Measurements for temperature and pressure of the crude oil inside the feed tank are also provided.

Table 3.1: Design details of feed tank

Characteristic	Value
Outer diameter	406.4 mm
Wall thickness	15 mm
Height	650 mm
Capacity	72 liter
Thickness of tori-spherical bottom and top head	19 mm
Number of bolts	20
Outer diameter of the gasket	478 mm
Inner diameter of the gasket	408 mm
Outer diameter of the flange	650 mm
Inner diameter of the flange	409 mm
Flange thickness	75 mm
Material of construction	SS – 304
Top and bottom head material	SS – 304
Flange material	Carbon steel
Bolts material	Stainless steel
Support type	Lug
Flange type	Loose ring

3.2.2 Pump

A high temperature, high suction-pressure customized TEIKOKU canned motor seal-less pump (P-100) with a maximum capacity of 120 liters per minute is used to pump the crude oil from the feed tank through the flow loop. It is equipped with a three phase induction motor with a rated output power of 1.5 kW and a rated current of 4.7 amperes. The casing, impeller and shaft are fabricated from SS316 and bearing made of graphite material. The pump is designed for a suction pressure of 60 bar and develops a discharge head of 2.4 bar. The pump and motor assembly are firmly mounted on a base plate of SS400 material. A strainer is fitted at the pump suction to remove any suspended solid particles in the test crude oil to prevent the wear out of the pump bearing.

3.2.3 Annular test sections

Two identical test sections with annular flow geometry are fitted in the flow loop. With the identical test sections, experiments could be tested for repeatability or experiments at different surface temperatures/heat flux or velocities and constant bulk temperature may be simultaneously performed. The annular cross section is formed by an outer pipe and the fouling probe as the inner pipe. The heat exchanger fouling probes (HEFP) are equipped with a WATLOW firerod cartridge heater rated @ 1 kW / 4 kW power. The outer pipe of the test section is fabricated from 1¼" 160-schedule stainless steel pipe. The schematic diagram of the HEFP is shown in Figure 3.2.

The cartridge heater has a heating length of 100 mm with a nichrome resistance coil. The remainder of the fouling probe is insulated with mica to prevent heat loss in the axial direction. Two *K*-type thermocouples are embedded in the cartridge heater at the axial centre close to the sheath to measure the heater temperatures. The heater is sheathed in a stainless steel tube of ¾" diameter. The bottom of the fouling probe is capped with an ellipsoidal plug for the even transition of flow from the tubular section to annular section. The top portion is welded with ANSI blind flange capable of withstanding 60 bar pressure. The fouling probe is held concentric to the outer pipe in the test section by four rounded holder pins at the bottom of the test section. The two test sections are referred to as K-200 and K-201. The major dimensions of HEFP are shown in Table 3.2.

Table 3.2: Dimensions of heat exchanger fouling probes

Characteristic	Value
Outside diameter	19.05 mm
Length of heated section	100 mm
Total length	1155 mm
Inside diameter of the outer pipe	29 mm
Maximum power input	1000 W / 4000 W
Voltage	230 V
Ellipsoidal length	15 mm
Material of construction	SS 316

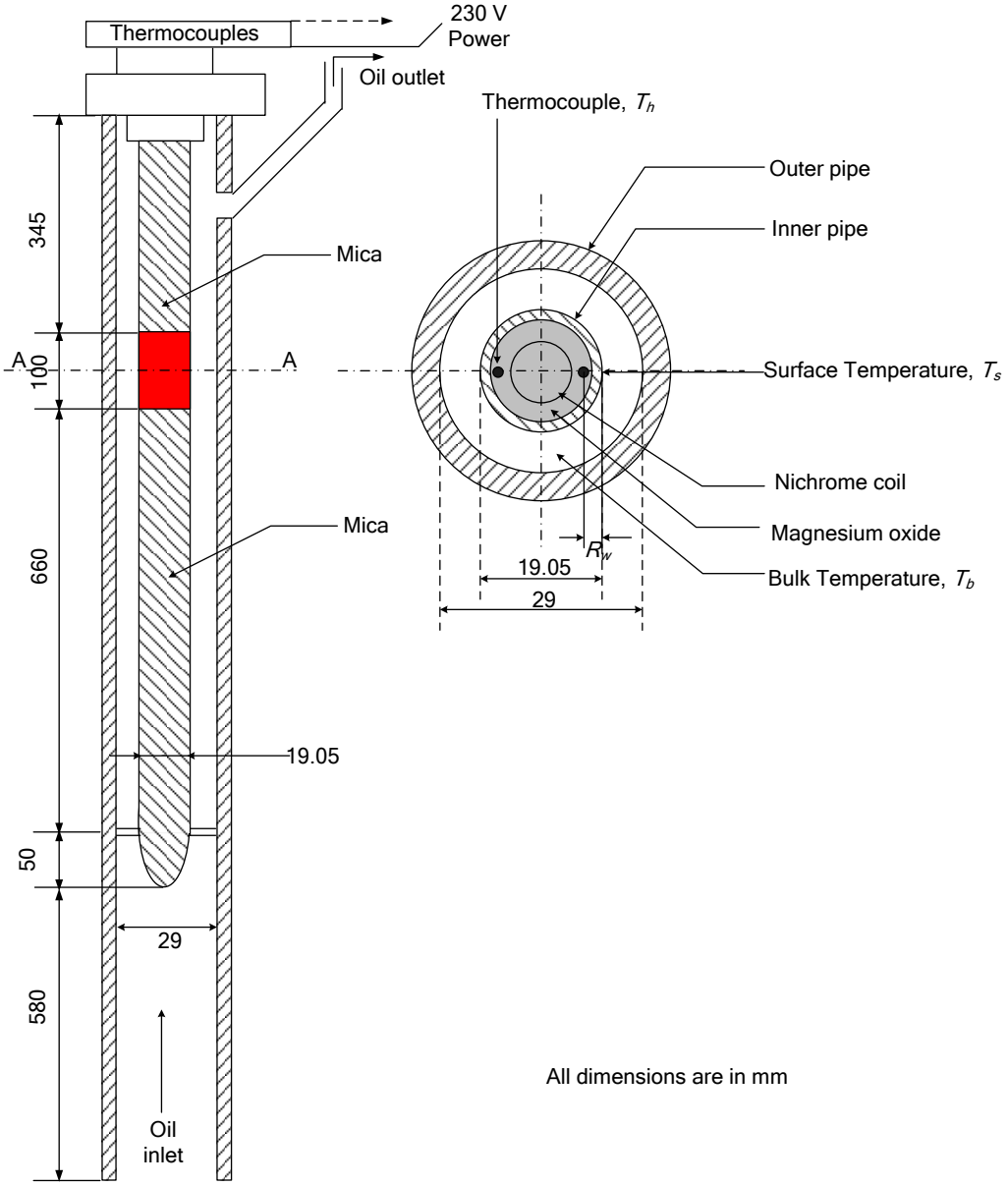

Fig.3.2: Schematic diagram of fouling probe with annular flow geometry. (a) cross sectional view in the axial direction and (b) cross sectional view across A-A

3.2.4 Double pipe heat exchanger

Since the flow loop is a closed system, heat added at the test sections must be removed to maintain the bulk temperature of the crude. A double-pipe heat exchanger (E-401) with an outer pipe of 65 mm outer diameter, an inner pipe of 49 mm outer diameter and a length of 1200 mm is provided in the flow loop after the

test sections. The hot crude oil leaving the test sections is cooled to a temperature of approximately 1^{o}C less than the desired bulk temperature using cooling water. The crude after cooling returns to the feed tank.

3.2.5 Instrumentation

The flow loop is fully equipped with necessary instruments to measure flow rates, temperatures, pressures and differential pressures. A piping and instrumentation diagram is shown in Figure 3.3 and a list of instrumentation used in the unit is summarized in Table 3.3.

Table 3.3: Instrumentation in AFFRU

Tag no	Instrument type and location	Range	Unit	Accuracy
FT-301	Colioris flowmeter	0-150	LPM	±0.15% of flow rate
FT-302	DP flow transmitter for column K-200	0-40	LPM	± 0.04%
FT-303	DP flow transmitter for column K-201	0-60	LPM	± 0.04%
TT-100	Pt100 RTD for temperature in the feed tank	0-350	^{o}C	±1.45^{o}C
TT 102	Pt100 RTD for the outlet bulk temperature for column K-200	0-350	^{o}C	±1.45^{o}C
TT 103	Pt100 RTD for the outlet bulk temperature for column K-201	0-350	^{o}C	±1.45^{o}C
TT 104, 105	*K*-type thermocouples embedded in the cartridge heater in column K-200	0-1000	^{o}C	±0.1% full scale
TT 106, 107	*K*-type thermocouples embedded in the cartridge heater in column K-201	0-1000	^{o}C	±0.1% full scale
TT 108	Pt100 RTD for bulk temperature after cooling	0-350	^{o}C	±1.45^{o}C
TT 109	Pt100 RTD for temperature in cooling water tank	0-100	^{o}C	±0.8^{o}C

Tag no	Instrument type and location	Range	Unit	Accuracy
PT 200	Pressure transmitter in the feed tank	0-60	bar	±0.50% best fit straight line
PT 201	Pressure transmitter at the inlet line of the test sections	0-60	bar	±0.50% best fit straight line
PT 202	Pressure transmitter in the outlet of column K-200	0-60	bar	±0.50% best fit straight line
PT 203	Pressure transmitter in the outlet of column K-201	0-60	bar	±0.50% best fit straight line

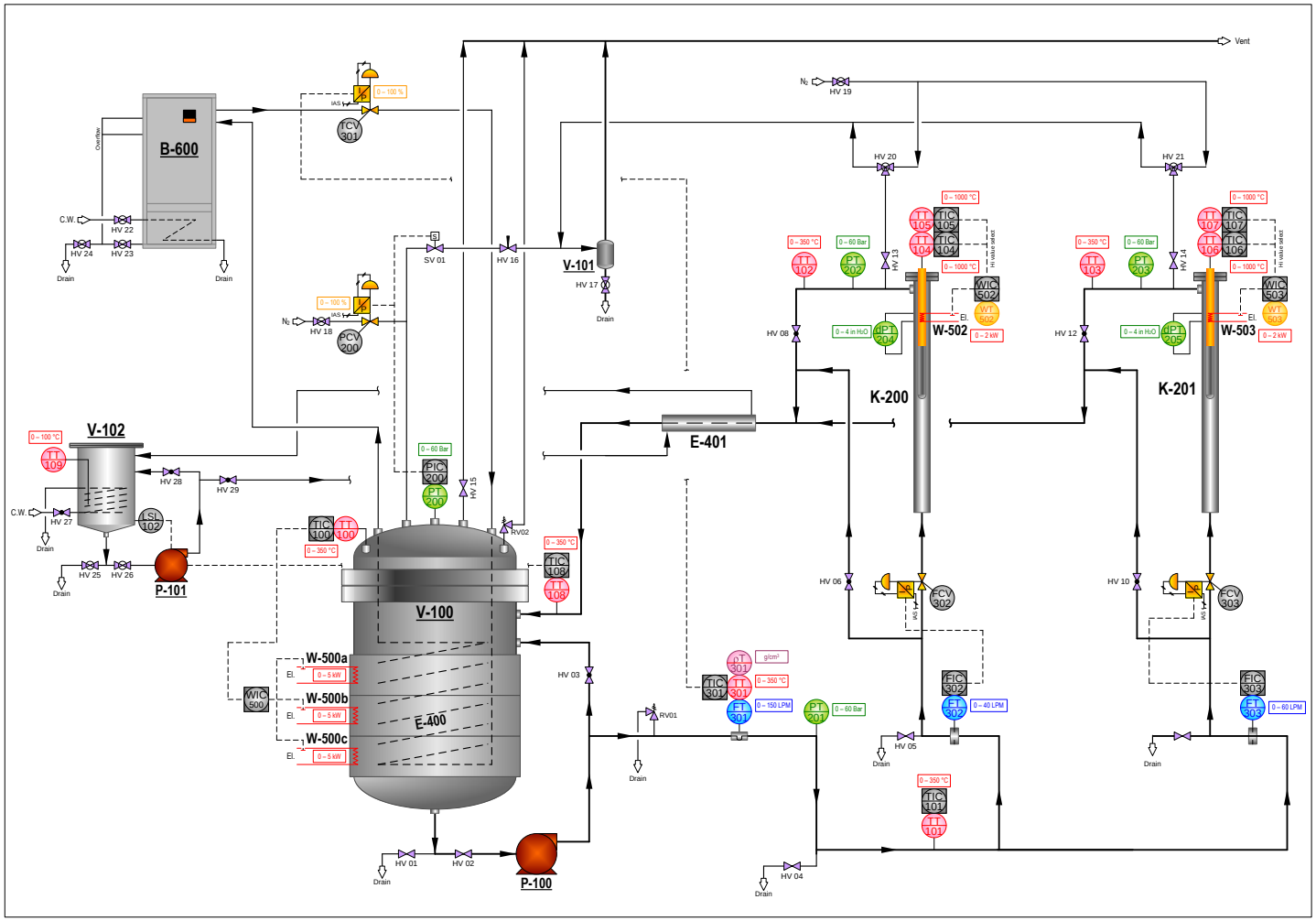

Fig.3.3: Piping and Instrumentation diagram of AFFRU

3.2.6 Data Acquisition and Control System

National Instrument LabVIEW version 8.6 data logging software is programmed to acquire, store and trend all the measurements in the system. The data can be acquired at intervals of one second or higher. The data recorded can be exported to Microsoft Excel or Matlab for further data analysis.

The experimental unit is provided with conventional feedback control systems with digital PID controllers. The pressure inside the feed tank and the rest of the flow loop is controlled using a split range control system (PCV 200). When the pressure exceeds the set-point, the vent valve (SV 01) is operated and when the pressure is below the set-point, the control valve (PCV 200) on the high pressure N_2 gas line is used.

The mass flow rate of the crude oil entering into the fouling test sections is measured by a Micro Motion® F100 colioris flowmeter (FT 301). The mass flowmeter also measures the temperature and the density of the crude oil. The custom-made mass flowmeter operates at the temperature range of -40 to 350^{o}C and a pressure rating of 100 bar. The flowmeter consists of Micro Motion® Model 1700 analog transmitter along with a sensor and a core processor. The sensor provides measurement functions and the core processor provides memory and processing functions. It has a high speed signal processing technology embedded in electronics and delivers accuracy under the toughest conditions such as high noise and high turndown.

The bulk temperature of the crude oil as measured by the mass flowmeter is controlled by a PI controller (TCV 301) by manipulating the circulation rate of hot thermal oil from a thermostat through the coil in the feed tank. The temperature of the thermal oil is closely controlled by a digital ON/OFF controller in the thermostat. Water is used as the cooling medium when the temperature is above the set point.

The flow rate of the crude oil entering the test sections is measured through the differential pressure across the orifice plates. PID controllers (FCV 302 and FCV

303) are used to regulate the flow rates corresponding to the desired flow velocities in the test sections.

The measurement of power supplied to the cartridge heaters contain a high level of noise and is filtered using a low-pass filter with cut off frequency at 0.01 Hz. The power is controlled to maintain a constant heat flux through PI controllers (WIC 502 and WIC 503). An Ashley-Edison automatic voltage stabilizer provides power to the heaters at a constant voltage.

Two *K*-type thermocouples with an accuracy of ±0.1% full scale are embedded into each cartridge heater to measure the heater temperature, T_h. The thermocouple sensors are connected to the transmitters supplied by STATUS Instruments. The transmitters are calibrated for the temperature range of 0 to 1000^{o}C and convert the sensors temperature to a linear current signal.

The hot crude oil leaving the test sections is slightly cooled in a double pipe heat exchanger using cooling water. The flow rate of the cooling water is manipulated manually and is measured using a rotameter.

Table 3.4 summarizes the list of controllers active during the experiments along with their tuning parameters.

Table 3.4: Controllers and their tuning parameters

Controller tag no.	Tuning parameters		
	Proportional gain, K_c	Integral time constant, τ_I, min	Derivative time constant, τ_D, min
TCV 301	10.0	5.00	0
FCV 302	0.04	0.01	0
FCV 303	0.04	0.01	0
WIC 500	10.0	10.0	0
WIC 502	0.01	1.00	0
WIC 503	0.01	0.60	0

3.3 Determination of surface temperature

The heat flux across the heat transfer surface, q, is given by:

$$q = h_o \left(T_s - T_b \right) \tag{3.1}$$

where h_o is the film heat transfer coefficient at clean conditions, T_b and T_s are the bulk and surface temperatures, respectively. In order to determine the film heat transfer coefficient, measurements on heat flux, bulk and surface temperatures are required. Direct measurement of surface temperature is not possible as the presence of thermocouples on the metal surface may disturb the fluid flow. Therefore, the temperature measurements from the thermocouples embedded inside the cartridge heater are used to estimate the surface temperature. The temperatures measured by the thermocouples inside the heater are referred to as the heater temperature, T_h.

An effective heat transfer coefficient, h_{eff}, can be defined with the use of T_h by rewriting Equation (3.1) as:

$$q = h_{eff} \left(T_h - T_b \right) \tag{3.2}$$

Equation (3.2) is rearranged with the introduction of Equation (3.1) as

$$\frac{1}{h_{eff}} = \frac{\left(T_h - T_b \right)}{q} = \frac{\left(T_h - T_s \right)}{q} + \frac{\left(T_s - T_b \right)}{q} = R_w + \frac{1}{h_o} \tag{3.3}$$

where R_w is the thermal wall resistance between the thermocouple location and the heater metal surface.

Since, the heat transfer coefficient, h_o, is a function of flow velocity, Equation (3.3) is rewritten as:

$$\frac{1}{h_{eff}} = R_w + \frac{C}{v^n} \tag{3.4}$$

where C is a constant and the value of n is generally taken as 0.8. The wall resistance, R_w, is usually unknown and needs to be determined through calibration experiments. For the determination of R_w, experiments were performed with non-

fouling heat transfer oil at fixed bulk and heater temperatures. The heat flux was adjusted to obtain the desired heater temperature for different fluid velocities and the corresponding heat flux values were noted. The effective heat transfer coefficient, h_{eff}, was estimated at different velocities and the reciprocal of effective heat transfer coefficient was plotted against $v^{-0.8}$ which resulted in a straight line. The intercept of the straight line is equal to R_w. Typical Wilson plot ($1/h_{eff}$ vs. $v^{-0.8}$) for HEFP1 is shown in Figure 3.4.

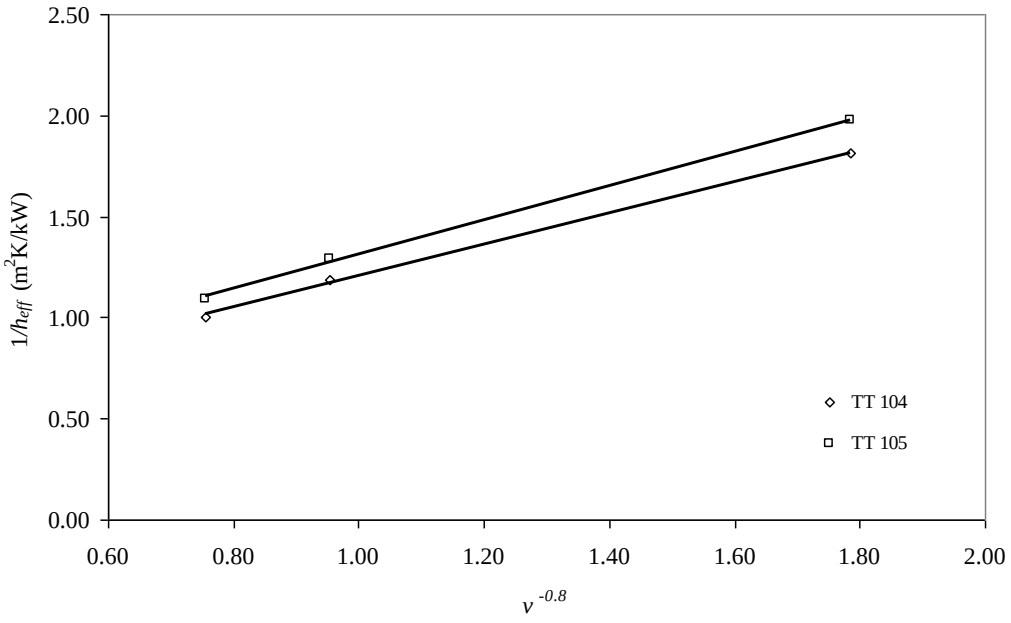

Fig. 3.4: Typical Wilson plot ($1/h_{eff}$ vs. $v^{-0.8}$) for HEFP1 with thermocouples TT104 and TT105

It was observed that the wall resistance, R_w, changed with the heater temperature, T_h. Calibration experiments were carried out following the same procedure as explained above at different heater temperatures and the corresponding wall resistances were obtained. The wall resistances were plotted against the heater temperatures as shown in Figure 3.5.

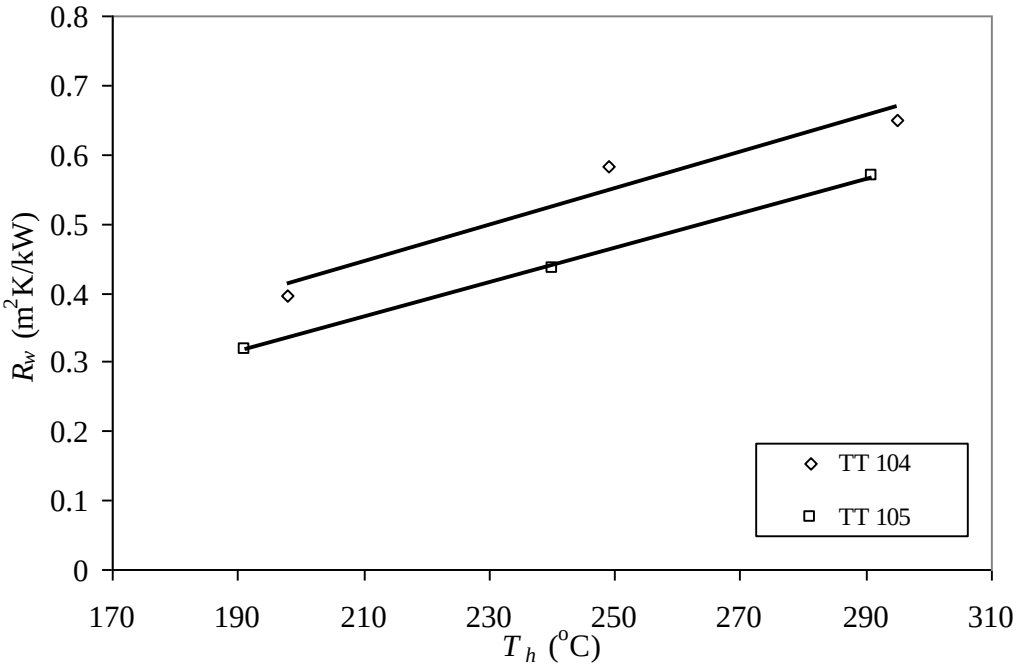

Fig. 3.5: The thermal wall resistance vs. the heater temperature for the two thermocouples in HEFP 1

It was observed from Figure 3.5 that the wall resistance changed linearly with the heater temperatures in the region of experiments carried out. Hence, a linear relationship was established for the given range of operating conditions, which is expressed as:

$$R_w = a + bT_h \tag{3.5}$$

where a and b are constants. The values of these constants for thermocouples embedded in the two probes HEFP 1 and HEFP 2 are tabulated in Table 3.5.

Table 3.5: Values of constants a and b for thermocouples embedded in the fouling probes

Fouling probe	Thermocouples	a	b
HEFP 1	TT 104	-0.1755	0.0026
	TT 105	-0.2465	0.003
HEFP 2	TT 106	-0.16	0.0025
	TT 107	-0.1132	0.0026

Noting that

$$q = \frac{T_h - T_s}{R_w}$$

the surface temperature, T_s, is calculated as:

$$T_s = T_h - R_w \times q \quad (3.6)$$

3.4 Crude oils and their properties

In this section, the test crude oil collection, storage and preparation before the experiments and their properties are discussed in detail and presented.

3.4.1 Crude collection, storage and preparation

The Malaysian crude oils used for the present study were collected directly from the ships using a sampler. The sampler draws crude oil from three different levels such as top, middle and bottom (TMB) to maintain the homogeneity of the crude oil. The crude oil samples were collected and stored in a 25 liter teflon coated drums to avoid the formation of corrosion products. The crude oil in the containers is well mixed by rolling the containers several times before the oil is charged into the reservoir.

3.4.2 Properties of crude oils

The crude oils used in this study are referred to as Crude oils A, B, C and D and their assay are summarized in Table 3.6.

Table 3.6: Assay of Malaysian crude oils used in this study

Properties	Units	Crude oils			
		A	B	C	D
Density @ 15^{o}C	kg/m^{3}	840.0	813.0	879.0	815.0
Viscosity @ 40^{o}C	cSt	1.97	2.58	4.6	2.56
Thermal conductivity @ 15^{o}C	W/m·K	1.4×10^{-1}	1.3×10^{-1}	1.5×10^{-1}	1.4×10^{-1}
Specific heat @ 15^{o}C	kJ/kg·K	1.80	1.99	1.76	1.96
Asphaltene content	wt%	0.168	0.039	0.055	0.038
API gravity	----	27.9	39.97	24.9	35.5
Basic Sediment & water	vol%	0.025	0.70	0.05	0.10
Total sulfur	wt%	0.048	0.027	0.056	0.019
Elemental compositions					
Fe	ppm	< 0.01	0.32	0.22	0.25
K	ppm	0.33	0.16	0.29	0.22
Mg	ppm	0.01	0.09	0.05	0.07
Na	ppm	0.51	0.68	0.44	0.39
Pb	ppm	< 0.01	0.76	0.66	0.47
V	ppm	0.07	2.01	5.35	15.07
Si	ppm	0.25	85.55	94.04	37.12
Al	ppm	< 0.01	0.85	0.32	0
Pour point	^{o}C	+3	+12	-12	-6
Total acid number	mg KOH/g	0.24	0.16	0.21	0.19

The physical properties such as density (ρ), dynamic viscosity (μ), thermal conductivity (k) and specific heat (C_p) for the crude oils in the temperature range of

0 to 470°C at a pressure of 50 bar were evaluated using the property package in PETROSIM simulation software. Expressions for the physical properties as functions of temperature were obtained as:

$$\rho = a_1 T + b_1 \text{ kg/m}^3 \tag{3.7}$$

$$\mu = a_2 T^{b_2} \text{ Pa.s} \tag{3.8}$$

$$k = a_3 T + b_3 \text{ W/m.K} \tag{3.9}$$

$$C_p = a_4 T + b_4 \text{ kJ/kg.K} \tag{3.10}$$

where a_i and b_i are constants which are summarized in Table 3.7.

Table 3.7: Values of constants for the crude oils

Constants	Crude oils			
	A	B	C	D
a_1	-1.14	-1.03	-1.08	-1.16
b_1	1216.2	1121.1	1216.6	1180.2
a_2	1×10^7	2×10^6	2×10^8	7×10^6
b_2	-3.999	-3.698	-4.383	-3.973
a_3	-0.0003	-0.0004	-0.0003	-0.0003
b_3	0.2468	0.2452	0.2469	0.2393
a_4	0.0039	0.0037	0.0038	0.0039
b_4	0.6924	0.9517	0.7241	0.855

The true boiling point (TBP) curves of the crude oils are shown in Figure 3.6. It may be noted that the true boiling temperature at 50% cumulative volume is between 225 and 260°C.

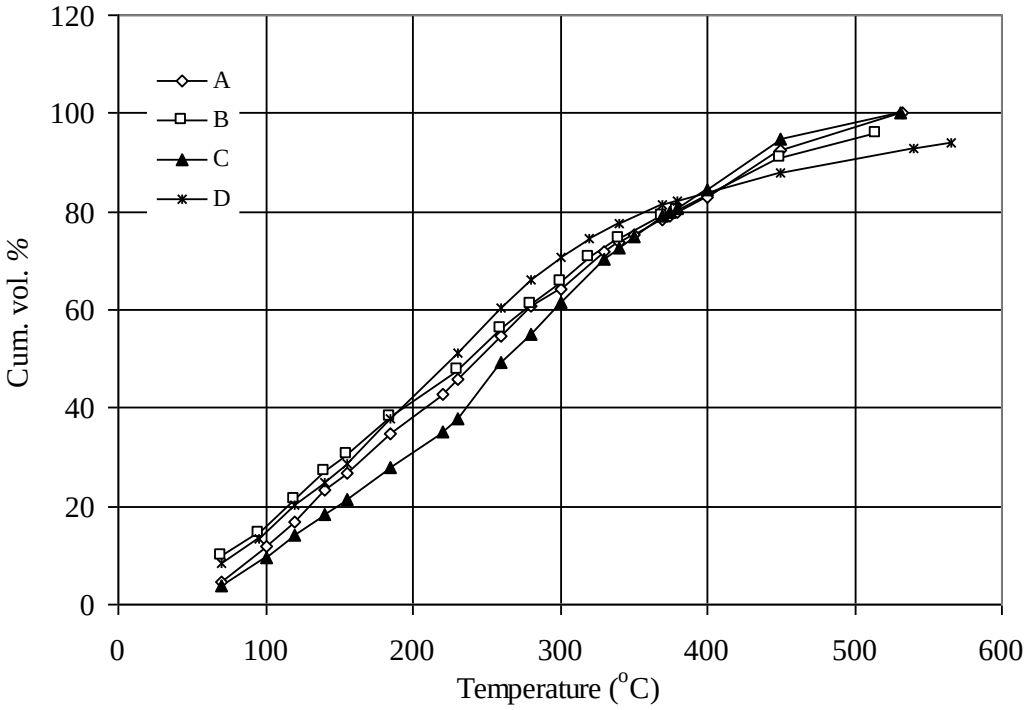

Fig. 3.6: True boiling point curves for the crude oils

3.5 Determination of maximum heat flux under the forced convective heat transfer regime

Forced convective heat transfer, generally prevails in the heat exchangers of the crude preheat train. It is, therefore, necessary that the heat transfer in the laboratory unit must also be in the same regime to understand the fouling in the crude preheat exchangers. At higher heat fluxes, there is a possibility of boiling with much higher heat transfer coefficients. It is necessary to identify the maximum heat flux, q_{max}, below which the forced convective heat transfer regime prevails.

In view of this, experiments to determine the boiling curve for the given crude oil at the desired operating conditions such as velocity and the bulk temperature need to be carried out. From the results of this experiment, the maximum heat flux for the given operating conditions and crude can be determined for the fouling experiments under forced convective heat transfer regime. The procedure is explained below.

The required volume of crude oil is charged into the feed tank, pressurized using high-pressure nitrogen gas and heated to raise the bulk temperature to the desired

value. During heating, the crude oil is pumped with the bypass valve open and the flow rate through the fouling probe is set to achieve the desired velocity. During this period, the heater in the fouling probe shall remain switched OFF. When the bulk temperature and the flow rates have been brought to the desired values, the flow is routed through the annular test sections and the cartridge heaters in the fouling probes are switched ON with low power output. The power and the heater temperatures are recorded when the values stabilize. The experiment is repeated with a small increment in the power to the heaters and the power and the corresponding heater temperatures readings are noted. With this information, R_w and T_s are calculated. The temperature difference between the surface and the bulk, (T_s-T_b), is plotted against the heat flux, q. Figure 3.7 shows a typical plot of (T_s-T_b) vs. q, for crude oil C at a bulk temperature of 120^{o}C, a velocity of 0.5 m/s and a pressure of 50 bar.

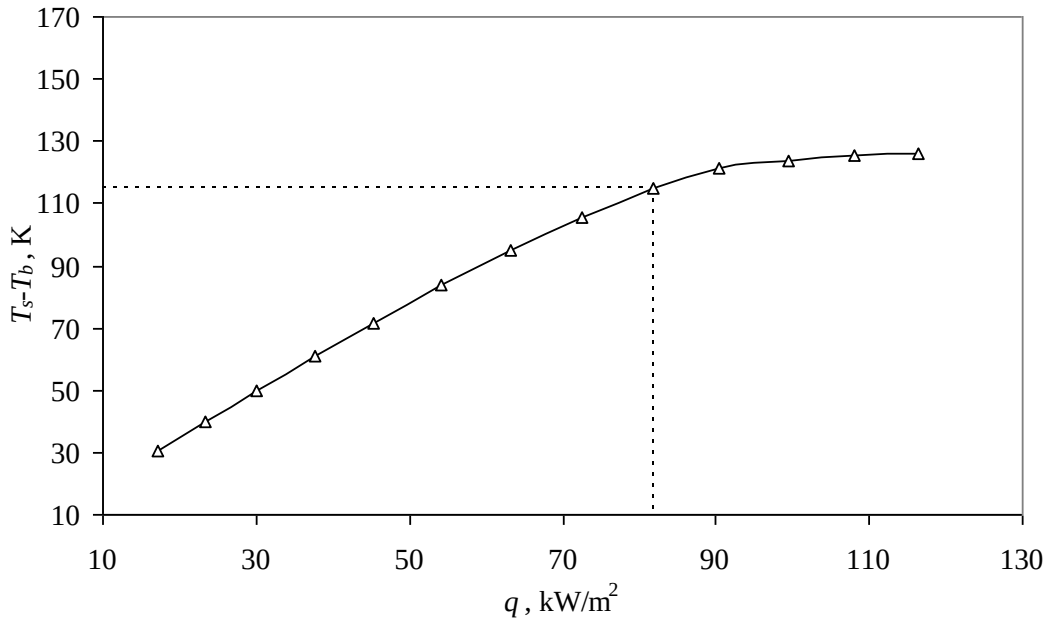

Fig. 3.7: The temperature difference, (T_s-T_b), vs. the heat flux, q, for crude oil C at T_b = 120^{o}C, v = 0.5 m/s, P = 50 bar

As the power is added gradually to the heater, the heat flux and T_s increases which results in an increase in (T_s-T_b) for a given bulk temperature. With further increase in the power, (T_s-T_b) remained fairly constant indicating the occurrence of boiling. Usually, the boiling curve is represented by plotting the heat flux, q or the heat transfer coefficient, h, vs. (T_s-T_b). Figure 3.8 shows a plot of h vs. (T_s-T_b).

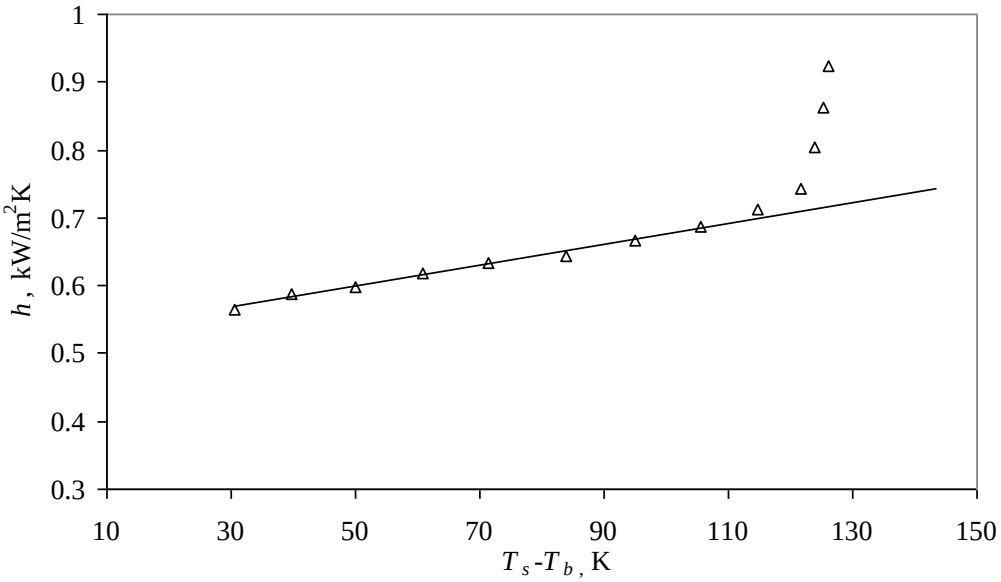

Fig. 3.8: The heat transfer coefficient, h, vs. the temperature difference (T_s-T_b) for crude oil C at T_b = 120^{o}C, v = 0.5 m/s, P = 50 bar

The plot of the heat transfer coefficient vs. the temperature difference shows the boiling curve and the different heating regimes. At lower heat fluxes, in the forced convective heat transfer regime, the heat transfer coefficient slightly increases with increasing (T_s-T_b). The increase in the power (heat flux) at a constant bulk temperature and flow velocity increases T_s and hence the film temperature, T_f, which therefore, decreases the viscosity of the crude oil. As the viscosity of the crude oil decreases, the Reynolds number increases, resulting in an increase in the heat transfer coefficient. At higher heat fluxes, the forced convective heat transfer regime changes to boiling regime and the heat transfer coefficient increases significantly with a minimal increase in (T_s-T_b). From the plot of h vs. (T_s-T_b), the maximum heat flux under the forced convective heat transfer can be obtained. In this example, a maximum temperature difference of 115^{o}C was observed for crude oil C from Figures 3.8 and 3.7 with a corresponding maximum heat flux of 82 kW/m^2. Similarly, the maximum heat fluxes under the forced convective heat transfer regime were obtained for all the crude oils at each bulk temperature and flow velocity. The corresponding plots of (T_s-T_b) vs. q and h vs. (T_s-T_b) for all the crude oils at each bulk temperature and flow velocity are discussed in Chapter 4.

3.6 Experimental procedure for determining fouling rates

Crude oil to be tested is well mixed and about 40 to 50 liters is charged into the feed tank. The feed tank and the rest of the flow loop is pressurized to about 30 – 40 bar using high pressure N_2 gas to prevent boiling of the crude oil at high temperatures. The feed pump is switched ON and the flow rate corresponding to the desired fluid velocities in the test sections are controlled by PI controllers (FCV 302 and FCV 303). The bulk temperature of the crude oil is quickly raised by heating using external band heaters in the feed tank along with the circulation of hot thermal oil through the heating coil immersed in the crude oil in the feed tank. The band heaters are turned OFF once the bulk temperature reaches nearer to the desired value. The bulk temperature is maintained at the desired value by a PI controller (TCV 301) by manipulating circulating hot thermal oil through the coil. The heater in the fouling probes are switched ON once the bulk temperature reaches 5^oC less than the desired value to prevent overshooting of the bulk temperature. Power is added gradually until the desired surface temperature is achieved. Usually, the fouling experiments are carried out by keeping either the power supplied (heat flux) to the fouling probe or the surface temperature of the fouling probe as constant. When the experiments are conducted with constant heat flux, the increase in the heater temperature with time indicates the fouling.

As the crude oil flows through the annular sections of the fouling probes, it gets heated at the heated zone. The crude oil leaving the test sections is cooled to a temperature of approximately 1^oC less than the desired bulk temperature in a double pipe heat exchanger and returned to the feed tank. During the experiment, the pressure, the crude oil flow rates and the heater power (heat flux) are maintained constant by well tuned PI controllers. The experiment is continued until either the fouling resistance value reaches a pre-set maximum value or the safe limit of the fouling probe heaters. Data is collected through the data acquisition system and stored.

At the end of each experiment, the flow loop is cooled, depressurized and the fouling probes are removed for the visual inspection and the micro-photographing. The deposit on the surface of the fouling probes is removed carefully and collected

for analytical tests. The flow loop is washed thoroughly after each experiment by flowing toluene for three hours through the flow loop at high velocities.

3.7 Experimental plan

A series of 40 experimental runs was planned to be carried out for different crude oils in the forced convective heat transfer regime ($q < q_{max}$) at bulk temperatures ranging from 80 to 120^{o}C, initial surface temperatures varying from 175 to 225^{o}C, and flow velocities from 0.4 to 0.6 m/s. The experiments were carried out at the bulk temperatures ranging from 80 to 120^{o}C, velocities from 0.4 to 0.6 m/s and surface temperatures varying from 178 to 226^{o}C. Since, the experiments were planned to be carried out under forced convective heat transfer regime, the maximum heat flux and the corresponding maximum surface temperature beyond which the heat transfer changes from forced convection to boiling were determined experimentally. All the experiments were carried out below the maximum heat flux/surface temperature conditions. It is believed that the fouling precursors are formed and deposited predominantly by chemical reaction in the range of bulk temperatures between 80 and 120^{o}C in the crude preheat train. Hence the operating bulk temperatures were selected in this range. In order to accelerate fouling and to reduce the duration of the experiments, the experiments were carried out at lower flow velocities. The summary of the operating conditions planned for the fouling runs at a pressure of 50 bar is summarized in Table 3.8.

Table 3.8: Summary of the operating conditions for the experiments

Crude oils	Run no.	Bulk temperature T_b	Flow velocity v	Initial surface temperature T_{so}
		^oC	m/s	^oC
A	1	120	0.5	198
	2	120	0.5	210
	3	120	0.5	223
B	4	80	0.4	213
	5	80	0.5	214
	6	105	0.4	214
	7	105	0.5	217
	8	120	0.4	212
	9	120	0.5	204
	10	120	0.5	216
	11	120	0.5	226
	12	120	0.6	213
C	13	80	0.4	178
	14	80	0.4	201
	15	80	0.4	223
	16	80	0.5	182
	17	80	0.5	201
	18	80	0.5	225
	19	100	0.4	181
	20	100	0.4	199
	21	100	0.4	216
	22	100	0.5	182
	23	100	0.5	200
	24	100	0.5	215
	25	120	0.4	196
	26	120	0.5	195
	27	120	0.5	216
	28	120	0.5	226

Crude oils	Run no.	Bulk temperature T_b	Flow velocity v	Initial surface temperature T_{so}
		^oC	m/s	^oC
D	29	80	0.4	191
	30	80	0.4	206
	31	80	0.4	219
	32	80	0.5	192
	33	80	0.5	204
	34	80	0.5	220
	35	100	0.4	185
	36	100	0.4	200
	37	100	0.4	215
	38	100	0.5	185
	39	100	0.5	200
	40	100	0.5	215

3.8 Estimation of initial fouling rates and induction periods

The extent of fouling on the heat transfer surface is related to the increase in surface temperature with time (or decrease in heat transfer coefficient). A continuous measurement of the heater temperatures provides the estimates of the surface temperatures with time at a constant heat flux. The estimates of surface temperature with time are used to determine the thermal fouling resistance, R_f, on the fouling probe as:

$$R_f = \left[\frac{T_s - T_b}{q}\right]_t - \left[\frac{T_s - T_b}{q}\right]_{t=0} \tag{3.11}$$

The first term in RHS of Equation (3.11) is the resistance to the heat transfer at time t or at fouled conditions while the 2nd term is the resistance to the heat transfer at $t = 0$ or at clean conditions.

Since, the thermal fouling experiments were carried out at constant heat flux conditions, the increase in the surface temperature with time indicates the occurrence

of the fouling. Surface temperature was monitored with time and the thermal fouling resistance, R_f, was calculated by Equation (3.11). The thermal fouling resistance, R_f, was plotted against time to get the thermal fouling profiles for all the experimental runs. Figures 3.9 and 3.10 show the thermal fouling resistance, R_f, vs. time profiles for crude oil A (Run 3) and crude oil C (Run 14), respectively.

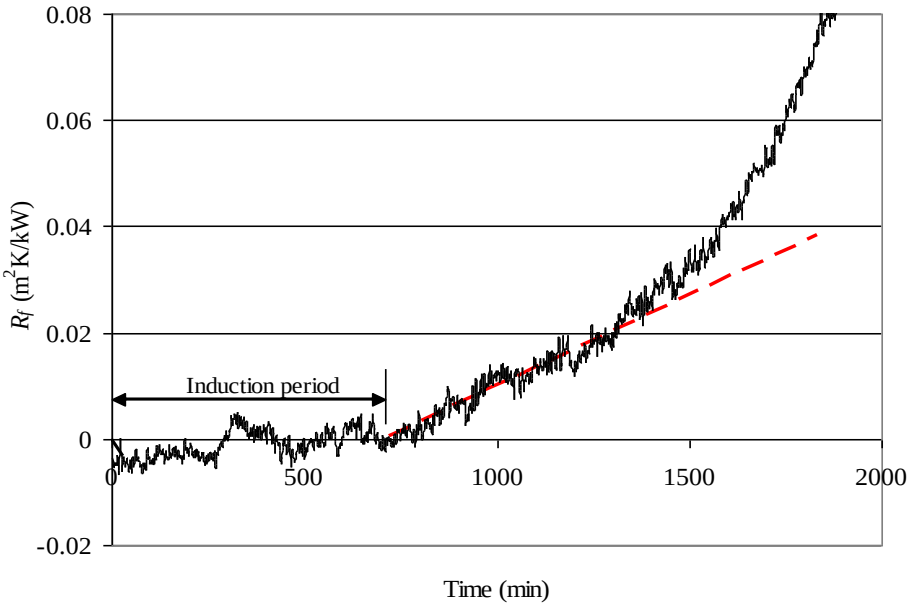

Fig.3.9: The thermal fouling resistance, R_f, vs. time for crude oil A at T_b = 120°C, v = 0.5 m/s, T_{so} = 223°C (Run 3)

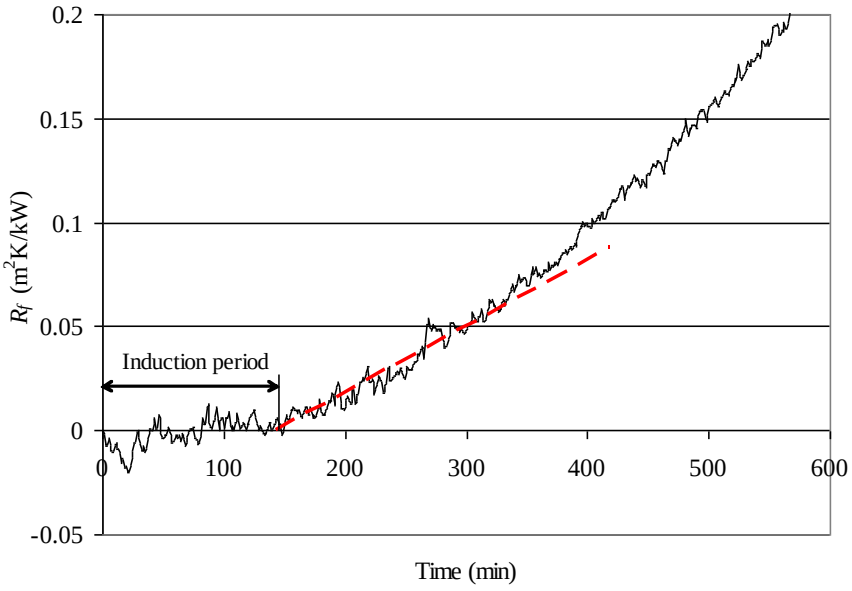

Fig.3.10: The thermal fouling resistance, R_f, vs. time for crude oil C at T_b = 80°C, v = 0.4 m/s, T_{so} = 201°C (Run 14)

Since the experimental unit is operated in a recirculation mode, the crude oil is exposed to continuous heating and cooling. This heating and cooling process results in a continuous generation of foulant precursors over time by reactions in the bulk fluid or on the heat transfer surface and changes the fluid composition. In view of this, the initial fouling rates were used for the analysis. The initial fouling rates were obtained by a fit of the linear section of the fouling resistance-time profiles after the induction period. The slope of the line gives the initial fouling rate. Figures 3.9 and 3.10 also show the estimation of the initial fouling rates and the induction periods for crude oils A and C, respectively, at different operating conditions. Induction periods of 700 and 150 minutes, where no measurable fouling was occurred were observed from R_f vs. time profiles for crude oils A (Run 3) and C (Run 14), respectively. The initial fouling rates of 0.68×10^{-5} and 15.0×10^{-5} $m^2K/kWmin$ were estimated from Figures 3.9 and 3.10, respectively, for Runs 3 and 14.

Similar procedure was followed for all the experimental runs for the estimation of the initial fouling rates and the induction periods. The analysis of the experimental results for the effects of initial surface temperature, bulk temperature and flow velocity on the initial fouling rates is discussed in detail in Chapter 5.

3.9 Summary

In this chapter, systematic procedures for (i) determination of the surface temperature, (ii) determination of maximum heat flux under the forced convective heat transfer regime, (iii) determination of fouling rates were discussed in detail. The experimental plan designed for the thermal fouling experiments was also presented in this chapter. Finally, the estimation of the initial fouling rates and the induction periods from the thermal fouling resistance, R_f, vs. time profiles were described in detail with examples.

CHAPTER 4

MAXIMUM HEAT FLUX UNDER FORCED CONVECTIVE HEAT TRANSFER REGIME

4.1 Introduction

Heat transfer in the preheat exchangers is mainly by forced convection. As the present investigation is limited to study on the fouling characteristics of crude oils in the preheat train, it is necessary to determine the maximum heat flux under the forced convective heat transfer regime for different crude oils at different operating conditions. Heat transfer experiments were carried out to determine the maximum heat flux for each crude oil and the results are discussed.

Experimental results for the estimation of the maximum heat flux under the forced convective heat transfer regime for each crude oil are described in Section 4.2. A model developed for the estimation of the maximum heat flux under the forced convective heat transfer regime for the crude oils are discussed in detail in Section 4.3.

4.2 Maximum heat flux under the forced convective heat transfer regime

The detailed experimental procedure for the determination of maximum heat flux, q_{max}, was described in Chapter 3, Section 3.5. All experiments were carried out at a pressure of 50 bar. The maximum heat fluxes were determined at different bulk temperatures and velocities for each crude oil, and the results are presented in the following sections for the crude oils individually.

4.2.1 Crude oil A

Experiments to determine the maximum heat flux for crude oil A were carried out at different bulk temperatures and flow velocities. Measurements on the heater temperature, T_h, at different heat fluxes were used to determine T_s (as explained in Section 3.5) at the respective operating conditions. The temperature differences between the surface and the bulk, (T_s-T_b), at a bulk temperature of 120^{o}C and a velocity of 0.5 m/s are shown in Figure 4.1 as a function of heat flux, q. The temperature difference, (T_s-T_b), increased with an increase in the heat flux, q, up to a limiting value of around 107^{o}C. Further increase in the heat flux resulted in minimal increase in (T_s-T_b) and remained fairly constant at much higher heat fluxes. From the experimental data, the heat transfer coefficient, h, was estimated and is shown in Figure 4.2 as a function of (T_s-T_b). It can be seen that the heat transfer coefficient increases drastically for the temperature differences beyond 107^{o}C which corresponds to a heat flux of 91 kW/m^2. This increase in heat transfer coefficient is associated with the change in heat transfer regime from forced convection to boiling. To study fouling in the forced convective heat transfer regime for crude oil A, the operating heat flux should be less than or equal to 91 kW/m^2.

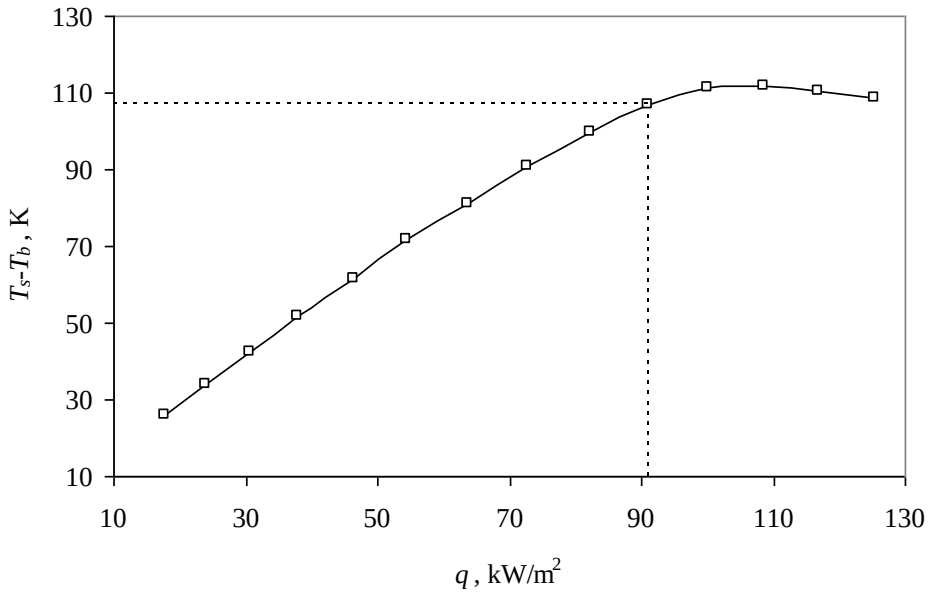

Fig. 4.1: The temperature difference, (T_s-T_b), vs. the heat flux, q, for crude oil A at T_b = 120^{o}C, v = 0.5 m/s, P = 50 bar

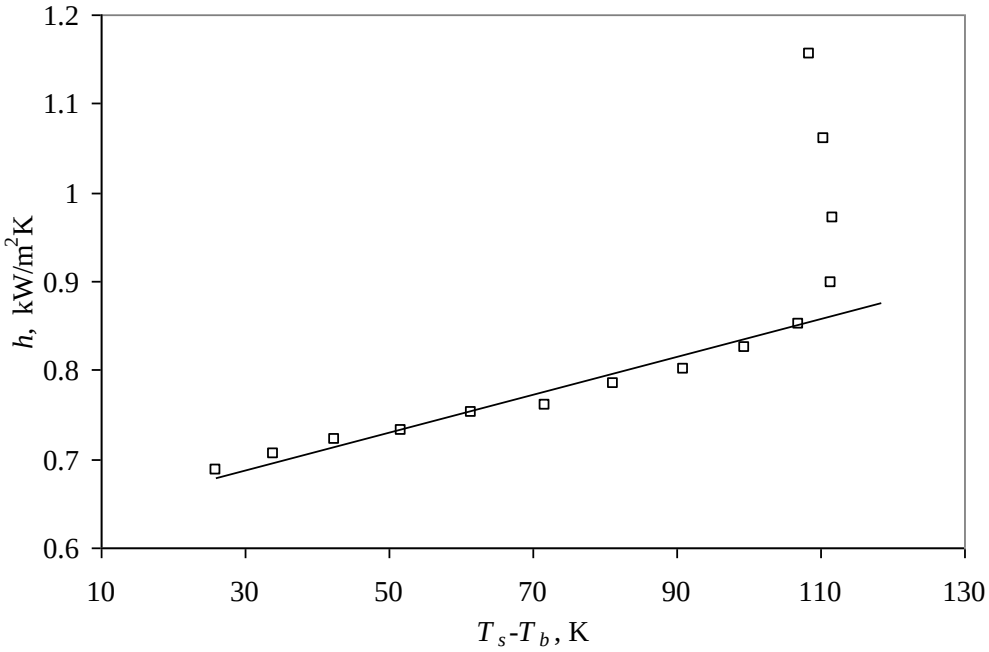

Fig. 4.2: The heat transfer coefficient, h, vs. the temperature difference, (T_s-T_b), for crude oil A at T_b = 120°C, v = 0.5 m/s, P = 50 bar

4.2.2 Crude oil B

Following the same procedure, the temperature differences, (T_s-T_b), as a function of heat flux, q, at bulk temperatures ranging from 90 to 120°C and a velocity of 0.5 m/s are shown in Figure 4.3. The increase in the heat flux resulted in an increase in (T_s-T_b) up to a limiting value of 131, 110, and 107°C for the bulk temperatures of 90, 105 and 120°C, respectively. The heat transfer coefficients were estimated at different bulk temperatures and plotted against (T_s-T_b) (Figure 4.4). The heat transfer coefficients increased significantly beyond these limiting temperature difference values. The significant increase in the heat transfer coefficient indicates the existence of the boiling regime. The maximum heat fluxes were determined to be 83, 81 and 78 kW/m^2, respectively, at bulk temperatures of 90, 105 and 120°C.

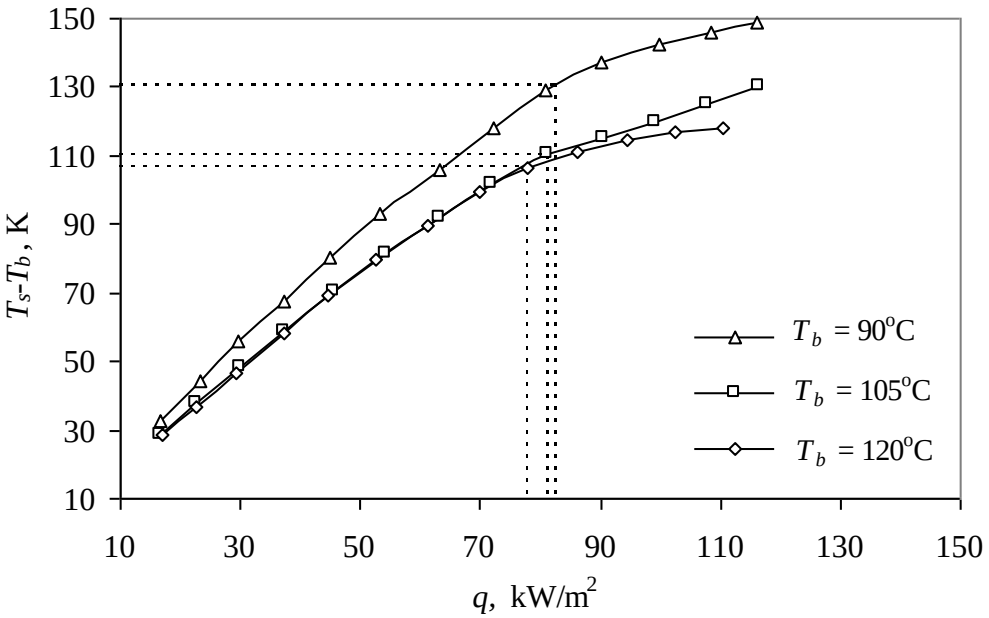

Fig. 4.3: The temperature difference, (T_s-T_b), vs. the heat flux, q, for crude oil B at v = 0.5 m/s, P = 50 bar for various bulk temperatures

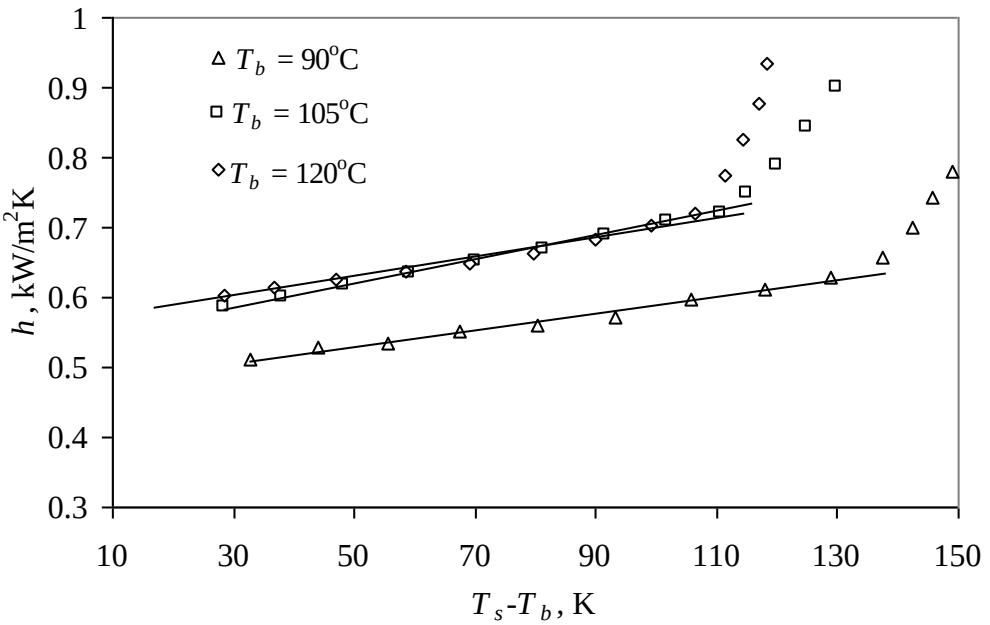

Fig. 4.4: The heat transfer coefficient, h, vs. the temperature difference, (T_s-T_b), for crude oil B at v = 0.5 m/s, P = 50 bar for various bulk temperatures

Figures 4.5 and 4.6 show (T_s-T_b) vs. q and h vs. (T_s-T_b), respectively, at a flow velocity of 0.4 m/s and different bulk temperatures. At lower temperature differences

and up to the temperature differences of 132 and 117°C for the bulk temperatures of 90 and 105°C, respectively, a slight increase in heat transfer coefficient was observed (Figure 4.6) with an increase in (T_s-T_b). Further increase in heat flux resulted in drastic increase in heat transfer coefficient. This drastic increase in the heat transfer coefficient shows the changes in the forced convective heat transfer regime to the boiling. The maximum heat fluxes were determined from Figure 4.5 for the corresponding temperature differences.

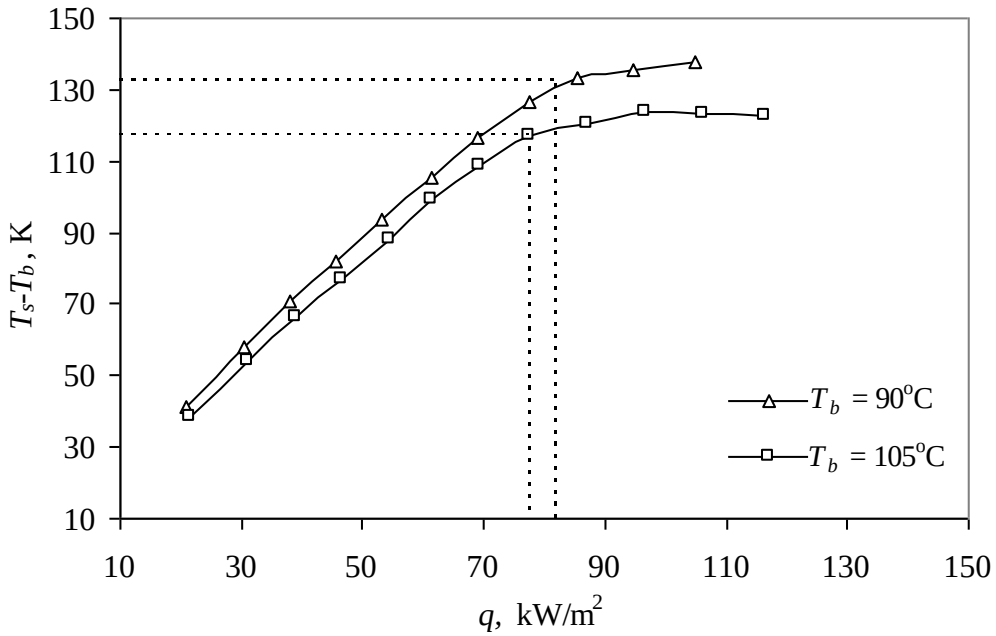

Fig. 4.5: The temperature difference, (T_s-T_b), vs. the heat flux, q, for crude oil B at v = 0.4 m/s, P = 50 bar, bulk temperatures of 90 and 105°C

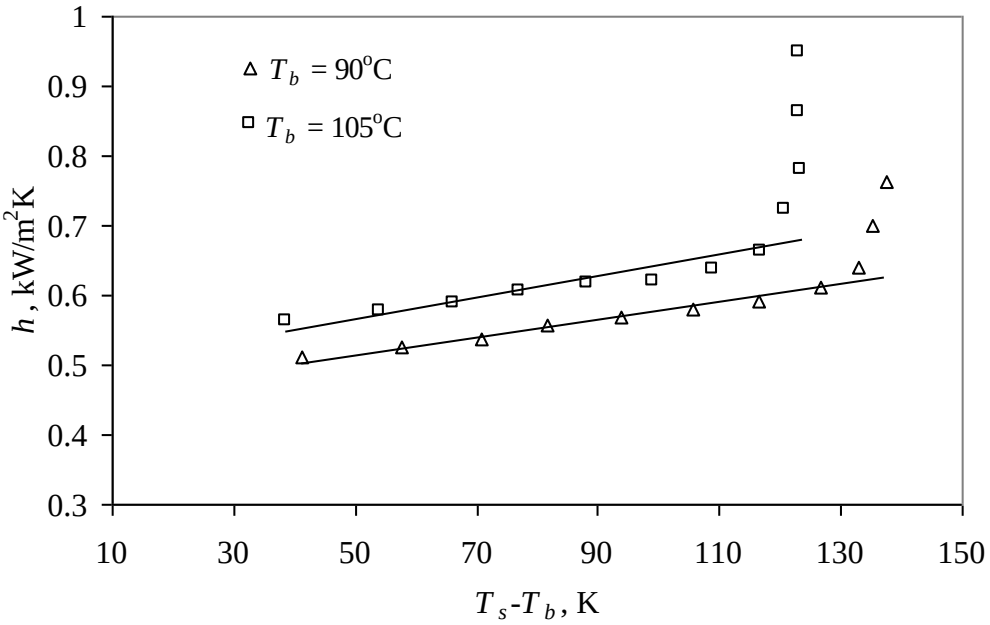

Fig. 4.6: The heat transfer coefficient, h, vs. the temperature difference, (T_s-T_b), for crude oil B at v = 0.4 m/s, P = 50 bar, bulk temperatures of 90 and 105^{o}C

4.2.3 Crude oil C

Experiments were carried out using crude oil C at bulk temperatures ranging from 80 to 120^{o}C and a velocity of 0.5 m/s. The temperature differences as a function of heat fluxes are shown in Figure 4.7. The heat transfer coefficient was estimated and plotted against (T_s-T_b) as shown in Figure 4.8. There was a significant increase in the heat transfer coefficient at temperature differences beyond 155, 135 and 115^{o}C for the bulk temperatures of 80, 100 and 120^{o}C, respectively. The maximum heat fluxes were determined at different bulk temperatures.

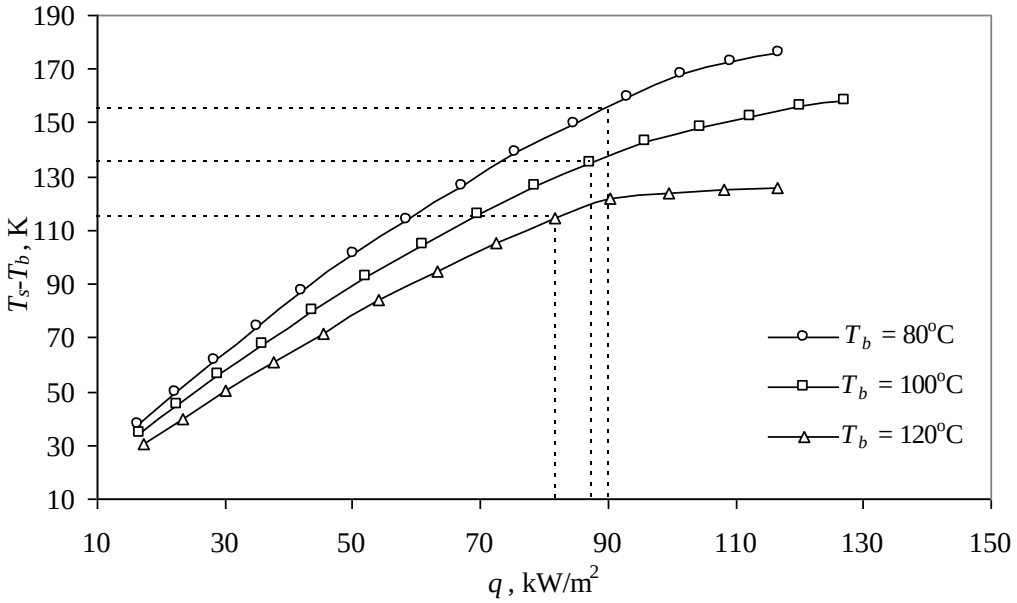

Fig. 4.7: The temperature difference, (T_s-T_b), vs. the heat flux, q, for crude oil C at v = 0.5 m/s, P = 50 bar for various bulk temperatures

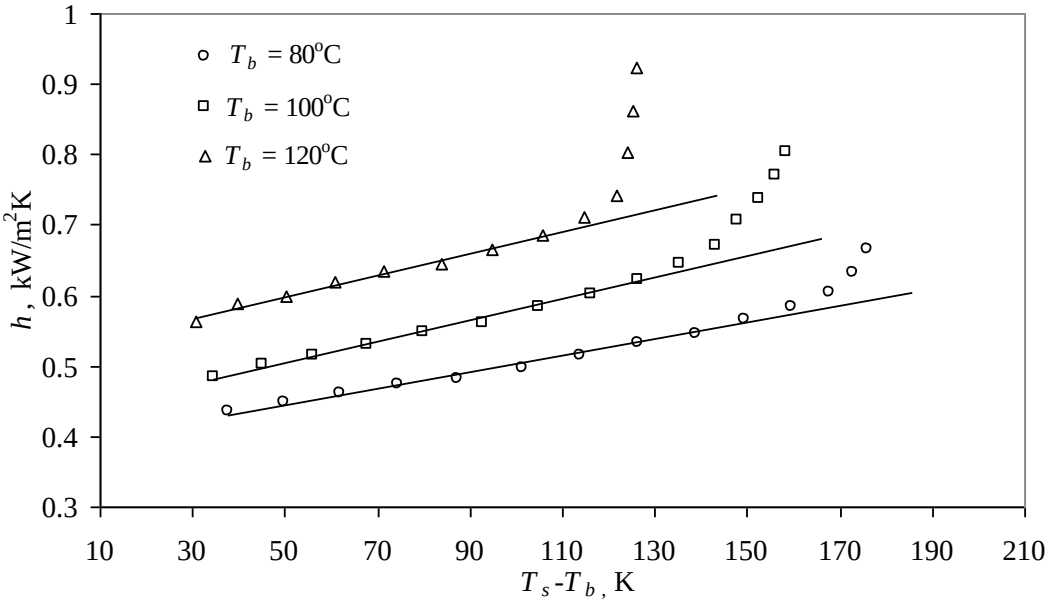

Fig. 4.8: The heat transfer coefficient, h, vs. the temperature difference, (T_s-T_b), for crude oil C at v = 0.5 m/s, P = 50 bar for various bulk temperatures

Similarly, Figures 4.9 and 4.10 show (T_s-T_b) vs. q and h vs. (T_s-T_b), respectively, for crude oil C at a velocity of 0.4 m/s and bulk temperatures of 80 and 100°C. The maximum temperature differences, 158 and 140°C for bulk temperatures of 80 and

100°C, respectively, were determined from Figure 4.10 and the corresponding maximum heat fluxes were determined from Figure 4.9.

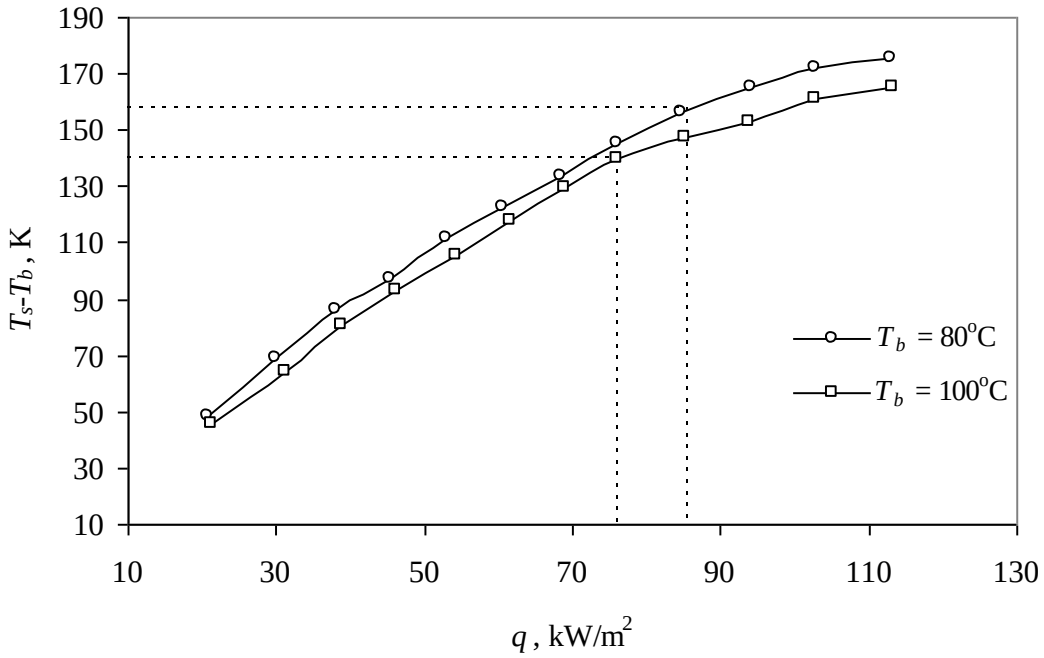

Fig. 4.9: The temperature difference, (T_s-T_b), vs. the heat flux, q, for crude oil C at v = 0.4 m/s, P = 50 bar, bulk temperatures of 80 and 100°C

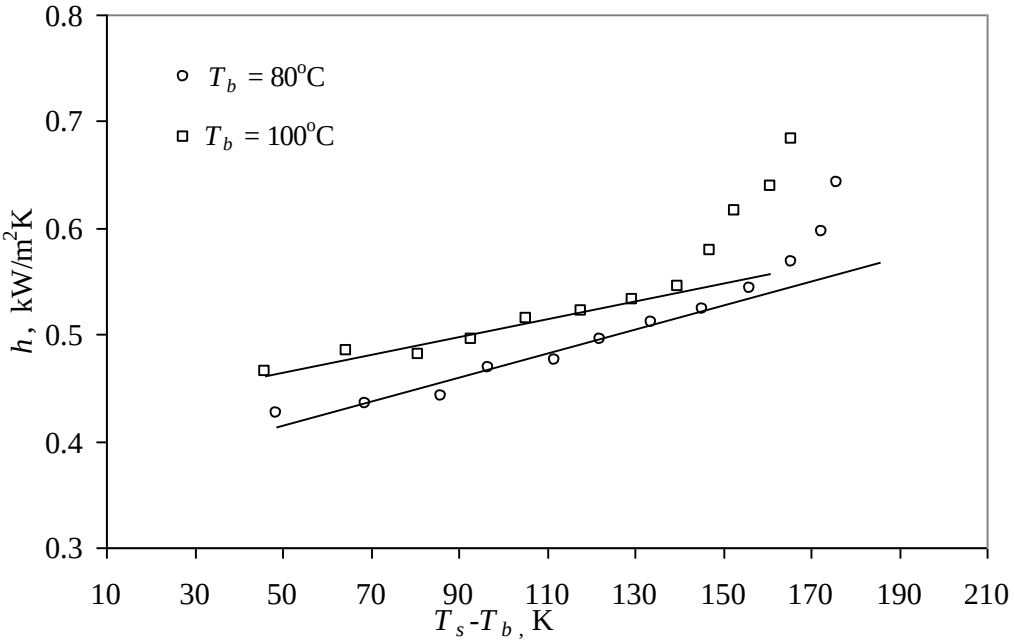

Fig. 4.10: The heat transfer coefficient, h, vs. the temperature difference, (T_s-T_b), for crude oil C at v = 0.4 m/s, P = 50 bar, bulk temperatures of 80 and 100°C

4.2.4 Crude oil D

Experiments were carried out using crude oil D at two bulk temperatures (80 and 100°C), a velocity of 0.5 m/s to determine the maximum heat flux. Figures 4.11 and 4.12 show (T_s-T_b) vs. q and h vs. (T_s-T_b), respectively. The drastic increase in the heat transfer coefficient was observed beyond the temperature differences of 141 and 122°C for the bulk temperatures of 80 and 100°C, respectively. The maximum heat fluxes were determined for these temperature differences from Figure 4.11.

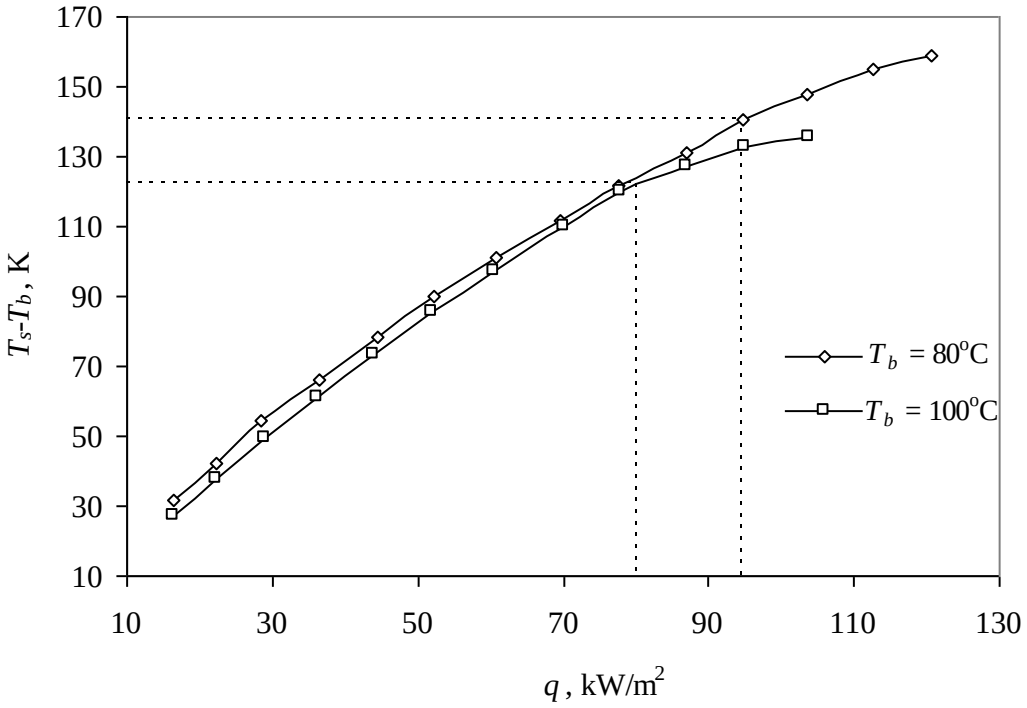

Fig. 4.11: The temperature difference, (T_s-T_b), vs. the heat flux, q, for crude oil D at v = 0.5 m/s, P = 50 bar, bulk temperatures of 80 and 100°C

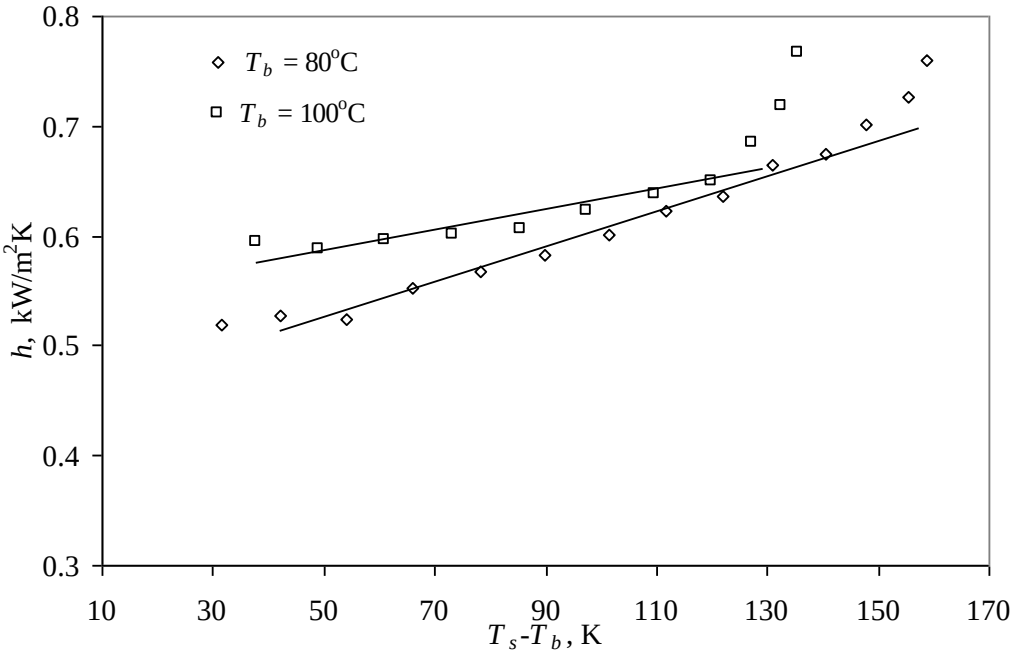

Fig. 4.12: The heat transfer coefficient, h, vs. the temperature difference, (T_s-T_b), for crude oil D at v = 0.5 m/s, P = 50 bar, bulk temperatures of 80 and 100^{o}C

Experiments were also carried out at a velocity of 0.4 m/s and the corresponding plots of (T_s-T_b) vs. q and h vs. (T_s-T_b) are shown in Figures 4.13 and 4.14, respectively. The maximum heat fluxes were determined for the temperature differences beyond which the heat transfer coefficient changed significantly from these plots at bulk temperatures of 80 and 100^{o}C, and velocity of 0.4 m/s.

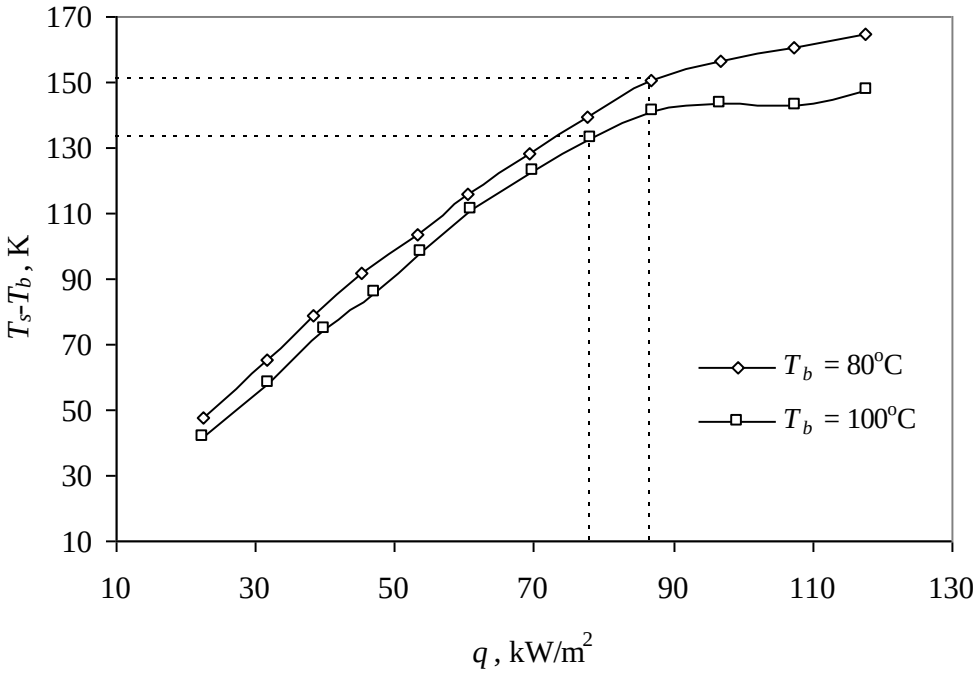

Fig. 4.13: The temperature difference, (T_s-T_b), vs. the heat flux, q, for crude oil D at v = 0.4 m/s, P = 50 bar, bulk temperatures of 80 and 100°C

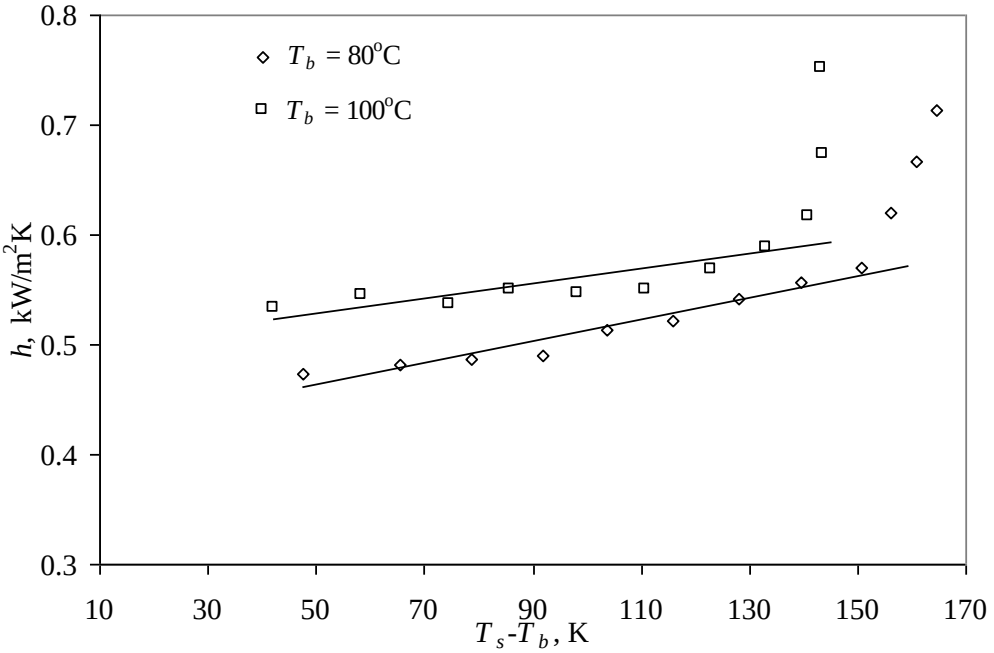

Fig. 4.14: The heat transfer coefficient, h, vs. the temperature difference, (T_s-T_b), for crude oil D at v = 0.4 m/s, P = 50 bar, bulk temperatures of 80 and 100°C

4.2.5 Discussion on the maximum heat flux for all crude oils

It was observed from (T_s-T_b) vs. q and h vs. (T_s-T_b) plots that in the forced convective heat transfer regime the increase in the heat flux resulted in the significant increase in the temperature differences and slight increase in the heat transfer coefficients. The slight increase in the heat transfer coefficient is mainly due to the fact that the viscosity of the crude oil is very sensitive to the temperature. As the temperature increases with increase in the heat flux, the viscosity decreases, resulting in an increase in the Reynolds number and, hence, increase in the heat transfer coefficient. Whereas in the boiling regime, the increase in the heat flux resulted in the minimal or no increase in (T_s-T_b) with drastic increase in the heat transfer coefficient.

The maximum temperature difference, $(T_s\text{-}T_b)_{max}$, the maximum heat flux, q_{max}, and the maximum heat transfer coefficient, h_{max}, below which the forced convective heat transfer regime prevails were determined for all the crude oils at different bulk temperatures and flow velocities as explained in the above sections and are summarized in Table 4.1.

Figure 4.15 shows $(T_s\text{-}T_b)_{max}$ vs. the bulk temperature for all the crude oils at different velocities. It was observed that higher $(T_s\text{-}T_b)_{max}$ can be achieved at lower bulk temperatures for all the crude oils at a constant flow velocity and a pressure.

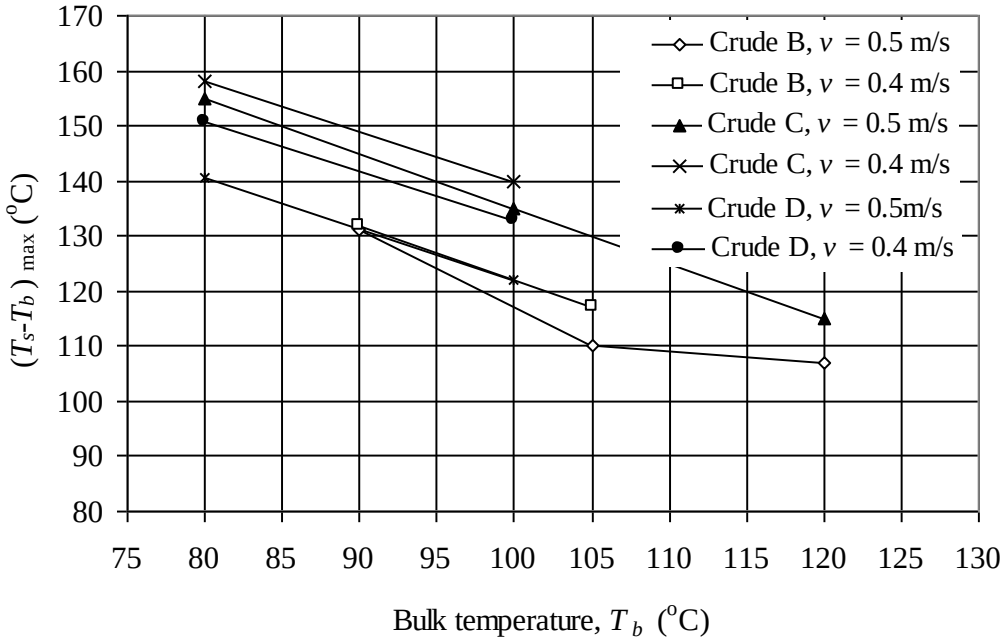

Fig. 4.15: Maximum temperature difference, $(T_s\text{-}T_b)_{max}$ vs. bulk temperature at different velocities

Figure 4.16 shows $(T_s\text{-}T_b)_{max}$ vs. the flow velocity for all the crude oils at different bulk temperatures. It was observed that higher $(T_s\text{-}T_b)_{max}$ can be achieved at lower flow velocities at a constant bulk temperature and a pressure.

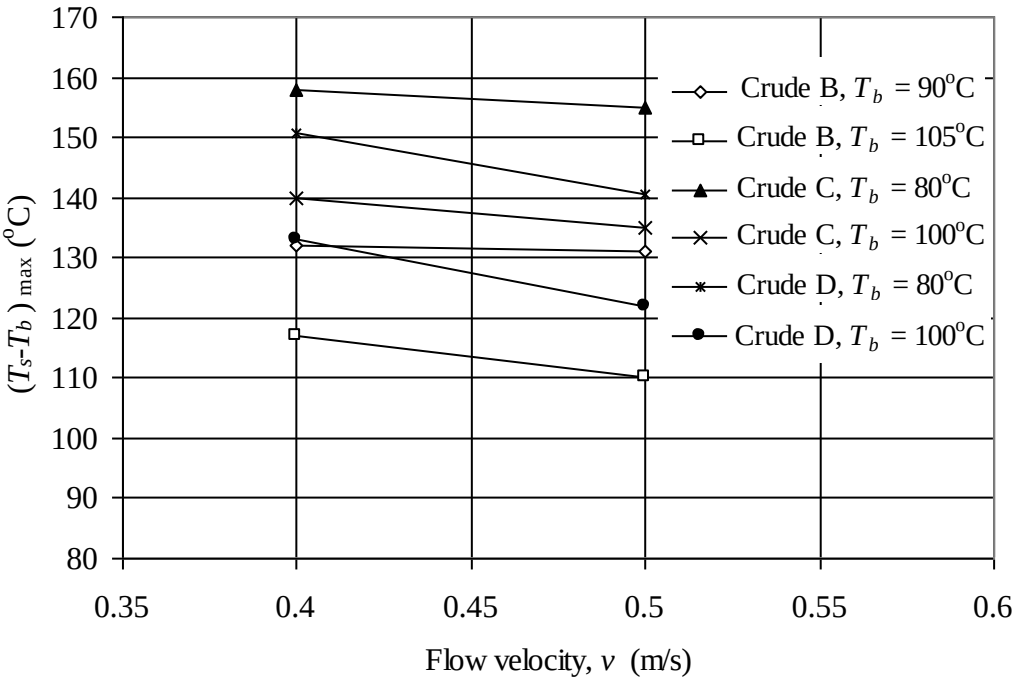

Fig. 4.16: Maximum temperature difference, $(T_s\text{-}T_b)_{max}$ vs. flow velocity

The maximum heat fluxes, q_{max}, determined for different crude oils are shown in Figure 4.17 as a function of T_b at different flow velocities. The q_{max} values decreased with an increase in the bulk temperature as seen from Figure 4.17.

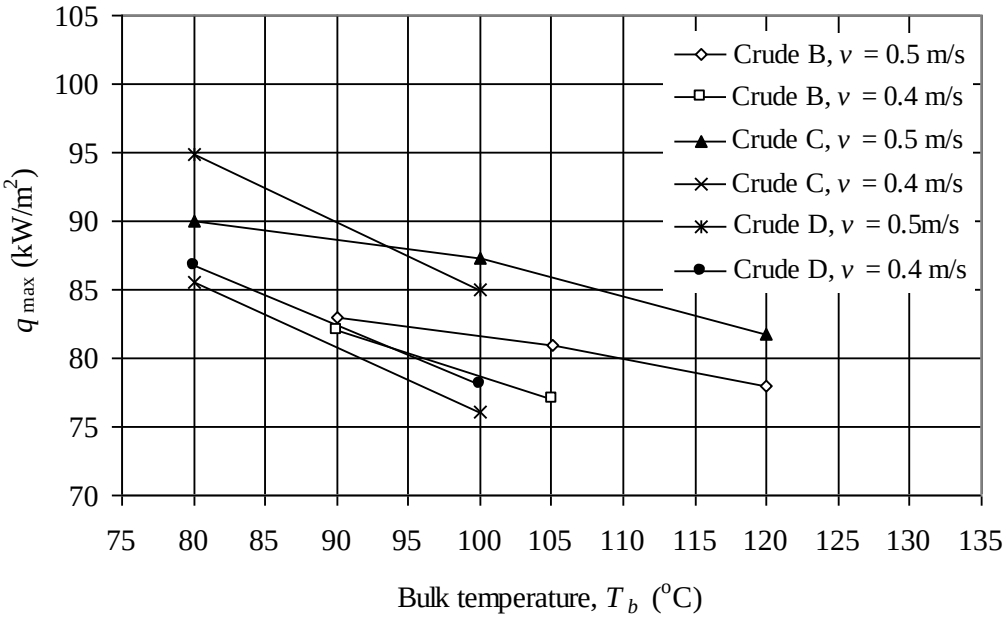

Fig. 4.17: Maximum heat flux, q_{max} vs. bulk temperature, T_b, for the crude oils at different velocities

Figure 4.18 shows q_{max} vs. flow velocity for different crude oils at different bulk temperatures. It can be seen that the q_{max} values increased with an increase in the flow velocities.

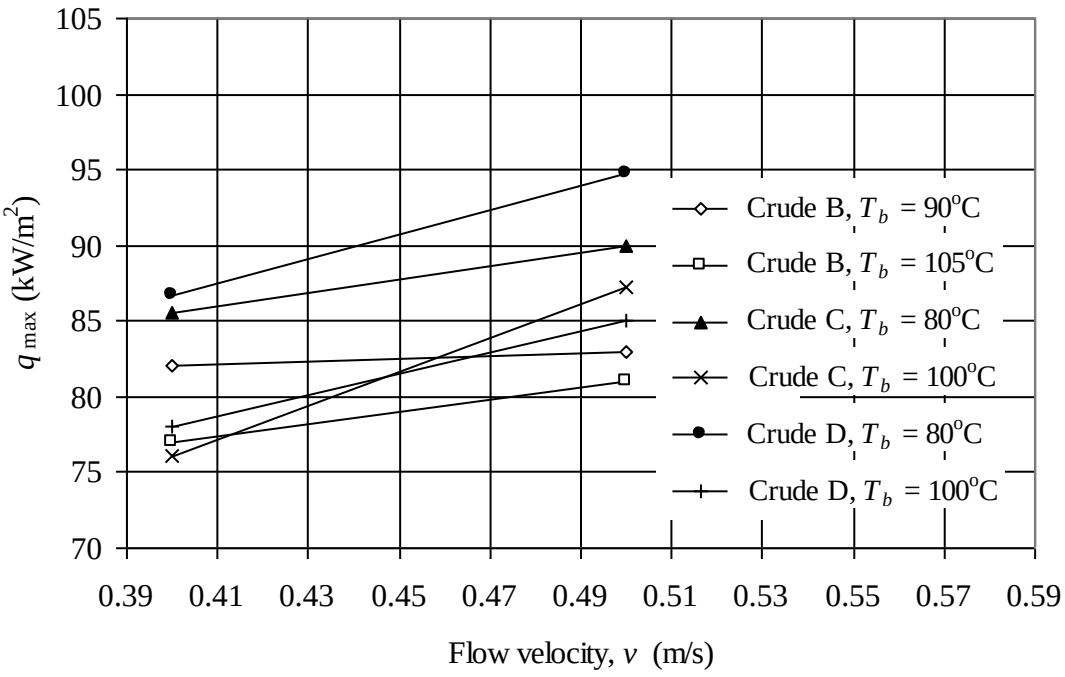

Fig. 4.18: Maximum heat flux, q_{max} vs. flow velocity, v, for the crude oils at different bulk temperatures

Figure 4.19 shows the h_{max} as a function of bulk temperature for all the crude oils at different velocities. It was observed that h_{max} values increased with an increase in the bulk temperature.

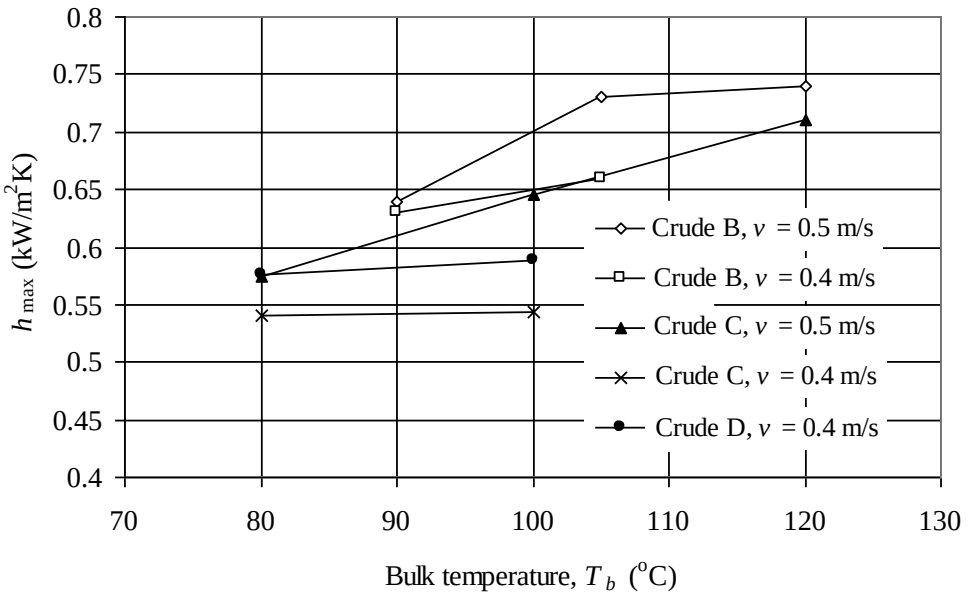

Fig. 4.19: Maximum heat transfer coefficient, h_{max} vs. bulk temperature, T_b, for the crude oils at different velocities

Figure 4.20 shows h_{max} vs. flow velocity for all the crude oils at different bulk temperatures. It was also observed that h_{max} values increased with an increase in the flow velocities.

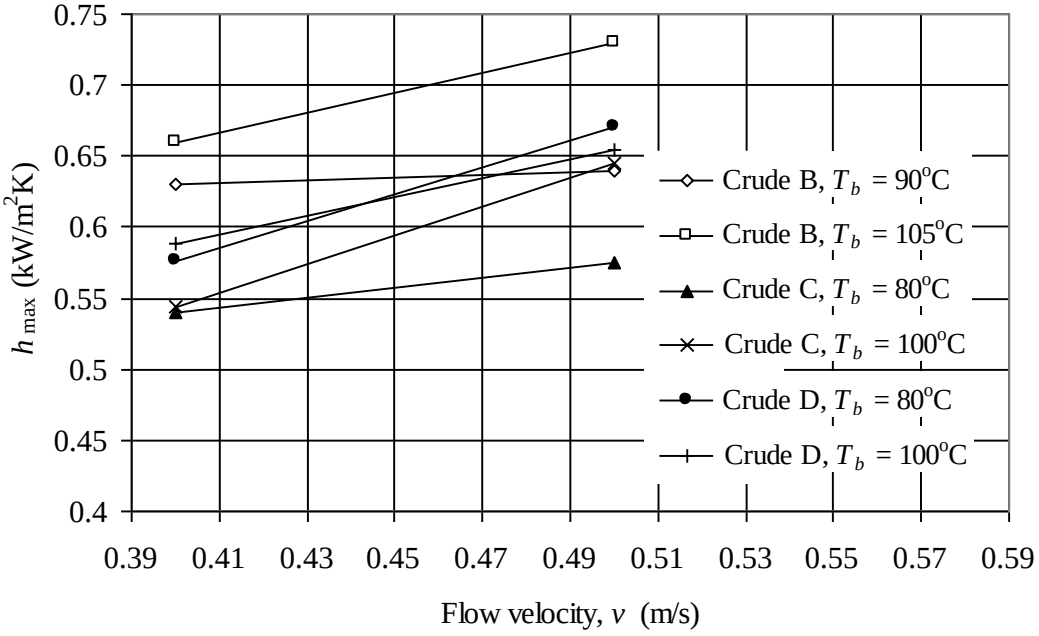

Fig. 4.20: Maximum heat transfer coefficient, h_{max} vs. flow velocity, v, for the crude oils at different bulk temperatures

Table 4.1: Maximum heat flux, heat transfer coefficients under forced convective heat transfer and physical properties of crude oils at the respective operating conditions

Crude oils	Avg. bulk temperature, T_b	Flow velocity, v	Maximum heat flux, q_{max}	Maximum heat transfer coefficient, h_{max}	Maximum temperature difference, $(T_s\text{-}T_b)_{max}$	Maximum surface temperature, $T_{s,max}$	$T_{bp0.5}$	Density, ρ	Viscosity, $\mu \times 10^4$	Reynolds number, Re $\times 10^{-3}$	Specific heat, C_p	Thermal conductivity, $k \times 10^4$	Prandtl number, Pr
	^oC	m/s	kW/m^2	kW/m^{2}K	^oC	^oC	^oC	kg/m^3	Pa.s	---	kJ/kg.K	kW/m.K	---
A	120	0.5	91	0.85	107	227	245	767.77	4.21	9.07	2.23	1.29	7.27
B	90	0.5	83	0.64	131	221	240	748.22	6.82	5.46	2.30	0.99	15.67
	105	0.5	81	0.73	110	215		732.82	5.87	6.21	2.35	0.94	14.70
	120	0.5	78	0.74	107	227		717.41	5.09	7.02	2.41	0.88	13.92
	90	0.4	82	0.63	132	222		748.22	6.82	4.37	2.30	0.99	15.67
	105	0.4	77	0.66	117	222		732.82	5.87	4.97	2.35	0.94	14.70
C	80	0.5	90	0.58	155	235	260	834.56	13.6	3.05	2.07	1.41	19.92
	100	0.5	87	0.65	135	235		812.93	10.7	3.79	2.14	1.35	16.95
	120	0.5	82	0.71	115	235		791.29	8.49	4.63	2.22	1.29	14.61
	80	0.4	86	0.54	158	238		834.56	13.6	2.44	2.07	1.41	19.92
	100	0.4	76	0.55	140	240		812.93	10.7	3.03	2.14	1.35	16.95
D	80	0.5	95	0.67	141	221	225	772.14	5.27	7.29	2.23	1.33	8.83
	100	0.5	80	0.66	122	222		749.03	4.24	8.80	2.31	1.27	7.69
	80	0.4	87	0.58	151	231		772.14	5.27	5.83	2.23	1.33	8.83
	100	0.4	78	0.59	133	233		749.03	4.24	7.04	2.31	1.27	7.69

4.3 A model for the estimation of maximum heat flux

The basic equation for the heat transfer by convection under steady state conditions is given by:

$$q = h(T_s - T_b) \tag{3.1}$$

Equation (3.1) holds good at conditions corresponding to the maximum heat flux under forced convection and can be written as:

$$q_{\max} = h_{\max}(T_{s,\max} - T_b) \tag{4.1}$$

where $T_{s,\max}$ is the maximum surface temperature beyond which the forced convective heat transfer regime changes to boiling.

Dittus – Boelter equation for the forced convective heat transfer is given by:

$$\frac{hD}{k} = 0.023\mathrm{Re}^{0.8}\,\mathrm{Pr}^{1/3} \tag{4.2}$$

Applying Equation (4.2) at the maximum heat flux conditions and rearranging yields:

$$\frac{h_{\max}D}{0.023\,k}\mathrm{Pr}^{-1/3} = \mathrm{Re}^{0.8} \tag{4.3}$$

The maximum heat transfer coefficient was estimated for different crude oils at different bulk temperatures and velocities as explained in the above sections. A plot of $(h_{\max} D\mathrm{Pr}^{-1/3})/0.023k$ vs. $\mathrm{Re}^{0.8}$ is shown in Figure 4.21. It was observed from Figure 4.21 that the experimental data matched fairly well with the Dittus – Boelter equation.

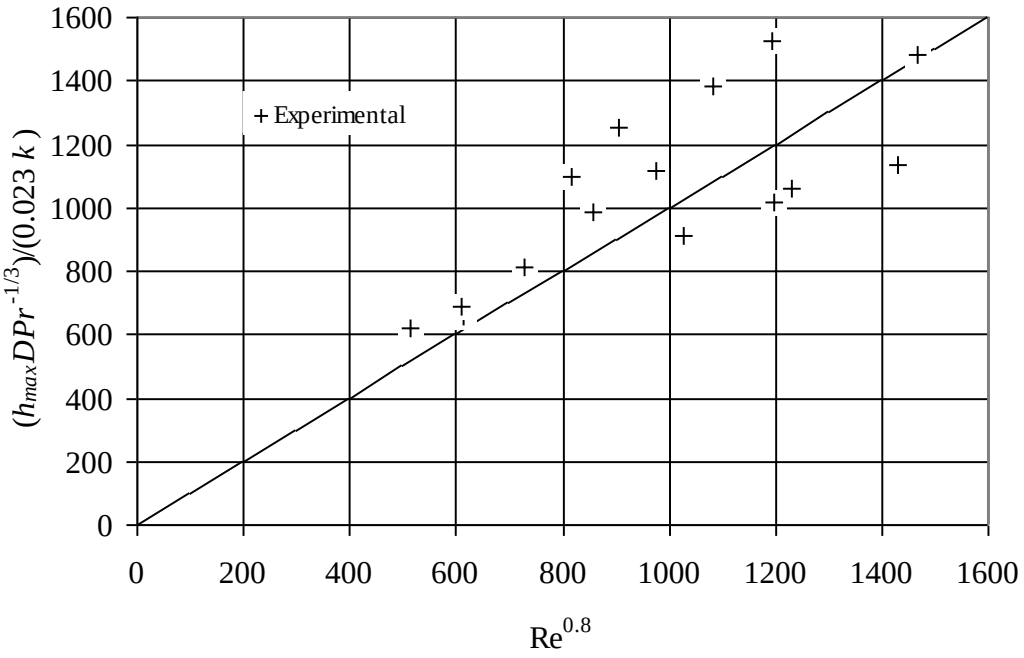

Fig. 4.21: $(h_{max}D\mathrm{Pr}^{-1/3}/0.023k)$ vs. $\mathrm{Re}^{0.8}$

Since the crude oil is a mixture of hydrocarbons with a different range of boiling points, the average boiling point of the mixture can be taken as $T_{bp0.5}$. The value of $T_{bp0.5}$ can be determined from the true boiling point curves for the respective crude oils at 50 cumulative volume percent recovery. It can be seen from Table 4.1 that $T_{s,\max}$ is very close to $T_{bp0.5}$. Hence $T_{s,\max}$ is taken as $T_{bp0.5}$.

Equation (4.1) can be written as:

$$q_{\max} = h_{\max}(T_{bp0.5} - T_b) \tag{4.4}$$

By estimating $h_{\max}$ from Dittus – Boelter equation and the $T_{bp0.5}$ of the crude oils, the maximum heat flux can be estimated. The physical properties such as density, dynamic viscosity, specific heat and thermal conductivities required for the estimation of Reynolds number and Prandtl number for different crude oils were evaluated at different bulk temperatures and are tabulated in Table 4.1. The calculated maximum heat flux values were compared with the experimentally determined values as shown in Figure 4.22. The experimental and calculated values of $q_{\max}$ were found to have a good agreement within ±20%. Hence, the experiments to determine the maximum heat fluxes under the forced convective heat transfer for

the crude oils can be avoided by calculating q_{max} by Equation (4.4) and by considering ±20% error.

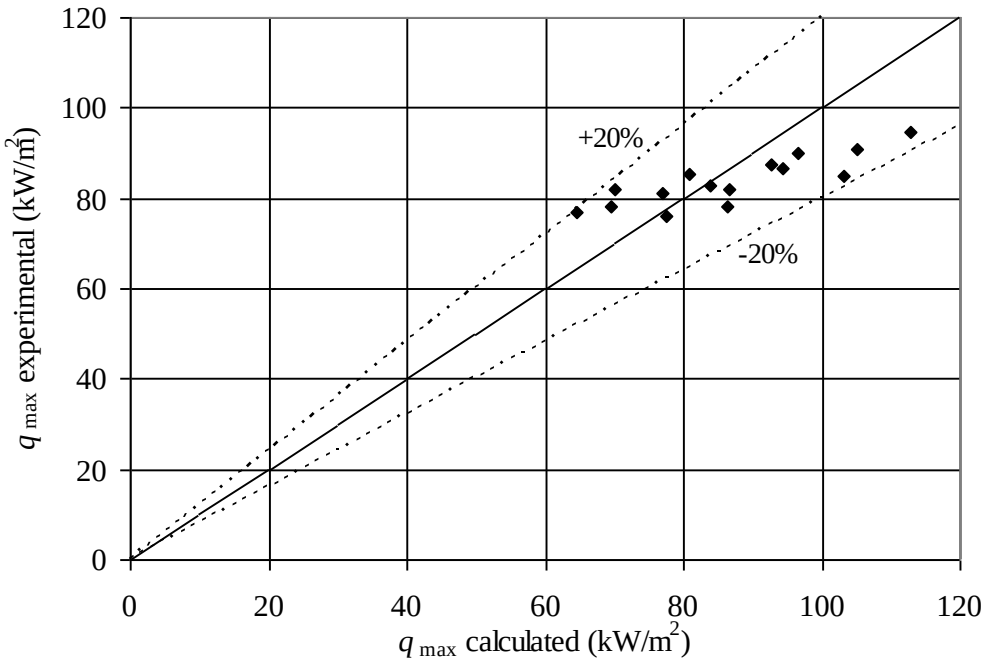

Fig. 4.22: Comparison of the calculated maximum heat flux with the experimental values for different crude oils

4.4 Summary

In this chapter, the experimental results for the estimation of the maximum heat flux for the forced convective heat transfer regime for the crude oils were described in detail for each crude oil individually. A model developed for the estimation of the maximum heat flux was presented. The q_{max} values estimated based on the model and the experiment were compared and found to have a good agreement within ±20%.

CHAPTER 5

RESULTS AND DISCUSSIONS

5.1 Introduction

In the present study, different crude oils were used as the hydrocarbons to understand their fouling characteristics. Experiments to study the fouling characteristics and the effects of surface temperature, bulk temperature and flow velocity on the initial fouling rates and the induction periods for different crude oils were carried out and the results are reported and discussed.

Experimental results on the fouling characteristics of different crude oils are presented and discussed in Section 5.2. Section 5.3 describes the evaluation of the experimental data by Panchal et al. [10] model. A new threshold fouling model is developed to account for the effect of bulk temperature on initial fouling rate and is presented in Section 5.4. Section 5.4 also covers a comparison between the experimental and the predicted initial fouling rates. Section 5.5 describes the correlation developed for the induction period and the initial fouling rate.

5.2 Fouling characteristics of crude oils

As explained in Chapter 3, a series of 40 experimental runs were carried out for four different crude oils (A, B, C and D) in the forced convective heat transfer regime in the absence of boiling (at heat fluxes, $q < q_{max}$) at a pressure of 50 bar, bulk temperatures ranging from 80 to 120^{o}C, flow velocities from 0.4 to 0.6 m/s and initial surface temperatures varying from 178 to 226^{o}C.

Table 5.1: Induction periods and the initial fouling rates of the crude oils

Crude oil	Run no.	Inlet bulk temperature	Outlet bulk temperature	Flow velocity	Heat flux	Initial surface temperature	Induction period	Initial fouling rate
		$T_{b,\,in}$	$T_{b,\,out}$	v	q	T_{so}	θ	dR_f/dt
		^oC	^oC	m/s	kW/m^2	^oC	min	m^{2}K/kWmin×10^5
A	1	120.25±0.18	121.09±0.25	0.48± 0.002	64 ± 0.23	198	2000	0.38
	2	120.33±0.10	121.09±0.25	0.48± 0.002	75 ± 0.23	210	750	0.52
	3	120.33 ± 0.10	122.47±0.10	0.48± 0.002	82 ± 0.57	223	700	0.68
B	4	89.94 ± 0.38	90.96 ± 0.30	0.39±0.005	72±0.50	213	378	4.72
	5	89.94 ± 0.38	92.14 ± 0.39	0.48±0.006	76±0.24	214	375	3.87
	6	105.14 ± 0.37	106.42 ± 0.33	0.39±0.002	68±0.38	214	1080	4.55
	7	105.14 ± 0.37	107.44 ± 0.36	0.48±0.004	79±0.38	217	700	1.38
	8	120.22 ± 0.04	121.16 ± 0.05	0.38±0.004	65±0.38	212	210	0.96
	9	120.25 ± 0.32	121.27 ± 0.32	0.48±0.002	64±0.28	204	700	0.29
	10	120.25 ± 0.32	122.34 ± 0.31	0.48±0.002	70±0.28	216	270	0.52
	11	119.96 ± 0.19	122.32 ± 0.19	0.48±0.002	75±0.28	226	18	0.67
	12	120.22 ± 0.04	122.30 ± 0.03	0.6±0.001	83±0.38	213	810	0.35
C	13	79.94±0.27	80.72±0.28	0.38±0.001	48±0.28	178	1000	6.15
	14	79.88±0.27	80.94±0.26	0.38±0.004	59±0.39	201	150	15.0

Crude oil	Run no.	Inlet bulk temperature	Outlet bulk temperature	Flow velocity	Heat flux	Initial surface temperature	Induction period	Initial fouling rate
		$T_{b,\,in}$	$T_{b,\,out}$	v	q	T_{so}	θ	dR_f/dt
		^oC	^oC	m/s	kW/m^2	^oC	min	$m^2K/kWmin\times10^5$
	15	80.47±0.56	81.71±0.67	0.39±0.006	75±0.88	223	42	16.0
	16	79.94±0.27	81.64±0.28	0.49±0.001	52±0.28	182	1100	4.53
	17	79.88±0.27	81.77±0.26	0.49±0.001	63±0.39	201	438	8.1
	18	80.47±0.56	82.64±0.58	0.49±0.002	80±0.63	225	60	9.18
	19	99.98±0.31	101±0.23	0.38±0.002	39±0.48	181	1410	4.33
	20	100.07±0.31	102.0±0.31	0.38±0.002	49±0.56	199	500	4.43
	21	100.21±0.66	101.2±0.67	0.38±0.003	59±0.25	216	162	9.77
	22	99.98±0.31	101.67±0.15	0.49±0.002	43±0.38	182	2424	1.5
	23	100.07±0.31	102.03±0.31	0.48±0.002	57±0.24	200	510	2.05
	24	100.21±0.66	102.29±0.68	0.49±0.002	67±0.47	215	282	3.18
	25	120.01±0.04	121.99±0.05	0.37±0.007	51±0.63	196	1500	0.87
	26	120.23±0.06	120.83±0.25	0.49±0.002	54±0.42	195	1900	0.60
	27	120.11±0.06	122.28±0.05	0.48±0.003	65±0.20	216	132	0.87
	28	120.01±0.038	120.75±0.092	0.49±0.002	69±0.32	226	70	1.20
D	29	80.09±0.33	80.85±0.32	0.38±0.002	58 ± 0.50	191	2300	2.35

Crude oil	Run no.	Inlet bulk temperature	Outlet bulk temperature	Flow velocity	Heat flux	Initial surface temperature	Induction period	Initial fouling rate
		$T_{b,\,in}$	$T_{b,\,out}$	v	q	T_{so}	θ	dR_f/dt
		^oC	^oC	m/s	kW/m^2	^oC	min	$m^2K/kWmin\times10^5$
	30	81.01±0.31	82.20±0.32	0.39±0.005	65 ± 0.61	206	1980	2.42
	31	80.00±0.20	81.38±0.21	0.38±0.003	80 ± 0.40	219	1098	4.42
	32	80.09±0.33	82.01±0.33	0.49±0.002	65 ± 0.29	192	2420	2.18
	33	79.92±0.31	82.20±0.32	0.49±0.002	79 ± 0.31	204	2300	2.38
	34	80.00±0.20	82.39±0.20	0.49±0.004	86 ± 0.63	220	1884	4.05
	35	99.99±0.10	100.70±0.12	0.38±0.002	47 ± 0.05	185	9000	0.70
	36	99.99±0.09	101.02±0.09	0.38±0.003	60 ± 0.03	200	6500	0.87
	37	99.99±0.37	101.20±0.39	0.38±0.002	69 ± 0.06	215	4900	1.53
	38	99.99±0.10	102.21±0.17	0.49±0.004	53 ± 0.05	185	9798	0.30
	39	99.99±0.09	101.93±0.13	0.49±0.002	63 ± 0.05	200	7005	0.58
	40	99.99±0.37	101.81±0.38	0.49±0.002	73 ± 0.05	215	5000	0.67

The initial fouling rates and the induction periods estimated from R_f vs. time profiles are summarized in Table 5.1 for all the experiments. Data on initial fouling rates and induction periods are analyzed for the effects of initial surface temperature, bulk temperature and flow velocity. Experiments will be selected and grouped for the purpose of analysis of effect of different variables on the fouling characteristics.

5.2.1 Effect of initial surface temperature on fouling characteristics

The results from the experimental runs, where the initial surface temperatures were varied by maintaining the bulk temperature and flow velocity as constant, were selected from Table 5.1 for all the crude oils. The selected experimental data were analyzed for the effect of initial surface temperature on the initial fouling rate and the induction period.

5.2.1.1 Crude oil A

The experimental results from Runs 1 – 3 were used for the investigation of the effect of initial surface temperature on the fouling characteristics of crude oil A. These runs correspond to the experiments carried out at a bulk temperature of 120^{o}C, a velocity of 0.5 m/s and initial surface temperatures of 198, 210 and 223^{o}C, respectively. The estimated initial fouling rates and the induction periods are tabulated in Table 5.2 for crude oil A.

Table 5.2: Initial fouling rates and induction periods of crude oil A

(T_b = 120^{o}C, v = 0.5 m/s)

Initial surface temperature T_{so}, ^{o}C	Run No.	Initial fouling rate dR_f/dt, m^{2}K/kWmin × 10^5	Induction period θ, min
198	1	0.38	2000
210	2	0.52	750
223	3	0.68	700

A longer induction period of 2000 minutes was observed for the initial surface temperature of 198^{o}C; induction periods of 750 and 700 minutes were observed for

the initial surface temperatures of 210 and 223°C, respectively. The induction period vs. the initial surface temperature is shown in Figure 5.1. It was observed that the induction periods decreased with an increase in the initial surface temperatures.

Figure 5.2 shows the initial fouling rate vs. the initial surface temperature for the three runs. It was observed that the initial fouling rates increased with an increase in the initial surface temperatures.

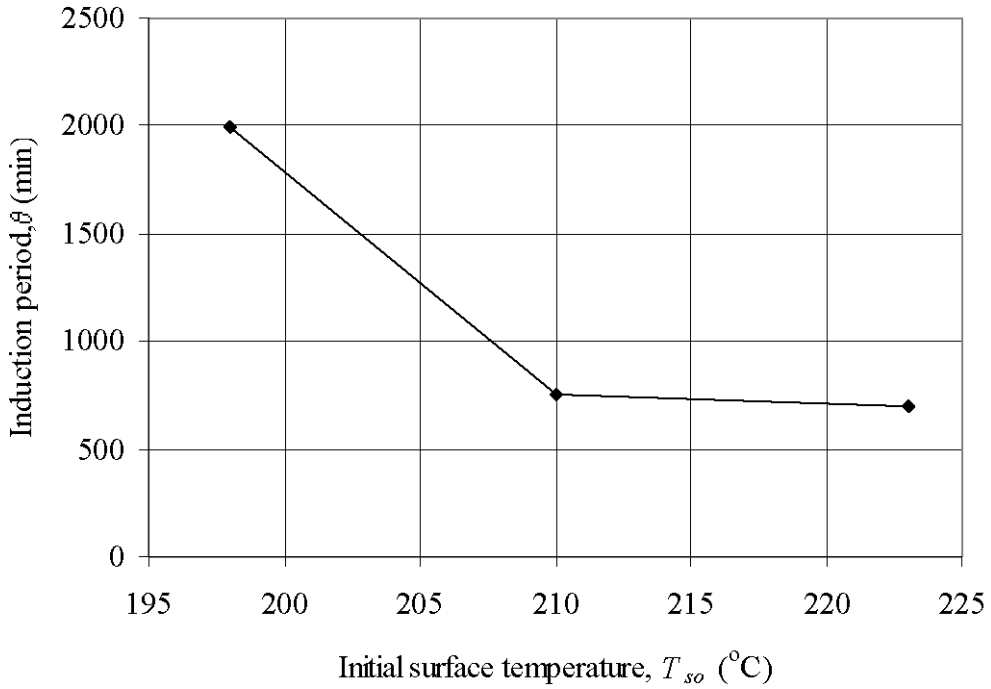

Fig. 5.1: Induction period vs. initial surface temperature of crude oil A at T_b = 120°C, v = 0.5 m/s

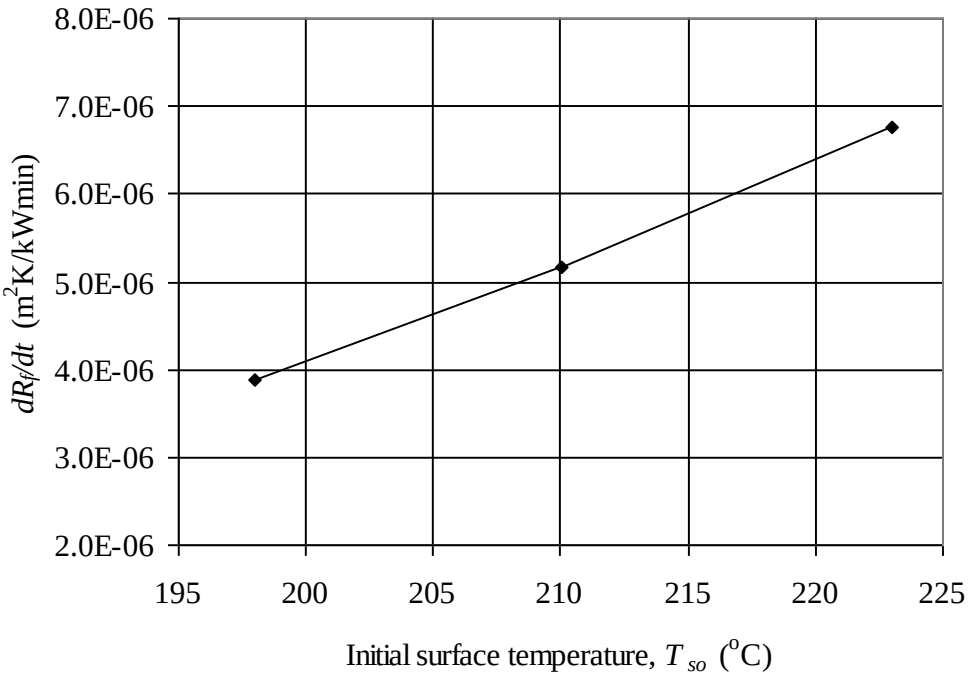

Fig. 5.2: Initial fouling rate vs. initial surface temperature of crude oil A at T_b = 120°C, v = 0.5 m/s

5.2.1.2 Crude oil B

The experimental results obtained by carrying out the experiments using crude oil B at a bulk temperature of 120°C, a velocity of 0.5 m/s and initial surface temperatures of 204, 216 and 226°C (corresponding to Runs 9 - 11, respectively) were used for the analysis. The estimated initial fouling rates and the induction periods from R_f vs. time plots of crude oil B are tabulated in Table 5.3.

Table 5.3: Initial fouling rates and induction periods of crude oil B (T_b = 120°C, v = 0.5 m/s)

Initial surface temperature T_{so}, °C	Run No.	Initial fouling rate dR_f/dt, $m^2K/kWmin \times 10^5$	Induction period θ, min
204	9	0.29	700
216	10	0.52	270
226	11	0.67	18

The induction periods of 700, 270 and 18 minutes were observed for the initial surface temperatures of 204, 216 and 226°C, respectively. The induction periods were plotted against the initial surface temperatures as shown in Figure 5.3. Longer induction periods were observed for lower initial surface temperatures of crude oil B.

Figure 5.4 shows the initial fouling rate vs. the initial surface temperature. It was observed that the increase in the initial surface temperature resulted in an increase in the initial fouling rates of crude oil B.

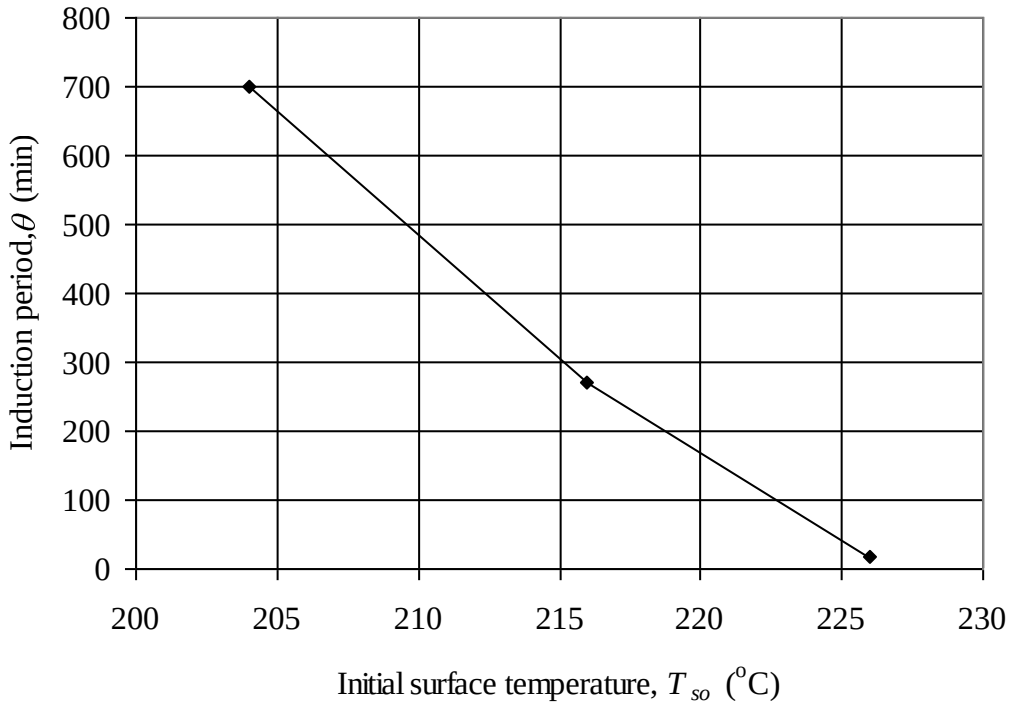

Fig. 5.3: Induction period vs. initial surface temperature of crude oil B at T_b = 120°C, v = 0.5 m/s

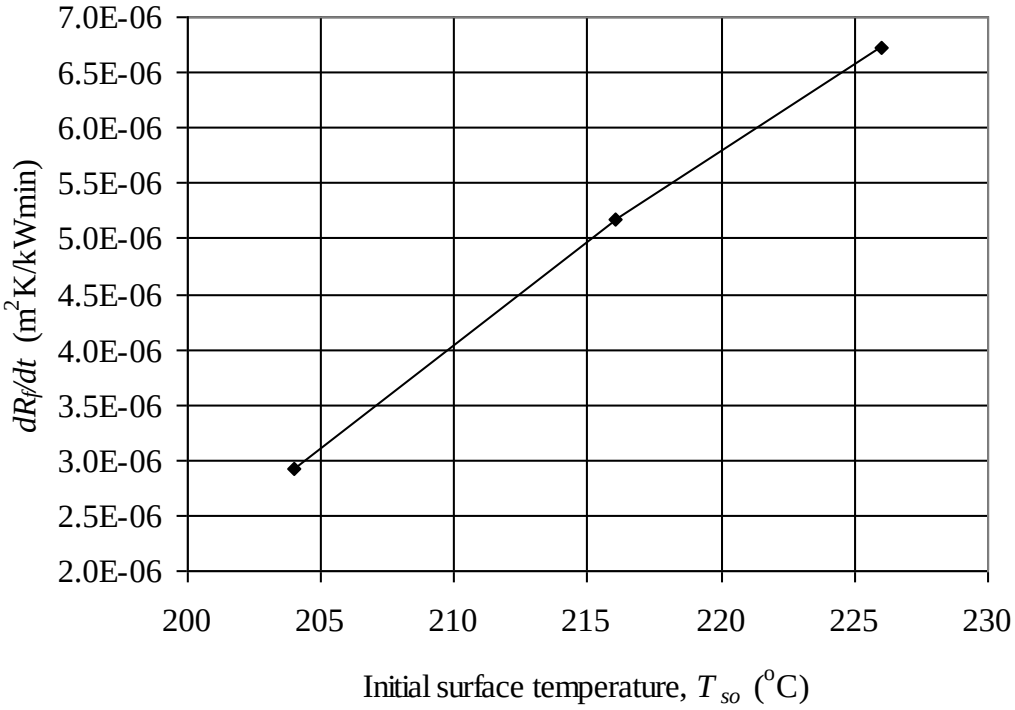

Fig. 5.4: Initial fouling rate vs. initial surface temperature of crude oil B at T_b = 120°C, v = 0.5 m/s

5.2.1.3 Crude oil C

Experimental results from Runs 26 - 28 were considered for the study of the effect of initial surface temperature on the fouling characteristics of crude oil C. The initial surface temperatures were varied as 195, 216 and 226°C; whereas the bulk temperature and flow velocity were kept constant at 120°C and 0.5 m/s for these experimental runs. Shorter induction periods of 132 and 70 minutes were observed for the initial surface temperatures of 216 and 226°C, respectively. A much longer induction period of 1900 minutes was observed for the initial surface temperature of 195°C. The results of other experiments which were carried out at bulk temperatures of 80 and 100°C, velocities of 0.4 and 0.5 m/s and different initial surface temperatures ranging from 178 to 225°C (Table 5.4, Runs 13 - 24) were also considered for the analysis. The possible groupings of the experimental results along with the operating conditions that account for the effect of initial surface temperature on the fouling characteristics of crude oil C are summarized in Table 5.4.

Table 5.4: Initial fouling rates and induction periods of crude oil C

Average bulk temperature T_b, °C	Velocity v, m/s	Initial surface temperature T_{so}, °C	Run No.	Initial fouling rate dR_f/dt, $m^2K/kWmin \times 10^5$	Induction period θ, min
120	0.5	195	26	0.60	1900
		216	27	0.87	132
		226	28	1.2	70
80	0.5	182	16	4.53	1100
		201	17	8.10	438
		225	18	9.18	60
100	0.5	182	22	1.50	2424
		200	23	2.05	510
		215	24	3.18	282
80	0.4	178	13	6.15	1000
		201	14	15.0	150
		223	15	16.0	42
100	0.4	181	19	4.33	1410
		199	20	4.43	500
		216	21	9.77	162

The induction periods were plotted against the initial surface temperatures at different flow velocities and bulk temperatures as shown in Figure 5.5. The experimental runs with lower initial surface temperatures resulted in the longer induction periods as compared with the experimental runs with higher initial surface temperatures (Figure 5.5).

Figure 5.6 shows the initial fouling rate vs. the initial surface temperature at different flow velocities and bulk temperatures. It was found that the initial fouling rates increased with an increase in the initial surface temperatures at all bulk temperatures and flow velocities.

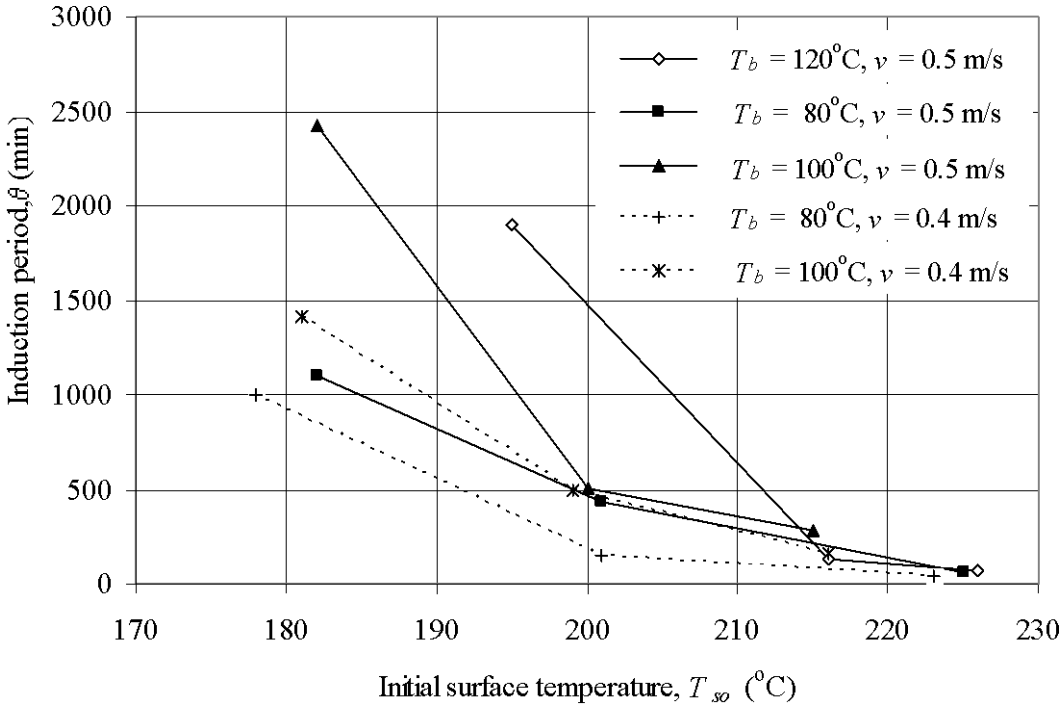

Fig. 5.5: Induction period vs. initial surface temperature at different bulk temperatures and flow velocities of crude oil C

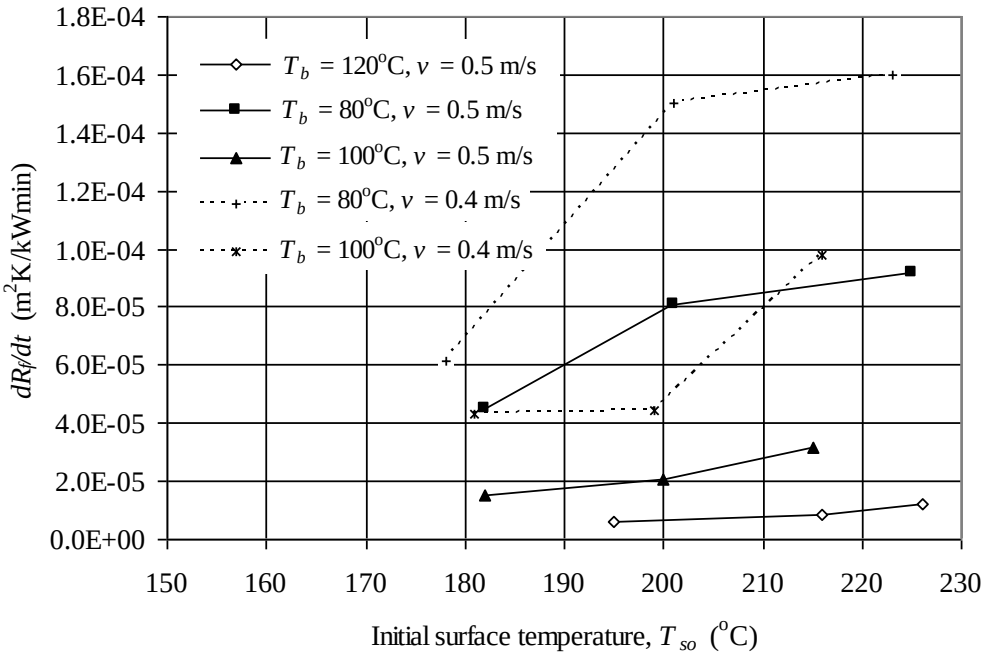

Fig. 5.6: Initial fouling rate vs. initial surface temperature at different bulk temperatures and flow velocities of crude oil C

5.2.1.4 Crude oil D

The possible groupings of the experimental runs that account for the effect of initial surface temperature on the induction period and the initial fouling rate of crude oil D are summarized in Table 5.5.

Table 5.5: Initial fouling rates and induction periods of crude oil D

Average bulk temperature T_b, ^oC	Velocity v, m/s	Initial surface temperature T_{so}, ^oC	Run No.	Initial fouling rate dR_f/dt, $m^2K/kWmin \times 10^5$	Induction period θ, min
80	0.5	192	32	2.18	2420
		204	33	2.38	2298
		220	34	4.05	1884
100	0.5	185	38	0.30	9798
		200	39	0.58	7005
		215	40	0.67	5000
80	0.4	191	29	2.35	2300
		206	30	2.42	1980
		219	31	4.42	1098
100	0.4	185	35	0.70	9000
		200	36	0.87	6500
		215	37	1.53	4900

Figure 5.7 shows the induction period vs. the initial surface temperature of crude oil D. The induction periods decreased with an increase in the initial surface temperatures.

Figure 5.8 shows the initial fouling rate vs. the initial surface temperature. The increase in initial fouling rates was observed with an increase in initial surface temperatures.

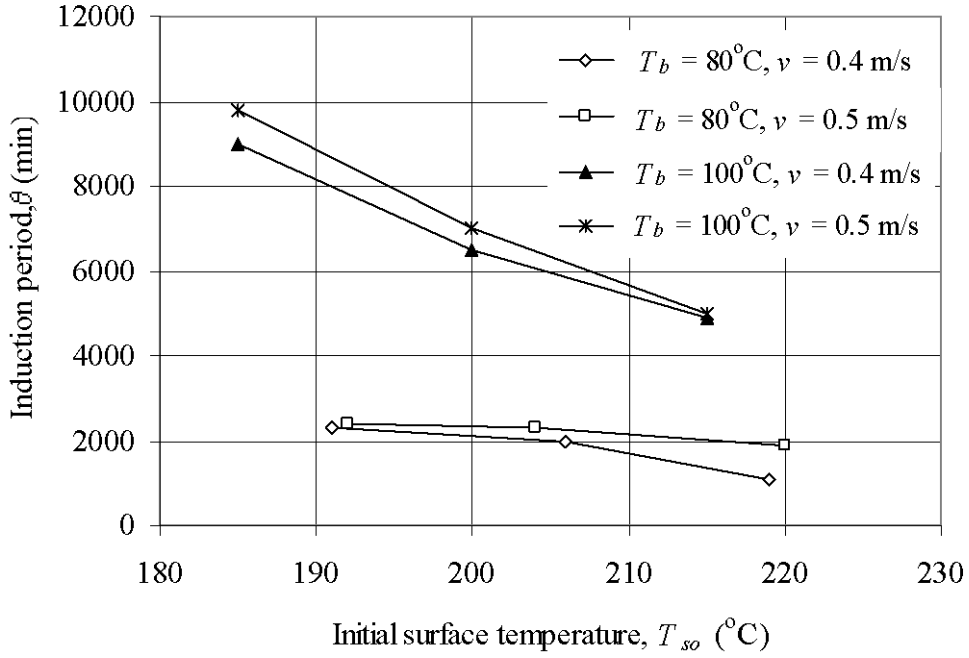

Fig. 5.7: Induction period vs. initial surface temperature at different bulk temperatures and flow velocities of crude oil D

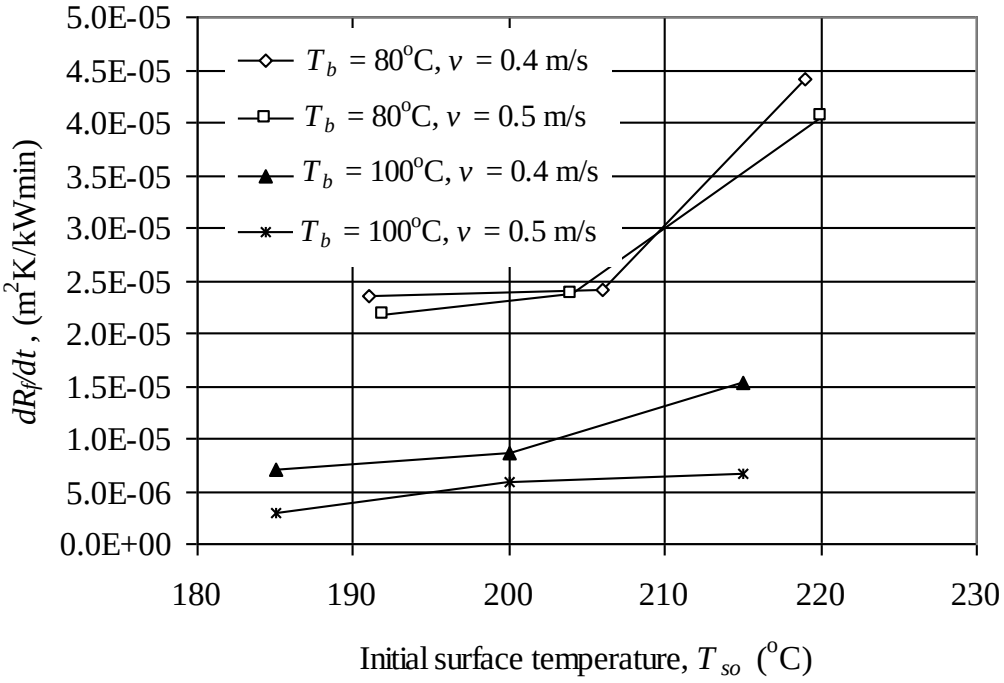

Fig. 5.8: Initial fouling rate vs. initial surface temperature at different bulk temperatures and flow velocities of crude oil D

5.2.1.5 Discussion on the effect of initial surface temperature on fouling characteristics

It was observed from the experimental investigations that the induction periods decreased with an increase in initial surface temperatures. Saleh et al. [23], Yang et al. [78], Troup and Richardson [79] and Srinivasan [80] reported similar observations on the effect of initial surface temperatures on induction periods.

It was also observed from the experimental investigations that the initial fouling rates increased with an increase in initial surface temperatures. Scarborough et al. [9], Eaton and Lux [14], Crittenden et al. [32, 81, 82], Asomaning [22], Saleh et al. [23], Srinivasan and Watkinson [24] and Fan et al. [72] reported similar observations on the effect of initial surface temperatures. However, Kovo [71] observed the decrease in fouling rate with an increase in surface temperature for refinery naphtha.

5.2.2 Effect of bulk temperature on fouling characteristics

The effect of bulk temperature on fouling characteristics was experimentally investigated for different crude oils. The experimental results are presented for each crude oil in the following sections.

5.2.2.1 Crude oil B

The experimental results from Runs 5, 7 and 10 were selected to study the effect of bulk temperature on fouling characteristics of crude oil B. These runs correspond to the experiments carried out at an initial surface temperature of 214±2^{o}C, flow velocity of 0.5 m/s and bulk temperatures of 90, 105 and 120^{o}C. The induction periods of 375, 700 and 270 minutes were noticed for the bulk temperatures of 90, 105 and 120^{o}C, respectively. Similarly, Runs 4, 6 and 8 were also considered for the study. In these runs, the flow velocity was maintained as 0.4 m/s and the bulk and initial surface temperatures were maintained almost similar to Runs 5, 7 and 10. The estimated initial fouling rates and the induction periods are summarized in Table 5.6.

Table 5.6: Initial fouling rates and induction periods of crude oil B at different bulk temperatures and flow velocities

Avg. bulk temperature T_b, °C	Initial surface temperature T_{so}, °C	Velocity v, m/s	Run No.	Initial fouling rate dR_f/dt, $m^2K/kWmin \times 10^5$	Induction period θ, min
90	214		5	3.87	375
105	216	0.5	7	1.38	700
120	216		10	0.52	270
90	213		4	4.72	378
105	214	0.4	6	4.55	1080
120	212		8	0.96	210

Figure 5.9 shows the initial fouling rate vs. the bulk temperature at two flow velocities (0.4 and 0.5 m/s) and a constant initial surface temperature of crude oil B. The initial fouling rates decreased with an increase in the bulk temperatures. No firm conclusions can be drawn on the effect of the bulk temperature on the induction period of crude oil B (Table 5.6).

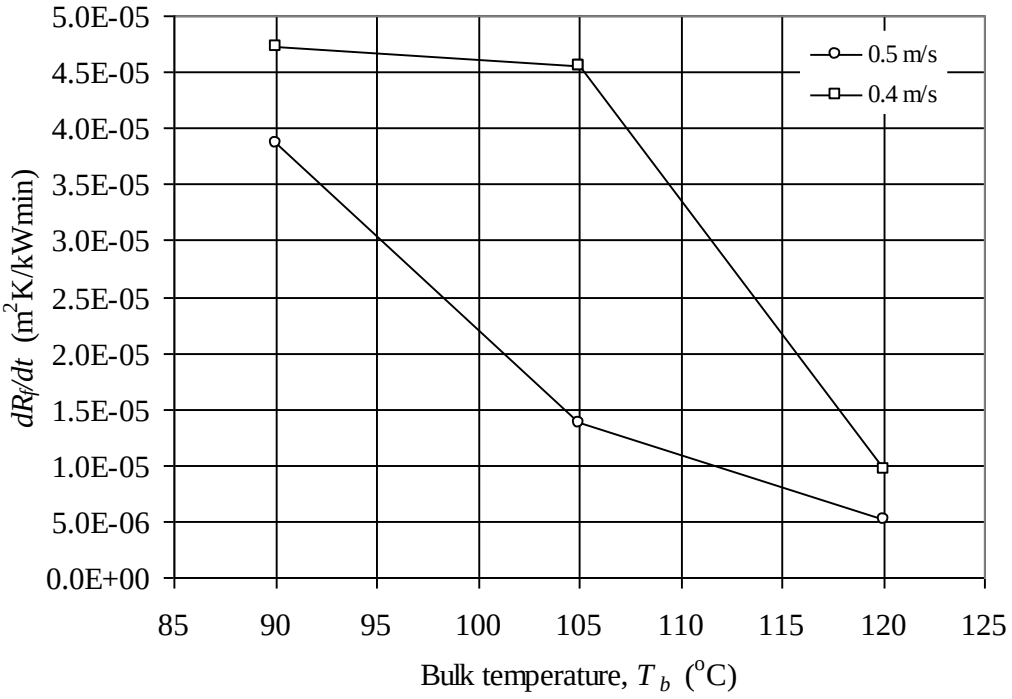

Fig. 5.9: Initial fouling rate vs. bulk temperature for different velocities of crude oil B (T_{so} = 214±2°C)

5.2.2.2 Crude oil C

Runs 17, 23 and 26 were considered for the investigation of the effect of bulk temperature on the fouling characteristics of crude oil C. These runs correspond to the experiments carried out at a flow velocity of 0.5 m/s, an initial surface temperature of 200^{o}C and the bulk temperatures of 80, 100 and 120^{o}C. The induction periods of 440 and 510 minutes were observed for the bulk temperatures of 80 and 100^{o}C, respectively and a longer induction period of 1900 minutes was observed for the bulk temperature of 120^{o}C. The results of the other experimental runs which were carried out at a constant flow velocity and initial surface temperature by varying the bulk temperatures using crude oil C were also considered for the study. The possible groupings of the experimental runs and their results that account for the effect of bulk temperature are summarized in Table 5.7.

Table 5.7: Initial fouling rates and induction periods of crude oil C at different bulk temperatures

Avg. bulk temperature T_b, ^{o}C	Initial surface temperatures T_{so}, ^{o}C	Velocity v, m/s	Run No.	Initial fouling rate dR_f/dt, $m^2K/kWmin \times 10^5$	Induction period θ, min
80	200	0.5	17	8.10	438
100			23	2.05	510
120			26	0.60	1900
80	225	0.5	18	9.18	60
120			28	1.2	70
100	215	0.5	24	3.18	282
120			27	0.87	132
80	178	0.4	13	6.15	1000
100			19	4.33	1410
80	201	0.4	14	15.0	150
100			20	4.43	500

The induction periods were estimated from the R_f vs. time profiles of crude oil C and are shown in Figure 5.10 as a function of the bulk temperature at different initial surface temperatures and flow velocities. It can be seen from Figure 5.10 that the induction periods increased with an increase in the bulk temperatures.

The initial fouling rates were estimated from R_f vs. time profiles and plotted against the bulk temperature as shown in Figure 5.11. It was observed that the initial fouling rates decreased with an increase in the bulk temperatures.

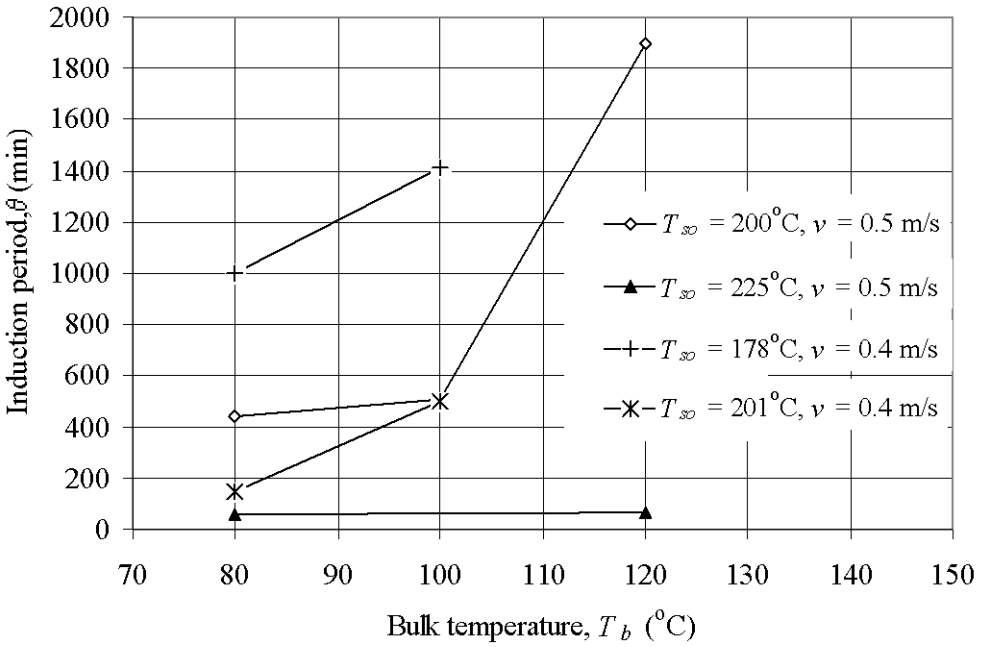

Fig. 5.10: Induction period vs. bulk temperature at different initial surface temperatures and flow velocities of crude oil C

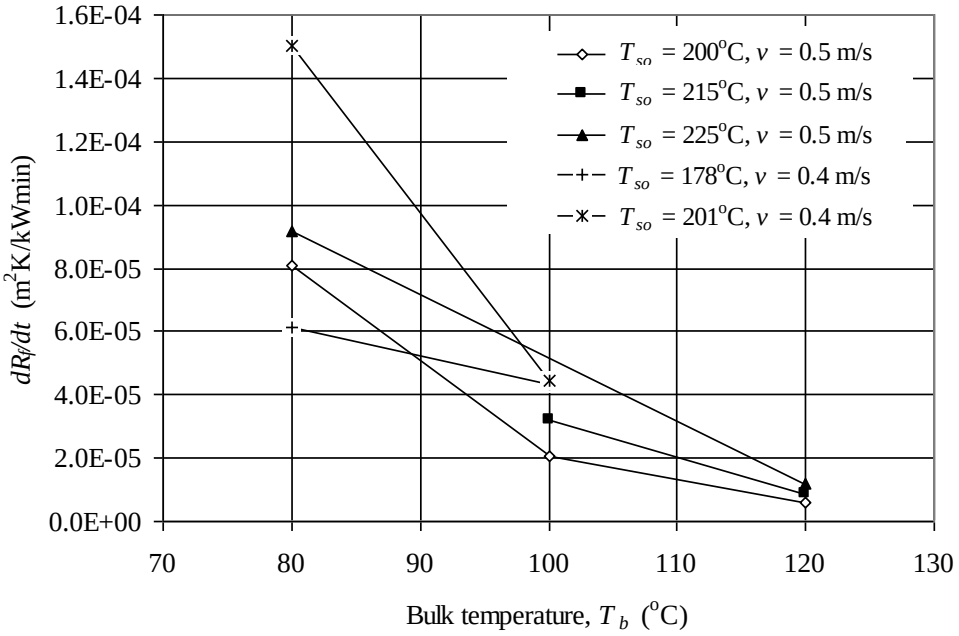

Fig. 5.11: Initial fouling rate vs. bulk temperature at different initial surface temperatures and flow velocities of crude oil C

5.2.2.3 Crude oil D

The possible groupings of the experimental runs and their results that account for the effect of bulk temperature on the fouling characteristics are considered from Table 5.1 and are summarized in Table 5.8 for crude oil D alone. In all these experimental runs, the flow velocity and the initial surface temperature were kept constant and the bulk temperatures were varied.

Table 5.8: Initial fouling rates and induction periods of crude oil D at different bulk temperatures

Avg. bulk temperature T_b, ^oC	Initial surface temperatures T_{so}, ^oC	Velocity v, m/s	Run no.	Initial fouling rate dR_f/dt, $m^2K/kWmin \times 10^5$	Induction period θ, min
80	204	0.5	33	2.38	2300
100	200		39	0.58	6700
80	220	0.5	34	4.05	1884
100	215		40	0.66	5000
80	206	0.4	30	2.42	1980
100	200		36	0.86	6500
80	219	0.4	31	4.42	1098
100	215		37	1.53	4900

Figure 5.12 shows the induction period vs. the bulk temperature plot of crude oil D at different initial surface temperatures and flow velocities. It was observed that the induction periods increased with an increase in the bulk temperatures. It was also observed that the fouling process started to occur after longer induction periods as compared with the other crude oils A, B and C.

The initial fouling rates were plotted against the bulk temperature as shown in Figure 5.13. It was found that the increase in the bulk temperature resulted in the decrease in the initial fouling rates.

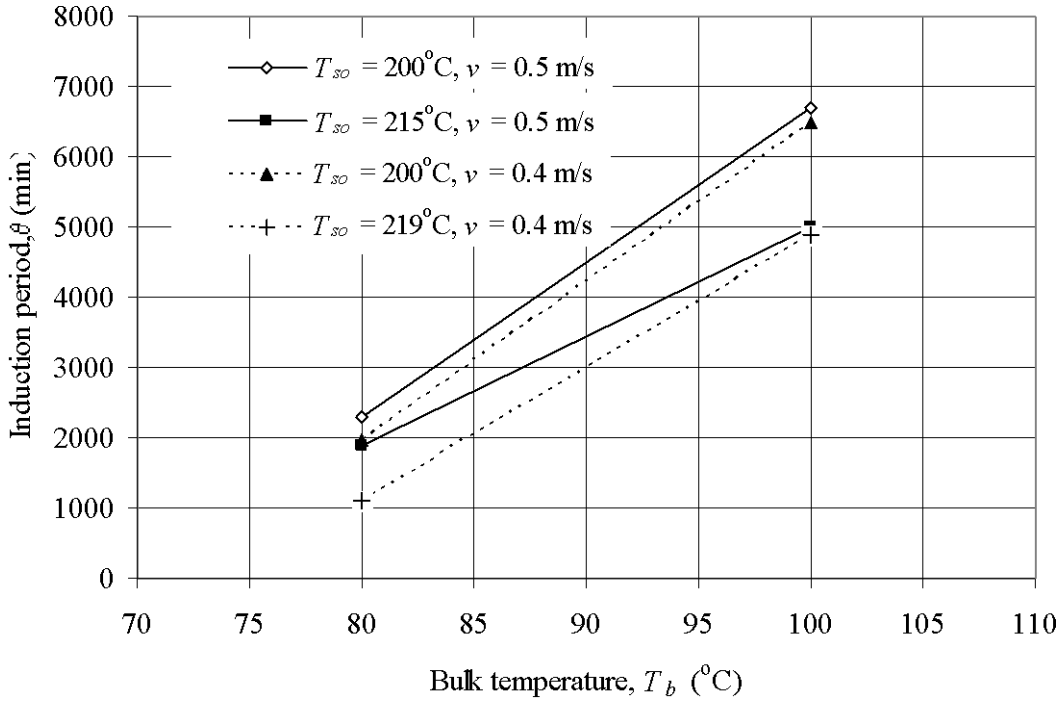

Fig. 5.12: Induction period vs. bulk temperature at different velocities and initial surface temperatures of crude oil D

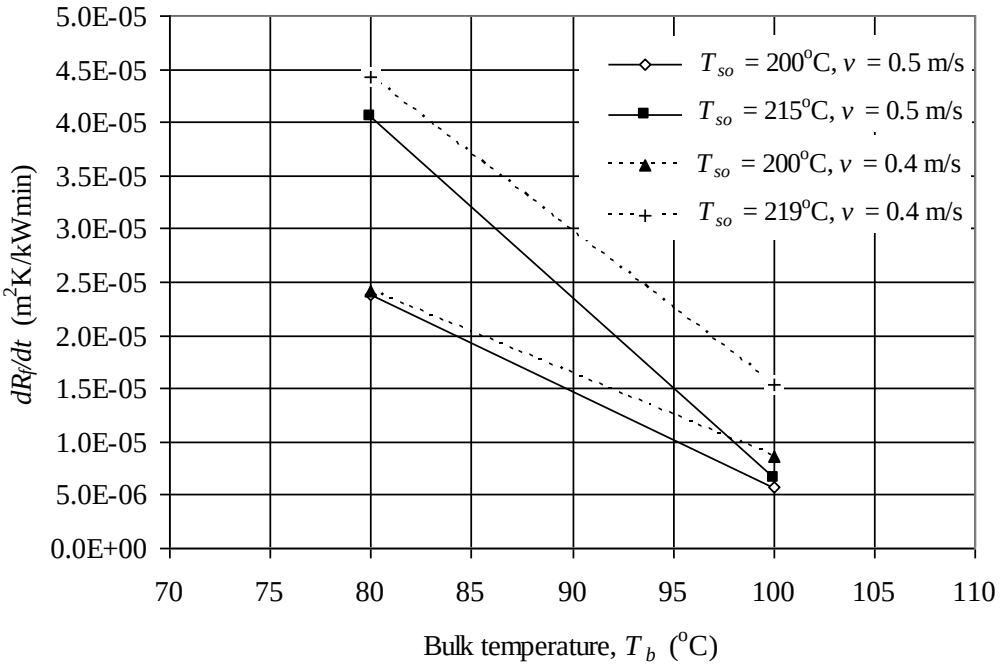

Fig. 5.13: Initial fouling rate vs. bulk temperature at different velocities and initial surface temperatures of crude oil D

5.2.2.4 Discussion on the effect of bulk temperature on fouling characteristics

It was found from the experimental investigations that the induction periods increased with an increase in bulk temperature. However, Srinivasan [80] reported longer induction periods for lower bulk temperatures for Canadian crude oils.

It was also found from the experimental observations that the initial fouling rates decreased with an increase in bulk temperature for Malaysian crude oils. The similar observations on the effect of bulk temperature were also reported by many researchers [14, 22, 25-27, 71]. However, Saleh et al. [23] and Srinivasan and Watkinson [24] reported that initial fouling rates increased with an increase in bulk temperature.

5.2.3 Effect of flow velocity on fouling characteristics

The effect of flow velocity on the initial fouling rate and the induction period were investigated for different crude oils. The experimental results that account for the effect of flow velocity on the fouling characteristics are analyzed for each crude oil in the following sections.

5.2.3.1 Crude oil B

The experimental results from Runs 8, 10 and 12 were used for the investigation of the effect of the flow velocity on the fouling characteristics of crude oil B. These experimental runs correspond to the experiments carried out at different flow velocities ranging from 0.4 to 0.6 m/s, a bulk and initial surface temperature of 120^{o}C and 214±2^{o}C, respectively. The significant increase in the thermal fouling resistance started after the induction periods of 210, 270 and 810 minutes for the flow velocities of 0.4, 0.5 and 0.6 m/s, respectively. The groupings of the experiments where the flow velocities were varied and the other operating conditions such as bulk and initial surface temperatures maintained constant were also used for this study. The possible groupings of the experimental runs and their results used for the analysis of the effect of flow velocity on the fouling characteristics are tabulated in Table 5.9.

Table 5.9: Initial fouling rates and the induction periods of crude oil B at different velocities

Avg. bulk temperature T_b, °C	Initial surface temperature T_{so}, °C	Velocity v, m/s	Run No.	Initial fouling rate dR_f/dt, $m^2K/kWmin \times 10^5$	Induction period θ, min
120	212	0.4	8	0.96	210
	216	0.5	10	0.52	270
	213	0.6	12	0.35	810
106	214	0.4	6	4.55	210
	217	0.5	7	1.38	702
90	213	0.4	4	4.72	373
	214	0.5	5	3.87	378

Figure 5.14 shows the induction period vs. the flow velocity of crude oil B. It was observed that the increase in the flow velocity increased the induction periods.

Figure 5.15 shows the initial fouling rate vs. the flow velocity. As seen from Figure 5.15, the initial fouling rates decreased with an increase in the flow velocities.

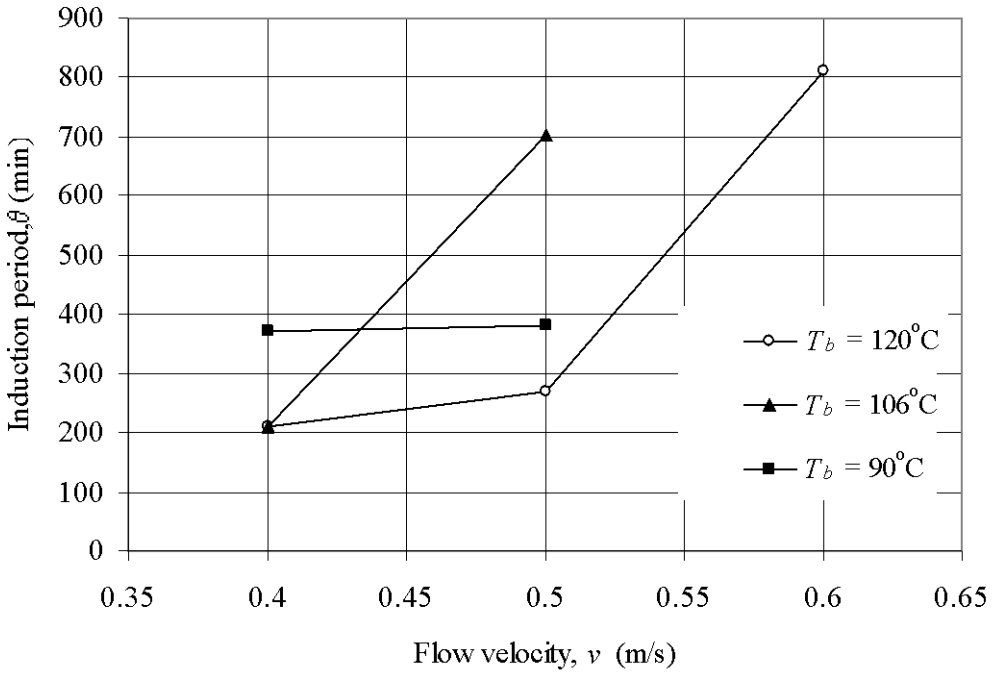

Fig. 5.14: Induction period vs. flow velocity at different bulk temperatures of crude oil B

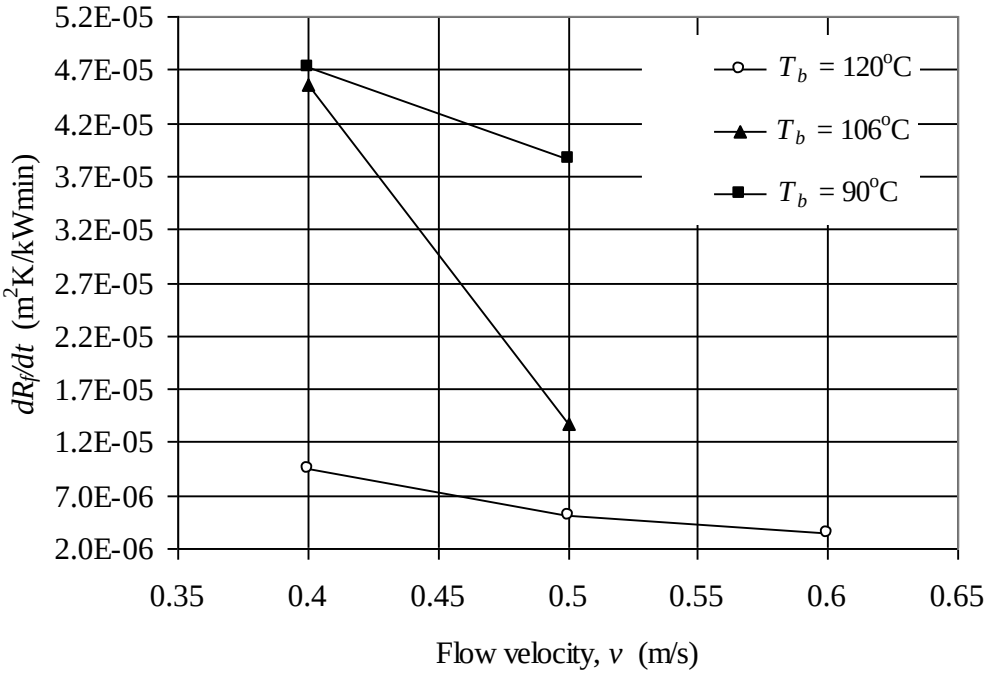

Fig. 5.15: Initial fouling rate vs. flow velocity at different bulk temperatures of crude oil B

5.2.3.2 Crude oil C

The experimental results obtained by carrying out the experiments at a bulk temperature of 80°C, an initial surface temperature of 201°C and flow velocities of 0.4 and 0.5 m/s, corresponding to Runs 14 and 17, respectively, were used for the investigation. A shorter induction period of 150 minutes was observed for the flow velocity of 0.4 m/s whereas the induction period of 440 minutes was observed for the flow velocity of 0.5 m/s. The possible groupings of the experiments and their results for the investigation of the effect of flow velocity are summarized in Table 5.10.

Table 5.10: Initial fouling rates and the induction periods of crude oil C at different velocities

Avg. bulk temperature T_b, °C	Initial surface temperature T_{so}, °C	Velocity v, m/s	Run no.	Initial fouling rate dR_f/dt, $m^2K/kWmin \times 10^5$	Induction period θ, min
80	201	0.4	14	15.0	150
		0.5	17	8.1	440
80	223	0.4	15	16.0	42
	225	0.5	18	9.18	60
80	178	0.4	13	6.15	1000
	182	0.5	16	4.53	1100
100	199	0.4	20	4.43	500
	200	0.5	23	2.05	510
100	181	0.4	19	4.33	1410
	182	0.5	22	1.5	2424
100	215	0.5	24	3.18	282
	216	0.4	21	9.77	162

The induction period as a function of flow velocity is shown in Figure 5.16 at different bulk and initial surface temperatures. It was found that the induction periods increased with an increase in the flow velocity.

The estimated initial fouling rate vs. the flow velocity at different bulk and initial surface temperatures of crude oil C is shown in Figure 5.17. The increase in flow velocity resulted in the decrease in the initial fouling rates.

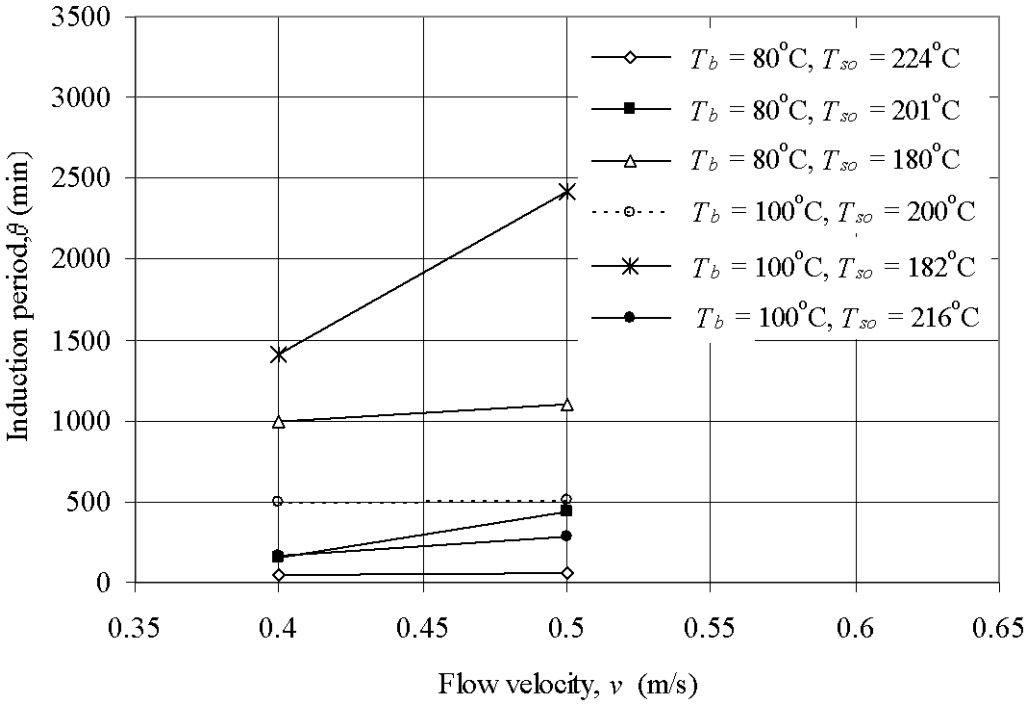

Fig. 5.16: Induction period vs. flow velocity at different bulk and initial surface temperatures of crude oil C

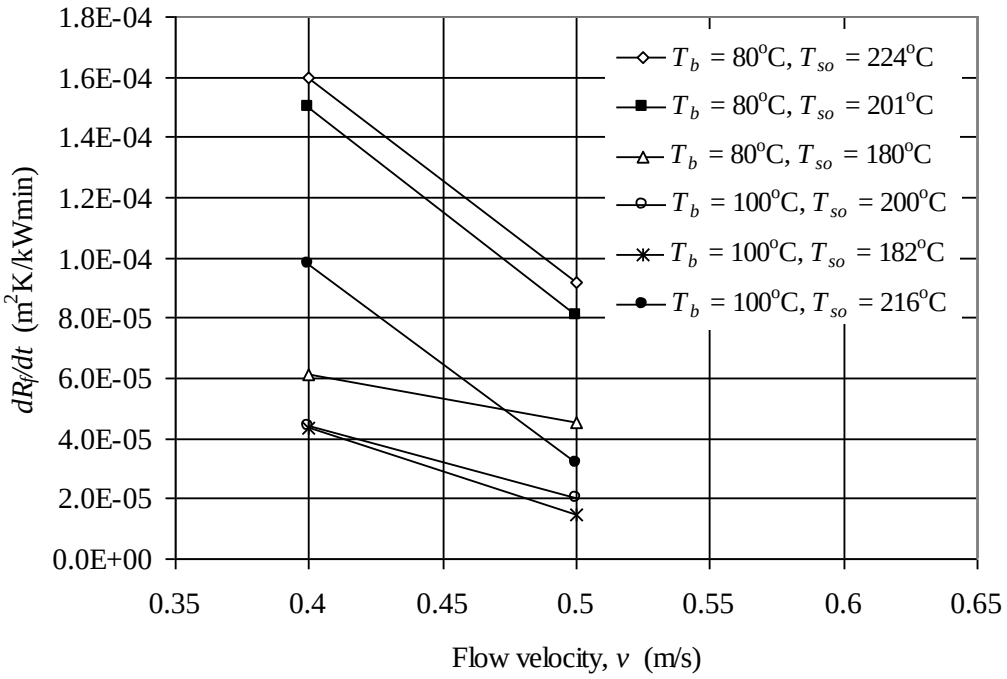

Fig. 5.17: Initial fouling rate vs. flow velocity at different bulk and initial surface temperatures of crude oil C

5.2.3.3 Crude oil D

The effect of flow velocity on fouling characteristics was experimentally investigated using crude oil D. The results of the experimental runs considered for the effect of flow velocity on fouling characteristics are tabulated in Table 5.11. It was observed that the occurrence of the fouling started after a much longer induction period for crude oil D as compared with the other crude oils A, B and C.

Table 5.11: Initial fouling rates and the induction periods of crude oil D at different velocities

Avg. bulk temperature T_b, ^oC	Initial surface temperature T_{so}, ^oC	Velocity v, m/s	Run no.	Initial fouling rate dR_f/dt, $m^2K/kWmin \times 10^5$	Induction period θ, min
80	206	0.4	30	2.42	1980
	204	0.5	33	2.38	2300
80	191	0.4	29	2.35	2300
	192	0.5	32	2.18	2420
80	219	0.4	31	4.42	1098
	220	0.5	34	4.05	1880
100	215	0.4	37	1.53	4900
		0.5	40	0.67	5000
100	200	0.4	36	0.87	6500
		0.5	39	0.58	7005
100	185	0.4	35	0.70	9000
		0.5	38	0.30	9798

The induction periods were plotted against the flow velocity as shown in Figure 5.18 at different bulk and initial surface temperatures. Longer induction periods were observed for higher flow velocities.

Figure 5.19 shows the initial fouling rate vs. the flow velocity of crude oil D. It was found that the initial fouling rates decreased with an increase in the flow velocities.

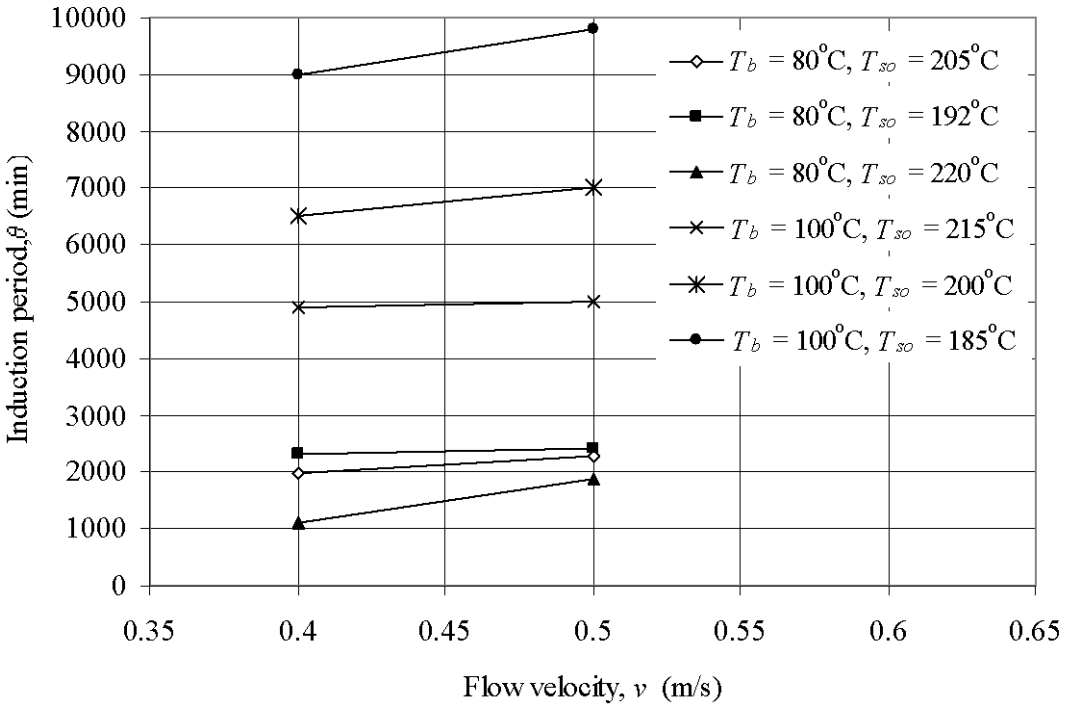

Fig. 5.18: Induction period vs. flow velocity at different bulk and initial surface temperatures of crude oil D

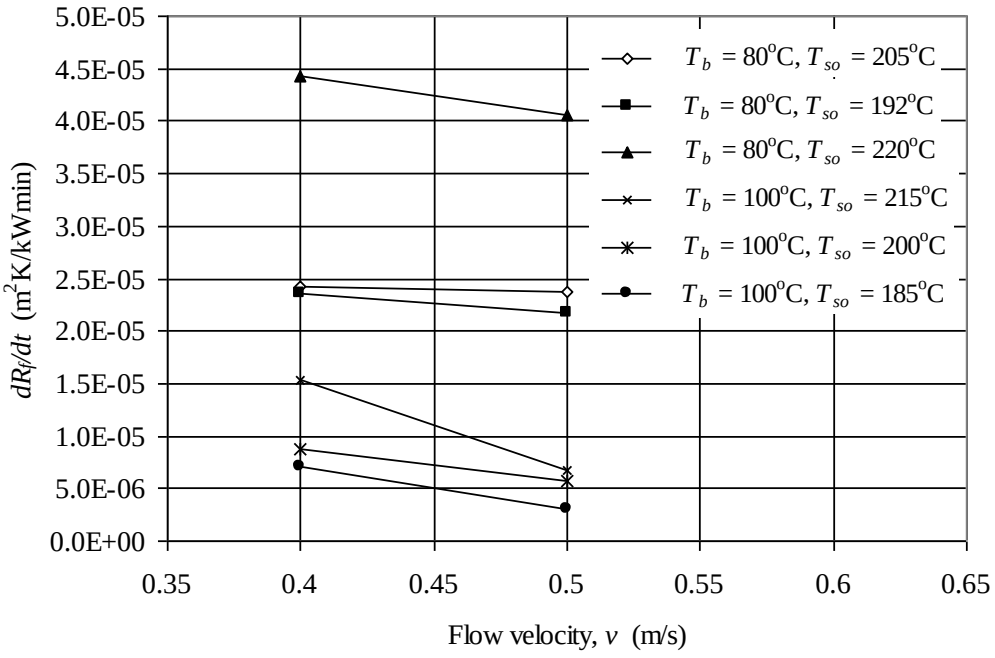

Fig. 5.19: Initial fouling rate vs. flow velocity at different bulk and initial surface temperatures of crude oil D

5.2.3.4 Discussion on the effect of flow velocity on fouling characteristics

It was noticed from the experimental investigations for the Malaysian crude oils that the induction periods increased with an increase in flow velocity. It was also noticed that the initial fouling rates decreased with an increase in flow velocity. Scarborough et al. [9], Knudsen et al. [13], Crittenden et al. [18], Asomaning [22], Saleh et al. [23], Watkinson and Epstein [53] and Fan et al. [72] reported similar observations on the effect of flow velocity.

5.3 Evaluation of the data in the light of the model of Panchal et al.

The threshold fouling model proposed by Panchal et al. (1997) is given by:

$$\frac{dR_f}{dt} = \alpha \,\mathrm{Re}^{-\beta}\,\mathrm{Pr}^{-0.33} \exp\left(-E/RT_f\right) - \gamma\tau_w \tag{2.19}$$

The first term on the RHS indicates the rate of deposition of foulant while the second term indicates the rate of removal of foulant. dR_f/dt is the initial fouling rate.

5.3.1 Estimation of the model parameters

Assuming that the rate of deposition is generally higher than the rate of removal during the initial period of fouling, Equation (2.19) can be written as:

$$\frac{dR_f}{dt} \approx \alpha \,\mathrm{Re}^{-\beta}\,\mathrm{Pr}^{-0.33} \exp\left(-E/RT_f\right) \tag{5.1}$$

Taking logarithm on both sides of the equation:

$$\ln\left(\frac{dR_f}{dt}\right) = \ln\left(\alpha \,\mathrm{Re}^{-\beta}\,\mathrm{Pr}^{-0.33}\right) - \left(E/RT_f\right) \tag{5.2}$$

Equation (5.2) can be written as:

$$\ln\left(\frac{dR_f}{dt}\right) = \ln A - \left(E/RT_f\right) \tag{5.3}$$

where A is α $Re^{-\beta}$ $Pr^{-0.33}$, E would be the apparent activation energy for fouling process, R is the universal gas constant and T_f is the absolute film temperature. Panchal et al. suggested an expression to determine the film temperature, T_f, as:

$$T_f = T_b + 0.55 \left(T_s - T_b \right) \tag{5.4}$$

The apparent activation energy, E, can be estimated from the slope of the linear relationship between ln (dR_f/dt) vs. $1/T_f$ (generally known as Arrhenius plot).

5.3.1.1 Crude oil A

The experimental results from Runs 1 – 3 carried out using crude oil A were used to estimate the apparent activation energy through Arrhenius plot. The film temperature used in the Arrhenius plot can be varied either by varying the surface temperature or the bulk temperature. In Runs 1 – 3 the film temperature was varied through the variation in the surface temperature at a constant bulk temperature. Figure 5.20 shows the Arrhenius plot for crude oil A. The apparent activation energy of 69 kJ/mol was obtained.

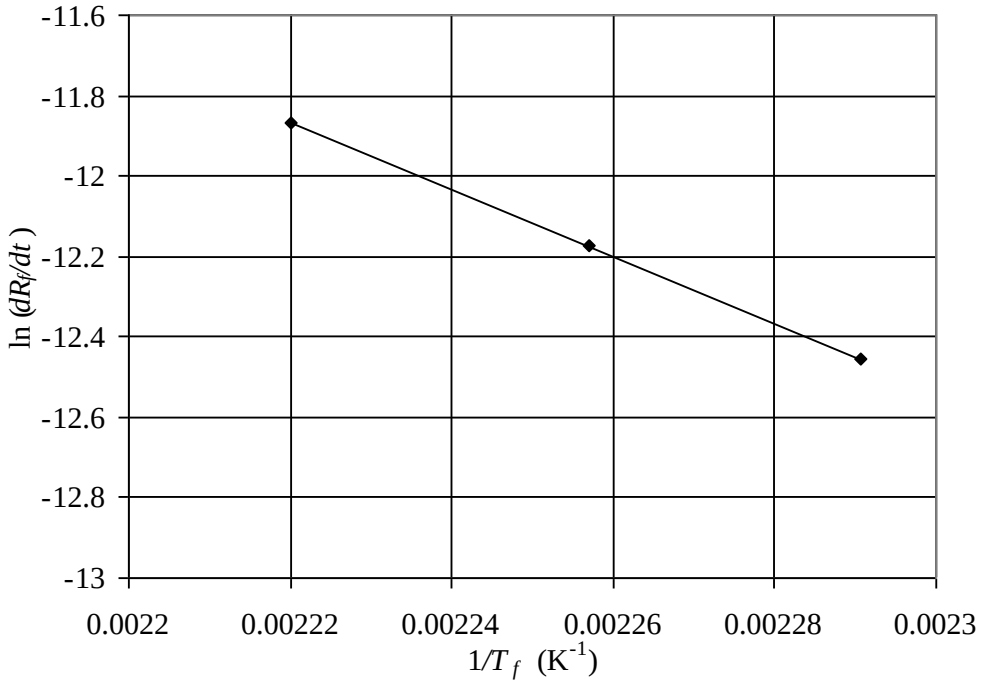

Fig. 5.20: Arrhenius plot for crude oil A

5.3.1.2 Crude oil B

The experimental results from Runs 9 - 11 were considered to estimate the apparent activation energy for crude oil B. In these runs, the bulk temperature and flow velocity were kept constant at 120°C and 0.5 m/s, respectively; whereas the initial surface temperatures were varied as 204, 216 and 226°C. The Arrhenius plot is shown in Figure 5.21. The apparent activation energy of 130.94 kJ/mol was obtained.

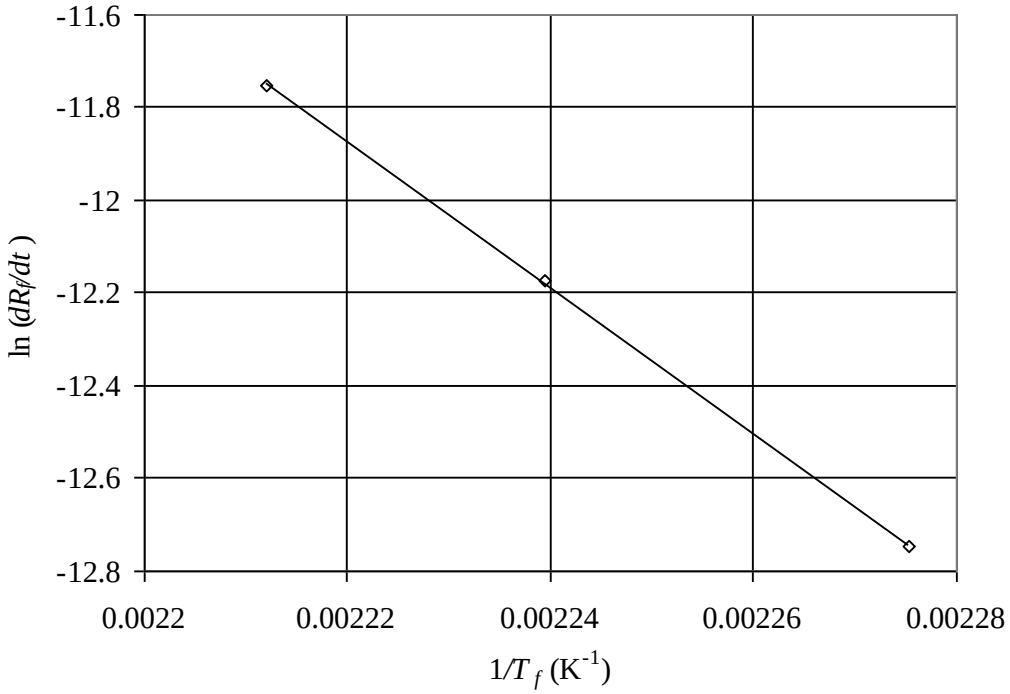

Fig. 5.21: Arrhenius plot for crude oil B

5.3.1.3 Crude oil C

Figures 5.22 - 5.24 show the Arrhenius plots for crude oil C at bulk temperatures of 80, 100 and 120°C respectively at flow velocities of 0.4 and 0.5 m/s. The apparent activation energy values estimated are summarized in Table 5.12.

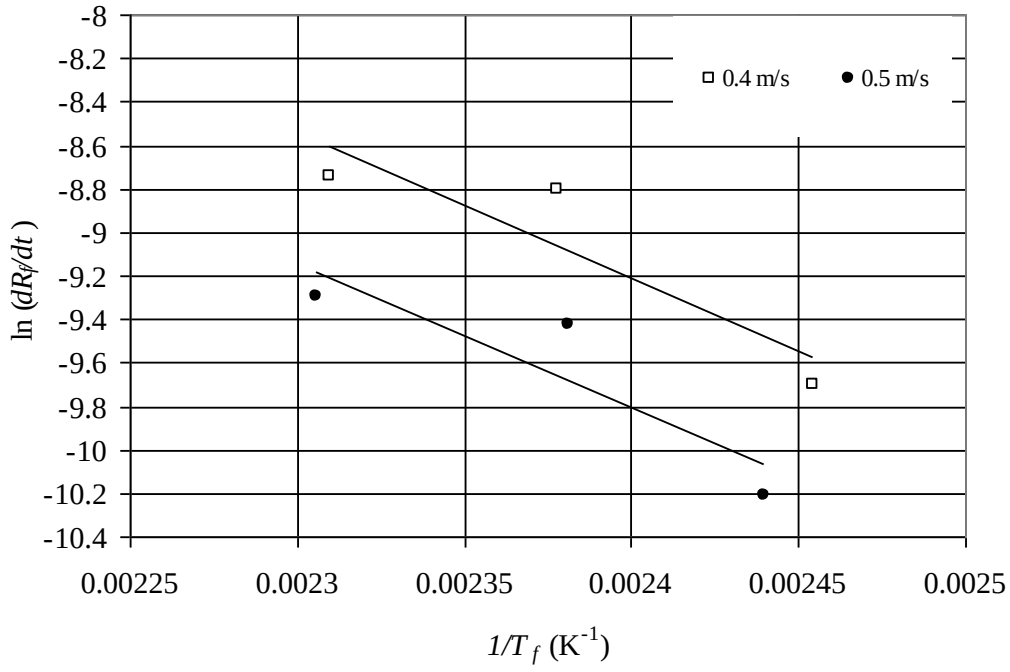

Fig. 5.22: Arrhenius plot for crude oil C at different velocities (T_b = 80°C)

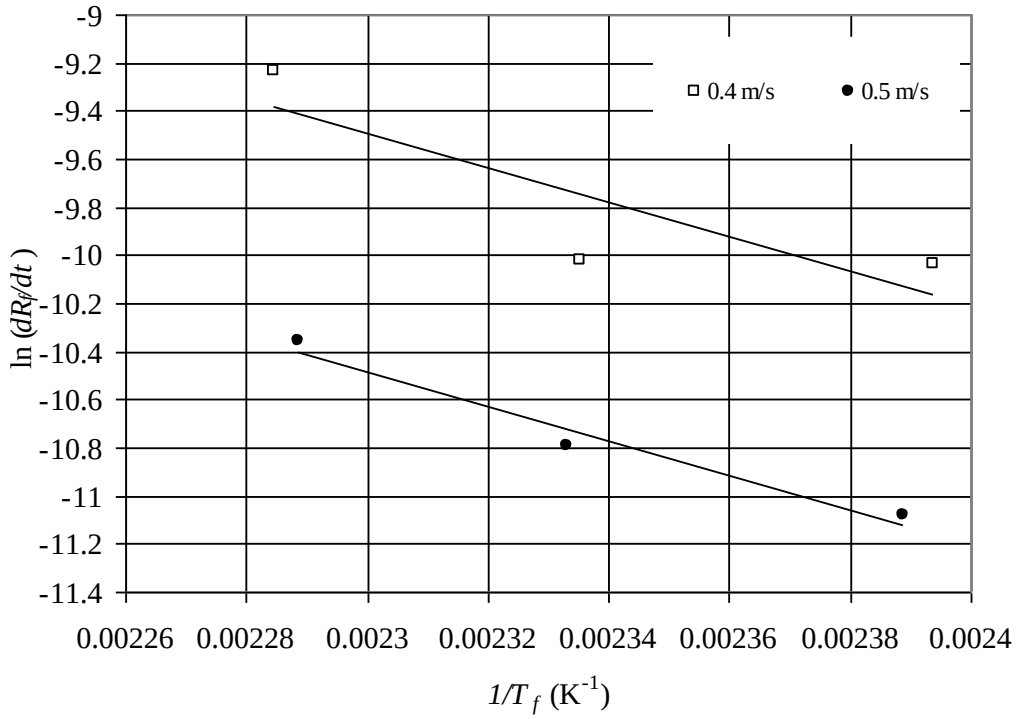

Fig. 5.23: Arrhenius plot for crude oil C at different velocities (T_b = 100°C)

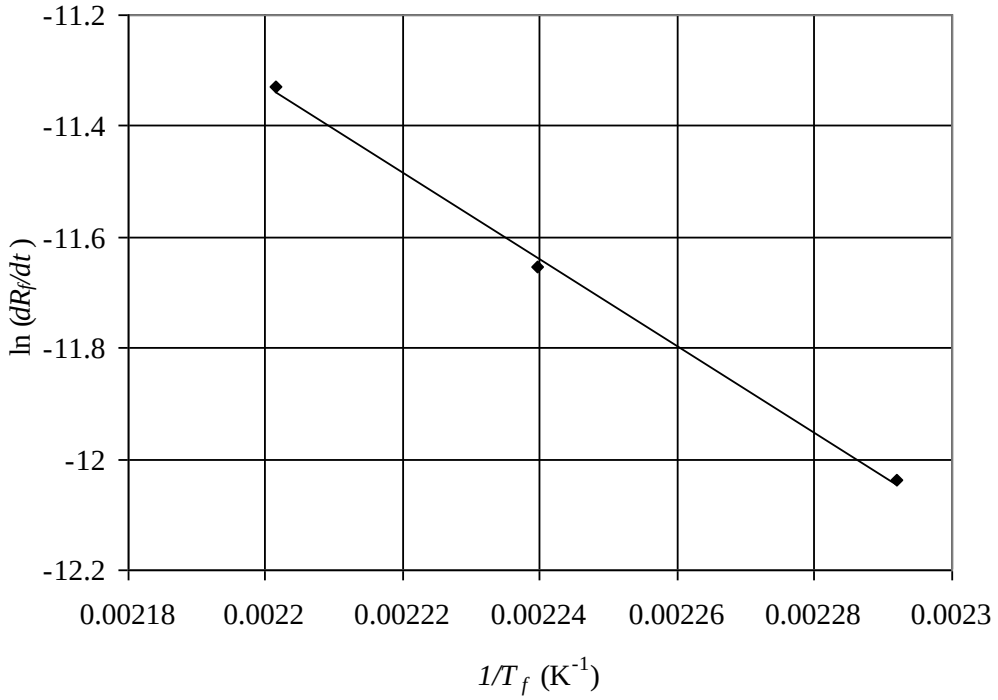

Fig. 5.24: Arrhenius plot for crude oil C (T_b = 120°C)

Table 5.12: Apparent activation energy values for crude oil C at different bulk temperatures

Avg. bulk temperature T_b, °C	Velocity v, m/s	Initial surface temperature T_{so}, °C	Run No.	Initial fouling rate dR_f/dt, $m^2K/kWmin \times 10^5$	Apparent activation energy E, kJ/mol
80	0.4	178	13	6.15	54.5
		201	14	15.0	
		223	15	16.0	
	0.5	182	16	4.53	55.8
		201	17	8.10	
		225	18	9.18	
100	0.4	181	19	4.33	59.39
		199	20	4.43	
		216	21	9.77	
	0.5	182	22	1.5	59.40
		200	23	2.05	
		215	24	3.18	
120	0.5	196	26	0.60	64.6
		216	27	0.87	
		226	28	1.2	

It was observed that there was not much of variation in the apparent activation energy values for the flow velocities of 0.4 and 0.5 m/s. However, Crittenden et al. [18] observed the variation of apparent activation energy with flow velocity (1 - 4 m/s) for Maya crude oil. It was experimentally observed that the apparent activation energy of 55 kJ/mol was estimated at the bulk temperature of 80^{o}C, the apparent activation energy of 59.4 kJ/mol was estimated at 100^{o}C and the apparent activation energy of 64.6 kJ/mol was estimated at 120^{o}C for crude oil C. The apparent activation energy values increased with an increase in the bulk temperature. This may be possibly due to the effect of solubility of fouling precursors in the crude oils at higher bulk temperatures and this might have affected the apparent activation energy. The strong influence of bulk temperature means that it is not possible to evaluate the true activation energy for the reaction aspects of the crude oil fouling process.

The observed apparent activation energies were unified for the crude oil C against the bulk temperature, T_b, as shown in Figure 5.25. It was observed that the apparent activation energy is linearly dependent on the bulk temperature. A linear relationship was, therefore, established between the apparent activation energy and the bulk temperature for a given range of operating conditions and is given by:

$$E = E_o + eT_b \tag{5.5}$$

where E_o and e are constants. For crude oil C, E_o = 35.707 kJ/mol and e = 0.2378 kJ/mol^{o}C were obtained.

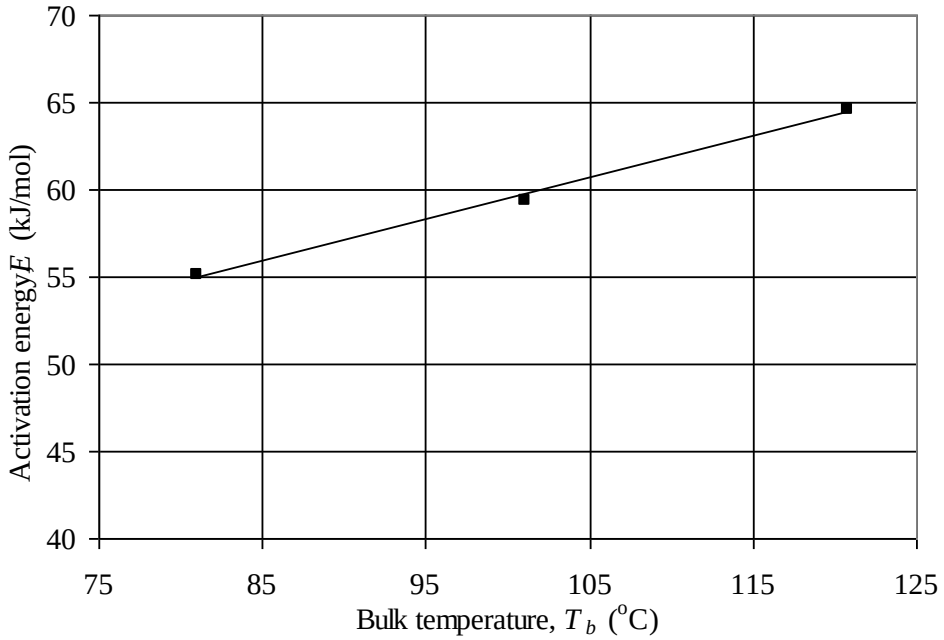

Fig. 5.25: Apparent activation energy, E, vs. bulk temperature, T_b, for crude oil C

5.3.1.4 Crude oil D

The apparent activation energy values were estimated at bulk temperatures of 80 and 100^{o}C, flow velocities of 0.4 and 0.5 m/s and at different initial surface temperatures. Figures 5.26 and 5.27 show the Arrhenius plots for crude oil D. The estimated apparent activation energy values are summarized in Table 5.13.

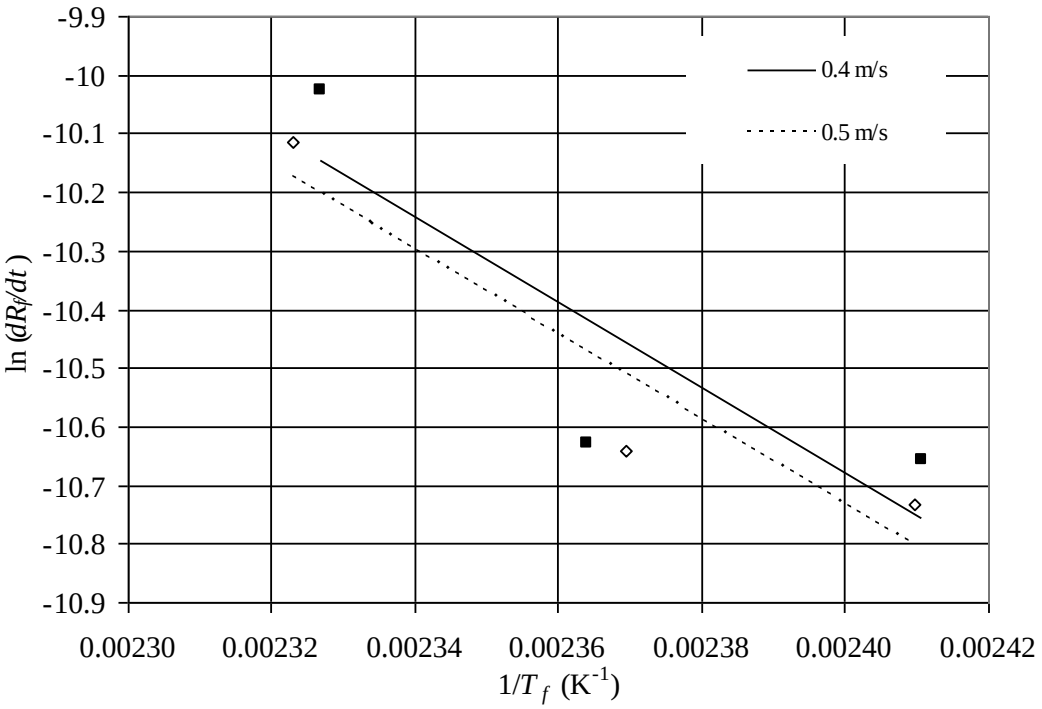

Fig. 5.26: Arrhenius plot for crude oil D at different velocities (T_b = 80°C)

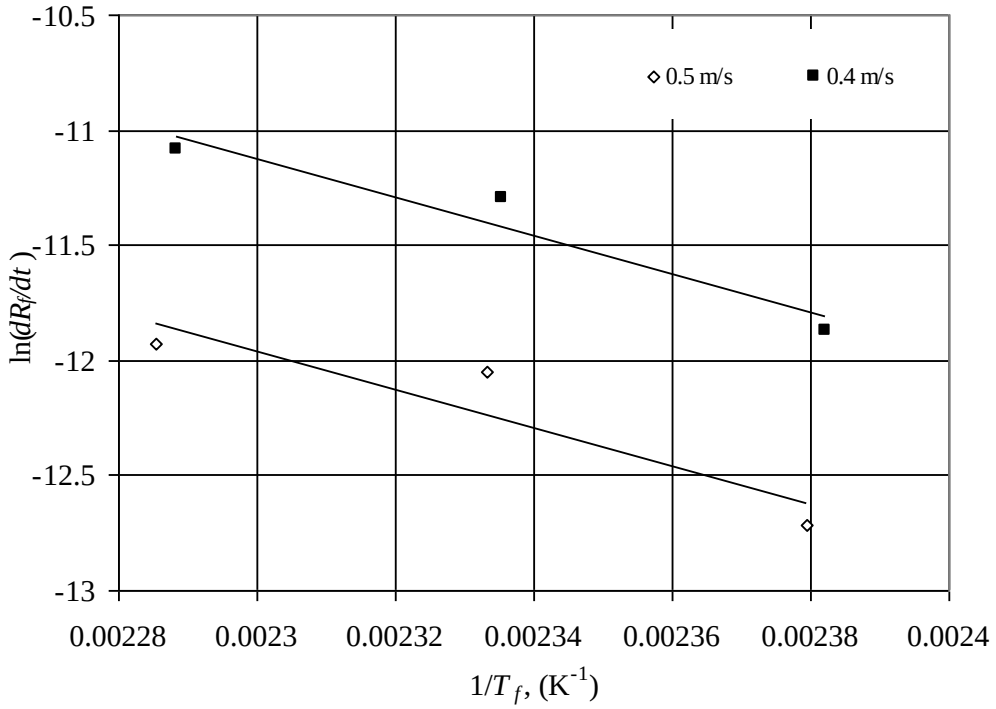

Fig. 5.27: Arrhenius plot for crude oil D at different velocities (T_b = 100°C)

Table 5.13: Apparent activation energy values for crude oil D at different bulk temperatures

Avg. bulk temperature T_b, °C	Velocity v, m/s	Initial surface temperature T_{so}, °C	Run No.	Initial fouling rate dR_f/dt, $m^2K/kWmin \times 10^5$	Apparent activation energy E, kJ/mol
80	0.4	191	29	2.35	60.45
		206	30	2.42	
		219	31	4.42	
	0.5	192	32	2.18	60.40
		204	33	2.38	
		220	34	4.05	
100	0.4	185	35	0.70	69.23
		200	36	0.87	
		215	37	1.53	
	0.5	185	38	0.30	69.54
		200	39	0.58	
		215	40	0.67	

It was observed that there was not much of variation in the apparent activation energy values for the flow velocities of 0.4 and 0.5 m/s. It was experimentally observed that the apparent activation energy of 60.4 kJ/mol was estimated at the bulk temperature of 80°C and the apparent activation energy of 69.4 kJ/mol was estimated at 100°C. The apparent activation energy values increased with an increase in the bulk temperature. This may be possibly due to the effect of solubility of fouling precursors in the crude oils at higher bulk temperatures and this might have affected the apparent activation energy.

The apparent activation energy values were unified for the crude oil D against the bulk temperature as shown in Figure 5.28. It was noticed that the apparent activation energy is linearly dependent upon the bulk temperature. Hence, a linear relationship between the apparent activation energy and the bulk temperature was established and the values of the constants E_o and e for crude oil D are tabulated in Table 5.14.

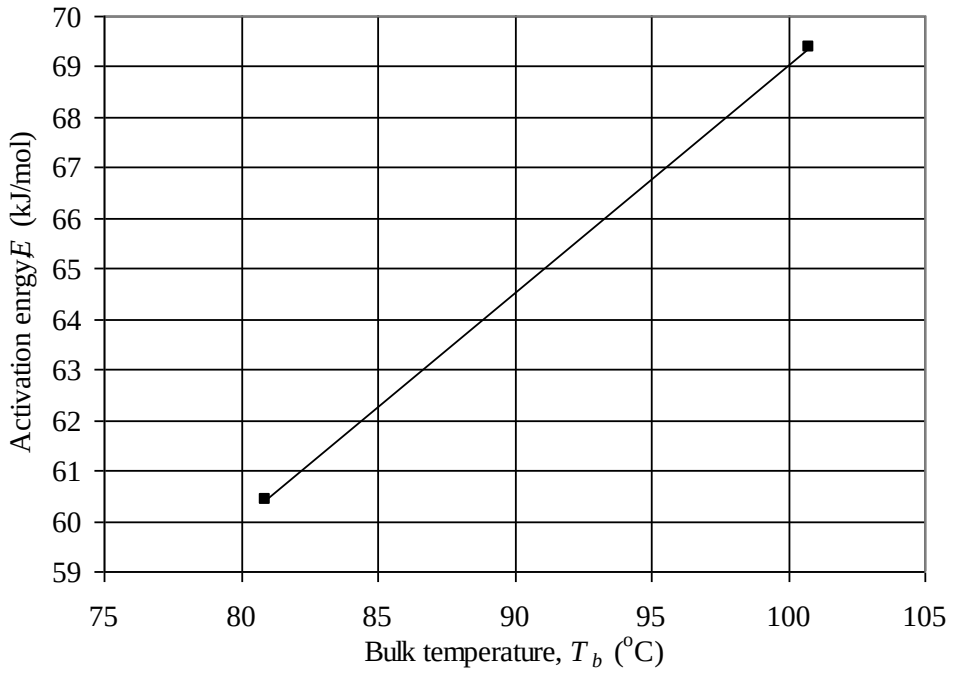

Fig. 5.28: Apparent activation energy, E, vs. bulk temperature, T_b, for crude oil D

Table 5.14: Constants for apparent activation energy determination for crude oil C and D

Constant	Unit	Crude C	Crude D
E_o	kJ/mol	35.707	24.005
e	kJ/mol ^{o}C	0.2378	0.4503

The Panchal et al. model (Equation 2.21) predicts an increase in the fouling rate with an increase in the film temperature. It was observed from the experimental investigations of the crude oils that the initial fouling rates decreased with increase in the film temperatures as a consequence of the increase in the bulk temperatures. This phenomenon is not explained by the Panchal et al. model. Hence, a new threshold fouling model, to account for the effect of bulk temperature on fouling, by considering the apparent activation energy as a function of bulk temperature is developed.

5.4 Development of a new threshold fouling model

The proposed threshold fouling model is given by:

$$\frac{dR_f}{dt} = \alpha \,\mathrm{Re}^{-\beta}\,\mathrm{Pr}^{-0.33} \exp\left(-E_o/RT_f\right) \exp\left(-eT_b/RT_f\right) - \gamma\,\tau_w \tag{5.6}$$

The model parameters such as α and γ were estimated by the regression analysis by maximizing R^2 value, whereas the value of β was fixed as 0.88. The physical properties such as density, dynamic viscosity, thermal conductivity and the specific heat required for the determination of Reynolds number and Prandtl number were evaluated at the bulk temperature.

The wall shear stress, τ_w, in the 2nd term of RHS of Equation (5.6) is determined by:

$$\tau_w = \frac{f}{2}\rho u^2 \tag{5.7}$$

where f is the friction factor and is determined for the turbulent flow conditions as [83]:

$$f = 0.0035 + \left(0.264/\mathrm{Re}^{0.42}\right) \tag{5.8}$$

Sixteen experimental runs (Runs 13 – 28) that were carried out at different bulk and initial surface temperatures and flow velocities were used for the estimation of model parameters for crude oil C. The proposed as well as the existing threshold fouling model (Ebert-Panchal, Panchal et al., Polley et al. and Nasr and Givi) parameters are summarized in Table 5.15. The initial fouling rates estimated from the models were compared with the experimental data as shown in Figure 5.29. It was found that the predicted data from the proposed model closely match with the experimental data with a R^2 value of 0.80. The relative percentage error between the experimental and predicted data from the proposed model is summarized in Table 5.16.

Table 5.15: Fouling model parameters for crude oil C

Model	E-P	Panchal et al.	Polley et al.	Nasr & Givi	Proposed model
α ($m^2K/kWmin$)	4.2×10^{5}	8.81×10^{5}	2×10^{5}	4.3×10^{5}	1.99×10^{6}
γ (m2K/kWmin/Pa)	1.17×10^{-6}	1×10^{-9}	1×10^{-9}	1.20×10^{-7}	8.61×10^{-7}
R^2	**0.04**	**0.08**	**0.4**	**0.05**	**0.8**

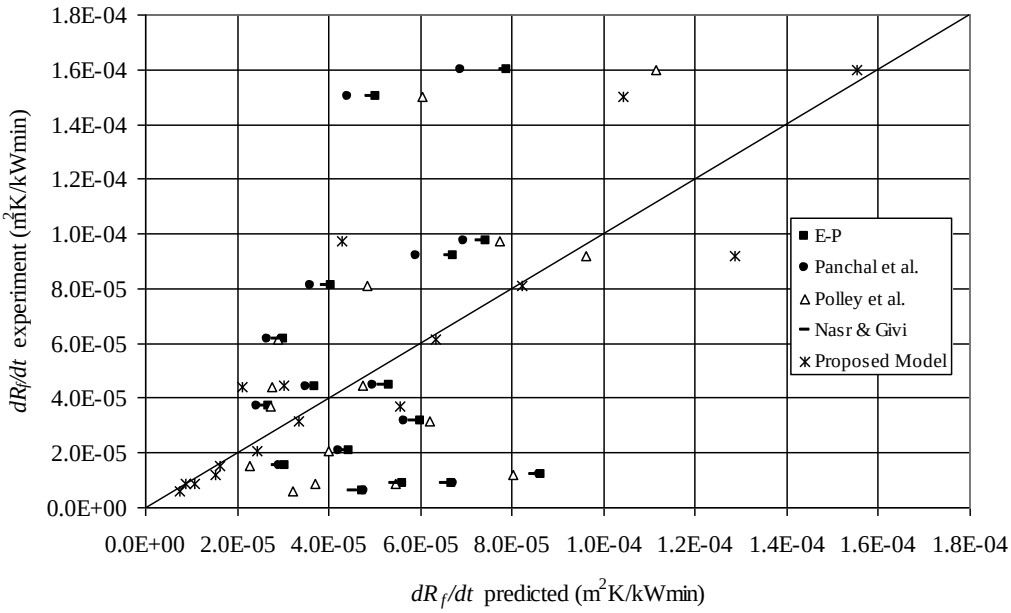

Fig. 5.29: Comparison of the model predicted values vs. the experimental values of crude oil C

Table 5.16: Relative percentage error between the experimental and the predicted values of crude oil C

dR_f/dt experiment	dR_f/dt predicted	Relative percentage error
$m^2K/kWmin \times 10^5$	$m^2K/kWmin \times 10^5$	
6.15	6.34	3.09
15.0	10.4	30.67
16.0	15.5	3.13
4.39	2.10	52.16
4.44	3.03	31.76
9.76	4.30	55.94
3.69	5.56	50.68
8.10	8.22	1.48
9.19	12.9	40.37
1.54	1.63	5.84
2.05	2.43	18.54
3.18	3.34	5.03
0.87	1.08	24.14
1.20	1.53	27.50
0.59	0.73	23.73
0.87	0.87	0.21

Runs 29 – 40 were used for the estimation of the model parameters for crude oil D. Table 5.17 summarizes the estimated model parameters and R^2 value for the proposed and the existing threshold fouling models. The initial fouling rates predicted from the proposed model were further compared with the experimental data as shown in Figure 5.30. The proposed model resulted in a good agreement in comparison with the experimental data. The relative percentage error between the experimental and the predicted data is summarized in Table 5.18.

Table 5.17: Fouling model parameters for crude oil D

Model	E-P	Panchal et al.	Polley et al.	Nasr & Givi	Proposed model
α ($m^2K/kWmin$)	1.36×10^{6}	4.62×10^{6}	4.78×10^{5}	1.61×10^{6}	4.62×10^{6}
γ (m2K/kWmin/Pa)	1×10^{-7}	1.55×10^{-5}	1×10^{-9}	1×10^{-7}	1.67×10^{-7}
R^2	**0.20**	**0.18**	**0.57**	**0.2**	**0.82**

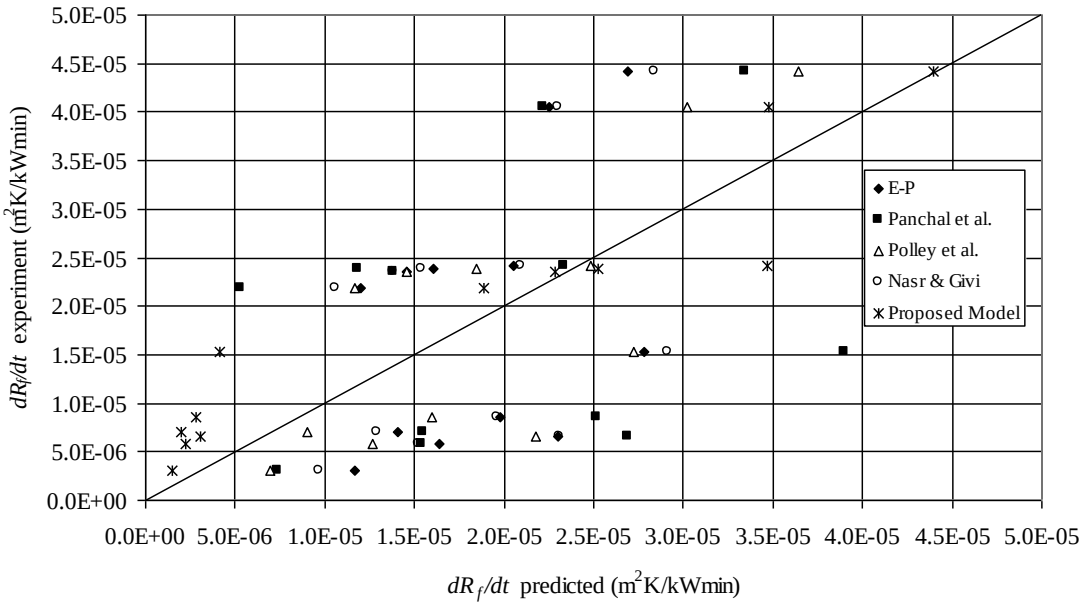

Fig. 5.30: Comparison of the model predicted values vs. the experimental values of crude oil D

Table 5.18: Relative percentage error between the experimental and the predicted values of crude oil D

dR_f/dt experiment	dR_f/dt predicted	Relative percentage error
$m^2K/kWmin \times 10^5$	$m^2K/kWmin \times 10^5$	
4.05	3.47	14.32
2.39	2.53	5.86
2.18	1.89	13.30
4.42	4.40	0.45
2.42	3.47	43.39
2.35	2.28	2.98
0.30	0.15	50.00
0.58	0.22	62.07
0.66	0.31	53.03
0.70	0.20	71.43
0.86	0.28	67.44
1.53	0.41	73.20

5.5 Induction period and initial fouling rate

The existing threshold fouling models (and the proposed threshold fouling model as well) does not account for induction period. In all the experiments, the fouling was preceded by an induction period in which no measurable fouling was observed. It was found that the induction period increased with:

- decrease in the initial surface temperatures (Figures 5.1, 5.3, 5.5 and 5.7),
- increase in the bulk temperatures (Figures 5.10 and 5.12) and
- increase in the flow velocities (Figures 5.14, 5.16 and 5.18).

In the present work, it was observed that the initial fouling rates increased with:

- increase in the initial surface temperatures (Figures 5.2, 5.4, 5.6 and 5.8)
- decrease in the bulk temperatures (Figures 5.9, 5.11 and 5.13) and
- decrease in the flow velocities (Figures 5.15, 5.17 and 5.19)

The summary of the effect of the parameters such as the initial surface temperature/heat flux, bulk temperature and flow velocity on the induction period

and the initial fouling rate is summarized in Table 5.19. It can be summarized from these observations that the initial fouling rate is inversely proportional to the induction period.

Table 5.19: Summary of the effect of parameters on the induction period and the initial fouling rate

Fouling characteristics	Operating parameters		
	Increase in T_b	Increase in T_{so}/q	Increase in flow velocity, v
Induction period: θ	Increases	Decreases	Increases
Initial fouling rate: dR_f/dt	Decreases	Increases	Decreases

5.6 Fouling Mechanism

It was observed from the experimental investigations that the initial fouling rate is inversely proportional to the induction period. This inverse relationship between the initial fouling rate and the induction period can be validated theoretically by considering a two-step chemical reaction as:

$$\underset{\text{(Reactants, Soluble)}}{A} \longrightarrow \underset{\text{(Precursors, Sparingly soluble)}}{R} \longrightarrow \underset{\text{(Foulant, Insoluble)}}{S}$$

Reactant *A* (heavier molecules in the crude) in the thermal boundary layer near the heat transfer surface get converted to soluble precursors *R* (smaller reactive molecules) which polymerize on the heat transfer surface to form insoluble foulant deposits of *S*. Assuming that the rate constants for the two steps as $k_{eff,}$ which is the effective rate constant and that depends upon the rate of heat transfer, fluid flow and the reaction temperature. The variation in concentrations of *A*, *R* and *S* with time, *t*, can be written as:

$$\frac{C_A}{C_{Ao}} = e^{-k_{eff}t} \tag{5.9}$$

$$\frac{C_R}{C_{Ao}} = k_{eff}te^{-k_{eff}t} \tag{5.10}$$

$$\frac{C_S}{C_{Ao}} = 1-e^{-k_{eff}t}-k_{eff}te^{-k_{eff}t} \tag{5.11}$$

where C_{Ao} is the initial concentration of A and C_A, C_R and C_S are the concentrations of A, R and S, respectively at time t. Graphical representation of the concentrations of A, R and S are shown in Figure 5.31.

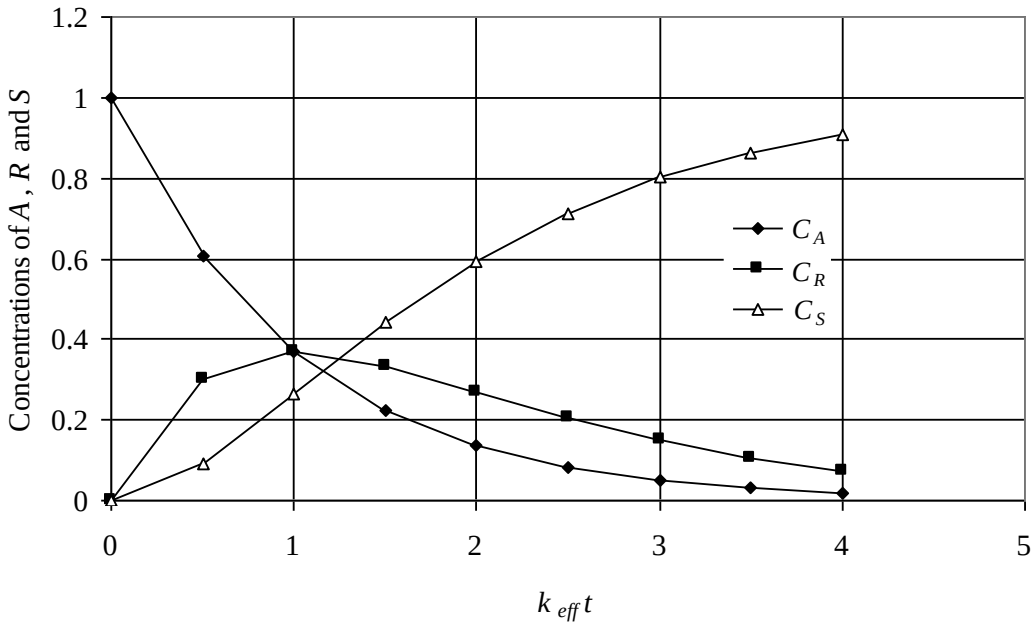

Fig. 5.31: Concentrations of A, R and S vs. $k_{eff}t$

The time at which the maximum concentration of R occurs can be found by setting $dC_R/dt = 0$. Thus

$$\frac{dC_R}{dt} = 0 = k_{eff}C_A - k_{eff}C_R \tag{5.12}$$

Rearranging Equation (5.12)

$$C_A = C_R \tag{5.13}$$

Substituting the values of C_A and C_R in Equation (5.13)

$$C_{Ao}e^{-k_{eff}t} = C_{Ao}k_{eff}te^{-k_{eff}t} \tag{5.14}$$

Rearranging Equation (5.14)

$$t = \frac{1}{k_{eff}} \tag{5.15}$$

Thus, the concentration of R passes through a maximum at $k_{eff}t$ = 1 where concentration of S passes through an inflection point.

The maximum slope (initial fouling rate) through the inflection point is estimated as:

$$\text{Maximum slope} = \frac{1}{C_{Ao}}\frac{dC_s}{dt} = \frac{C_R}{C_{Ao}}k_{eff} \tag{5.16}$$

Substituting Equation (5.10) into Equation (5.16) and rearranging

$$\text{Maximum slope} = k_{eff}e^{-1} = 0.3679k_{eff} \tag{5.17}$$

The tangent of the curve of C_S cuts the x-axis at X_2 (Figure 5.32) which is generally known as the induction period, θ, which can be determined as follows:

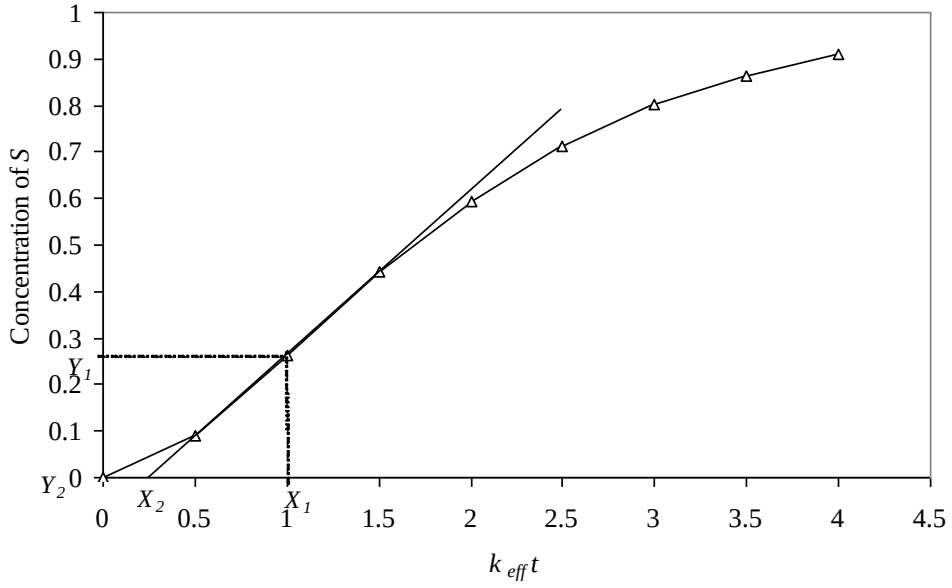

Fig. 5.32: Concentration of S vs. $k_{eff}t$

$$\text{Maximum slope} = \frac{Y_1 - Y_2}{X_1 - X_2} \tag{5.18}$$

where Y_1 indicates the concentration of C_S at the inflection point *i.e.* $\frac{C_S}{C_{Ao}} = 1 - 2e^{-1}$

Substituting X_1, X_2 and Y_1 and rearranging Equation (5.18):

$$\theta = \frac{3 - e}{k_{eff}} = \frac{0.2817}{k_{eff}} \tag{5.19}$$

The induction period as well as maximum slope (initial fouling rate) depends on the number of intermediate steps before the insoluble foulant is formed. As the number of intermediate steps increases, the induction period also increases with smaller slope. Rate of fouling can be estimated as:

$$\frac{dR_f}{dt} = \frac{1}{k_f}\frac{dx_f}{dt} = \frac{1}{Ak_f}\frac{dV_f}{dt} = \frac{V_{TB}}{Ak_f}\frac{dC_s}{dt} = \frac{V_{TB}}{Ak_f}k_{eff}C_R \tag{5.20}$$

where $V_f = V_{TB}C_s$, k_f is the thermal conductivity of the foulant, x_f is the thickness of the foulant, V_f is the volume of the film and V_{TB} is the volume of the thermal boundary layer.

It is interesting to note that maximum slope is proportional to reaction rate constant while the induction period is inversely proportional to reaction rate constant. This inverse relationship between the induction period and initial fouling rate is validated by the observations as summarized in Table 5.19. However, this model has to be investigated further before any firm conclusions can be drawn because the two parameters - induction period and initial fouling rate – were observed to be dependent on heat flux, flow velocity and surface as well as bulk temperatures. An attempt is made to empirically correlate these observations.

The deposition of the solid foulant on the heat transfer surface is controlled by three rate processes defined by their time scales as:

(i) Heating time, $\tau_h \quad \propto \quad \frac{V\rho C_p T_b}{Aq}$

(ii) Reaction time, $\tau_r \quad \propto \quad \frac{1}{k_{eff}}$

(iii) Residence time $\tau_f \propto \frac{V}{Av}$

The induction period is the time needed for foulant to form by heat transfer while it is being scavenged by the fluid flow. Based on the experimental observations, it is conjectured that they may be related as:

$$k_{eff}\theta \quad \propto \quad \frac{V\rho C_p T_b vA}{AqV} \quad \propto \quad \frac{v\rho C_p T_b}{q} \tag{5.21}$$

Equation (5.21) can be rearranged as

$$k_{eff} \propto \frac{v\rho C_p T_b}{q\theta} \propto \frac{\mathrm{Pr}\,\mathrm{Re}}{Nu}\frac{T_b}{\Delta T}\frac{1}{\theta} \tag{5.22}$$

Equation (5.22) can be expressed as

$$k_{eff} \propto \frac{v\rho C_p T_b}{h\Delta T\theta} \propto Da\,\frac{T_b}{\Delta T}\frac{v}{L} \tag{5.23}$$

where *Da* is the Damkohler number which is the ratio of the time scale of fouling to that of the heat transfer and can be expressed as:

$$Da \propto \frac{\rho C_p L k_{eff}}{h} \propto \frac{\rho C_p L}{h\theta} \tag{5.24}$$

where L is a length parameter such as equivalent diameter.

Since, the rate of fouling is directly proportional to the rate constant k_{eff}, it can be expressed as:

$$\frac{dR_f}{dt} \propto k_{eff} \propto Da\,\frac{T_b}{\Delta T}\frac{v}{L} \tag{5.25}$$

dR_f/dt is plotted against $Da\frac{T_b}{\Delta T}\frac{\nu}{L}$ as shown in Figure 5.33. As expected, the initial fouling rate increased with an increase in $Da\frac{T_b}{\Delta T}\frac{\nu}{L}$.

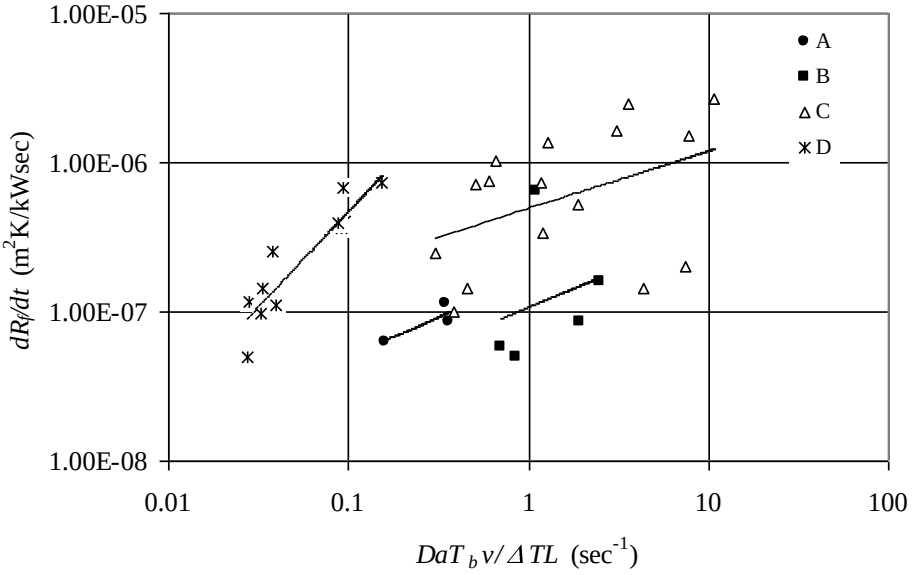

Fig. 5.33: The initial fouling rate vs. $Da\frac{T_b}{\Delta T}\frac{\nu}{L}$ for the crude oils

The initial fouling rate is inversely proportional to the induction period $\left(\frac{dR_f}{dt} \propto \frac{1}{\theta}\right)$ as shown in Fig. 5.34.

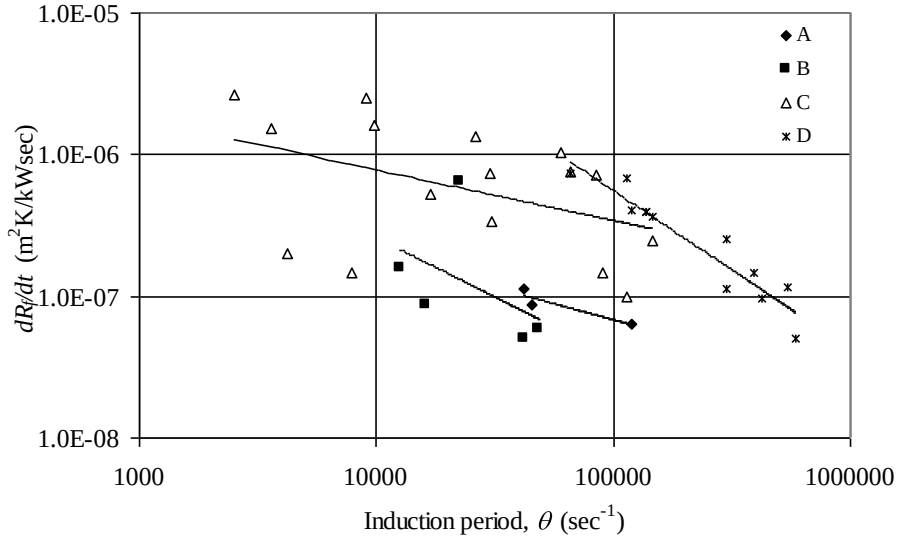

Fig. 5.34: The initial fouling rate vs. the induction period for the crude oils

5.7 Summary

In this chapter, the experimental results were analyzed for the effect of initial surface temperature, bulk temperature and flow velocity on the initial fouling rate and the induction periods of the crude oils. It was observed that the initial fouling rates increased with an increase in initial surface temperature; decreased with an increase in bulk temperature and flow velocity. It was also observed that the induction period decreased with an increase in the initial surface temperature; increased with an increase in the bulk temperature and flow velocity. The experimental data were analyzed by the Panchal et al. model. The apparent activation energy values were estimated for the crude oils. It was noticed that the variations in the apparent activation energy values for flow velocities of 0.4 and 0.5 m/s were insignificant. It was also noticed that the apparent activation energy increased with an increase in the bulk temperature. Based on the experimental observations, a new threshold fouling model to account for the effect of bulk temperature on the initial fouling rate was developed and further validated with the experimental data that were obtained at different bulk temperatures. The proposed model was found to have a good agreement with the experimental data with a R^2 value of about 0.8. Finally, an empirical correlation developed to consider the induction period as well as the initial fouling rate was presented in this chapter.

CHAPTER 6

CONCLUSIONS AND RECOMMENDATIONS

6.1 Conclusions

A high-temperature, high-pressure, annular flow fouling research unit (AFFRU) has been used to study the fouling characteristics of different crude oils at operating conditions very close to the conditions in the real plant. However, the operating conditions have been chosen to be slightly different from the plant conditions during the experiments to achieve accelerated fouling. Increased surface temperature and decreased flow velocity are the variables used to accelerate fouling. The major conclusions/observations made based on the experimental results are listed below.

1. The initial fouling rates increased with an increase in initial surface temperature and decreased with increase in bulk temperature and flow velocity.

2. The induction periods decreased with an increase in initial surface temperatures and increased with an increase in bulk temperature and flow velocity.

3. The initial fouling rates were observed to be inversely dependent on the induction periods.

4. The apparent activation energy values increased linearly with an increase in bulk temperature.

5. A new fouling model for the crude oils where the fouling rates decreases with an increase in film temperature as a consequence of increase in bulk temperature has been developed and validated.

6. A new fouling model that accounts for the induction periods and initial fouling rates has been proposed.

6.2 Recommendations

It was observed from the experimental investigations that the fouling rates decreased with an increase in the bulk temperature for this particular type of crude oils. This may be possibly due to (i) the solubility of the fouling precursors in the crude oils at higher bulk temperatures and (ii) the decrease in the thermal driving force, *i.e.* (T_s-T_b). A detailed study is, therefore, necessary to understand the effect of bulk temperature on fouling.

Crude blending is also an important factor influencing fouling. Blending of crude oils can cause unstable mixes which precipitate species such as asphaltene and result in rapid fouling. The crude oil incompatibility and the precipitation of asphaltene on blending of crude oils can cause significant fouling and coking in crude preheat train. A thorough investigation is also needed to establish the effects of crude blending on fouling characteristics.

Pressure is the least studied parameter in crude oil fouling. Pressure can have a significant effect on the fouling rate, especially where multi-component fluids are involved. A thorough investigation is also required to study the effect of pressure on fouling.

REFERENCES

[1] T. R. Bott, *Fouling of heat exchangers*: Elsevier Science B.V, 1995.

[2] H. Muller-Steinhagen, "Fouling of heat exchanger surfaces," *Chemistry and Industry*, vol. 5, pp. 171-175, 1995.

[3] W. L. V. Nostrand, S. H. Leach, and J. L. Haluska, "Economic penalties associated with the fouling of refinery heat transfer equipment," in *Fouling of heat transfer equipment, Somerscales, E.F.C.*, Hemisphere, Ed. Washington, 1981, p. 619.

[4] C. B. Panchal and E.-P. Huangfu, "Effects of mitigating fouling on the energy efficiency of crude oil distillation," *Heat Trans. Eng.*, vol. 21(3), pp. 3-9, 2000.

[5] A. P. Watkinson, "Deposition of crude oils in heat exchangers," in *E.C.I. Symp. Ser., vol. RP2: Proc. of 6th Intl. Conf. on heat exchanger fouling and cleaning- challenges and opportunities*, H. Muller-Steinhagen, A. P. Watkinson, and M. R. Malayeri, Eds. Kloster Irsee, Germany, 2005, pp. 7-15.

[6] H. Muller-Steinhagen, *Heat exchanger fouling – mitigation and cleaning technologies*: Publico Publications, 2000.

[7] E.S.D.U, "Heat exchanger fouling in the pre-heat train of a crude oil distillation unit," in *Data item 00016* ESDU Intl. London, 2000.

[8] W. A. Ebert and C. B. Panchal, "Analysis of Exxon crude oil slip-stream coking data," in *Fouling Mitigation of Industrial Exchange Equipment* Begell House, NY, 1995, pp. 451-460.

[9] C. E. Scarborough, D. C. Cherrington, R. Diener, and L. P. Golan, "Coking of crude oil at high heat flux levels," *Chem. Eng. Prog.*, vol. 75(7), pp. 41-47, 1979.

[10] C. B. Panchal, W. C. Kuru, C. F. Liao, W. A. Ebert, and G. W. Palin, "Threshold conditions for crude oil fouling," in *Eng. Foundation Conf., Understanding of Heat Exchanger Fouling and its Mitigation* Lucca, Italy, 1997.

[11] G. T. Polley, D. I. Wilson, B. L. Yeap, and S. J. Pugh, "Evaluation of laboratory crude oil threshold fouling data for application to refinery pre-heat trains," *Applied Thermal Eng.*, vol. 22, pp. 777-788, 2002.

[12] M. R. J. Nasr and M. M. Givi, "Modeling of crude oil fouling in preheat exchangers of refinery distillation units," *Applied Thermal Eng.*, vol. 26, pp. 1572-1577, 2006.

[13] J. G. Knudsen, D. Lin, and W. A. Ebert, "The determination of a threshold fouling curve for crude oil," in *Proc. of Understanding Heat Exchanger Fouling and its Mitigation*, T. R. Bott, Ed. Begell House, NY, 1999, pp. 265-272.

[14] P. Eaton and R. Lux, "Laboratory fouling test apparatus for hydrocarbon feedstocks," *Fouling in Heat Exchange Equipment, ASME HTD* vol. 35, pp. 33-42, 1984.

[15] A. Young, S. Venditti, C. Berrueco, M. Yang, A. Waters, H. Davies, S. Hill, M. Millan, and B. D. Crittenden, "Characterisation of crude oils and their fouling deposits using a batch stirred cell system," in *Proc. of Int. Conf. on Heat Exchanger Fouling and Cleaning VIII*, H. Muller-Steinhagen, M. R. Malayeri, and A. P. Watkinson, Eds. Schladming, Austria, 2009, pp. 17-26.

[16] G. Brons and T. M. Rudy, "Fouling of whole crude oils on heated surfaces," in *Heat Exchanger Fouling-Fundamental Approaches and Technical Solutions*, H. Muller-Steinhagen, Ed. Essen Germany: Publico Publications, 2002, pp. 249-257.

[17] A. P. Watkinson, "Comparison of crude oil fouling using two different probes," in *E.C.I conf. on Heat Exchanger Fouling and Cleaning: Fundamentals and applications*, A. P. Watkinson, H. Muller-Steinhagen, and M. R. Malayeri, Eds. Santa Fe, New Mexico, USA 2004, pp. 234-240.

[18] B. D. Crittenden, S. T. Kolaczkowski, T. Takemoto, and D. Z. Phillips, "Crude oil fouling in a pilot-scale parallel tube apparatus," *Heat Transfer. Eng*, vol. 30(10-11), pp. 777-785, 2009.

[19] D. I. Wilson and A. P. Watkinson, "Model experiments of auto-oxidation reaction fouling," *Trans IChemE Part A*, vol. 73, pp. 59-68, 1995.

[20] C. A. Bennett, R. S. Kistler, K. Nangia, W. Al-Ghawas, N. Al-Hajji, and A. Al-Jemaz, "Observation of an isokinetic temperature and compensation effect

for high temperature crude oil fouling," *Heat Transfer Eng.,* vol. 30(10-11), pp. 794-804, 2009.

[21] L. Oufer, "Fouling characteristics of organic fluids." vol. PhD: Oregon State University, 1990.

[22] S. Asomaning, "Heat exchanger fouling by petroleum asphaltenes." vol. PhD Canada: University of British Columbia, 1997.

[23] Z. S. Saleh, R. Sheikholeslami, and A. P. Watkinson, "Fouling characteristics of a light Australian crude oil," *Heat Transfer Eng.,* vol. 26(1), pp. 15-22, 2005a.

[24] M. Srinivasan and A. P. Watkinson, "Fouling of some Canadian crude oils," *Heat Transfer Eng.,* vol. 26(1), pp. 7-14, 2005.

[25] G. A. Lambourn and M. Durrieu, "Fouling in crude oil preheat trains," in *Heat Exchangers- Theory and Practice,* J. Taborek, G. F. Hewitt, and N. Afghan, Eds. NY: Hemisphere Publishing Corporation, 1983, pp. 841-852.

[26] B. J. Fuhr, C. Cathrea, L. Coates, H. Kalra, and A. I. Majeed, "Properties of asphaltenes in waxy crude," *Fuel,* vol. 70, pp. 1293-1297, 1991.

[27] D. A. Storm, R. J. Barresi, and E. Y. Sheu, "Flocculation of asphaltenes in heavy oil at elevated temperatures," *Fuel Sci. and Tech. Intl,* vol. 14, pp. 243-260, 1996.

[28] S. Asomaning, C. B. Panchal, and C. F. Liao, "Correlating field and laboratory data for crude oil fouling," *Heat Transfer Eng.,* vol. 21, pp. 17-23, 2000a.

[29] E. E. Wilson, "A basis for rational design of heat transfer apparatus," *Trans. A.S.M.E.,* vol. 37, pp. 47-82, 1915.

[30] J. Nesta and C. A. Bennett, "Reduce fouling in Shell -and-tube heat exchangers," *Hydrocarbon Processing,* vol. 83 (7), pp. 77-82, 2004.

[31] J. G. Knudsen, "Apparatus and techniques for measuring of fouling of heat transfer surfaces," in *Fouling of Heat Transfer equipment* Hemisphere, Washington, 1981, pp. 57-81.

[32] B. D. Crittenden, S. T. Kolaczkowski, and I. L. Downey, "Fouling of crude oil preheat exchangers," *Trans. IChemE,* vol. 70 Part A, pp. 547-557, 1992.

[33] A. P. Watkinson and D. I. Wilson, "Chemical reaction fouling: A review," *Experimental Thermal and Fluid Science,* vol. 14, pp. 361-374, 1997.

[34] J. H. J. Weiland, R. C. Mccay, and J. E. Barnes, "Rates of fouling and cleaning of unfired heat exchangers," *Trans. ASME,* vol. 71, pp. 849-853, 1949.

[35] NACE, "Materials protection," 1970.

[36] E. J. Latos and F. H. Franke, "Relative thermal fouling rates of petroleum and shale oils," in *Corrosion, 82, Int. Corrosion Forum*, 1982, pp. 103.1-103.12.

[37] G. Dickakian and S. Seay, "Asphaltene precipitation: primary crude exchanger fouling mechanism," *Oil and Gas Journal,* vol. 86 (10), pp. 47-50, 1988.

[38] G. Dickakian, "Crude oil fouling control by a fouling analyzer," *ASME HTD,* vol. 108, pp. 331-336, 1989.

[39] G. Dickakian, "Fluid cat cracker unit fouling: causes and mitigation," in *Preprint, Session 35, AIChE Meeting* San Diego, 1990.

[40] B. D. Crittenden, S. T. Kolaczkowski, and T. Takemoto, "Use of in-tube inserts to reduce fouling from crude oils," *AIChE Symp. (Am. lnst. Chem. Eng.) Ser.,* vol. 89(295), pp. 300-307, 1993.

[41] L. Oufer and J. G. Knudsen, "Modeling chemical reaction fouling under sub-cooled boiling conditions," in *AIChE (Am. Inst. Chem. Eng.) Symp. Ser.* . vol. 89(295), 1993, pp. 308-313.

[42] L. Oufer and J. G. Knudsen, "The effect of various sulfur compounds on chemical reaction fouling under local boiling conditions," in *Proc. 10th Intl. Heat Transfer Conf., I.Chem.E.* vol. 7 Brighton, UK, 1994, pp. 527-532.

[43] Y. Haquet, R. Loutaty, and T. Patureaux, "Turbotal: a mechanical means for continuously fighting heat exchanger fouling," in *Proc. Mitigation of Industrial Heat Exchanger Fouling, Eng., Foundation, CA*, 1995.

[44] G. Bach, G. Zimmermann, F. D. Kopinke, S. Barendregt, P. V. d. Oosterkamp, and H. Woerde, "Transfer-line heat exchanger fouling during pyrolysis of hydrocarbons I," *Ind. Eng. Chem. Res,* vol. 34, pp. 1132-1139, 1995.

[45] S. Asomaning and A. P. Watkinson, "Petroleum stability and heteroatom species effects in fouling of heat exchangers by asphaltenes," *Heat Transfer Eng.,* vol. 21(3), pp. 10-16, 2000b.

[46] C. A. Bennett, S. Appleyard, M. Gough, R. P. Hohmann, H. M. Joshi, D. C. King, T. Y. Lam, T. M. Rudy, and S. E. Stomierowski, "Industry-recommended procedures for experimental crude oil preheat fouling research," *Heat Transfer Eng.*, vol. 27(9), pp. 28-35, 2006.

[47] D. I. Wilson and A. P. Watkinson, "Solvent effects in chemical reaction fouling," in *3rd UK Natl. Heat Transfer Conf. IChemE* Birmingham, UK, 1992, pp. 987-994.

[48] A. P. Watkinson, "Critical review of organic fluid fouling. Final report - Contract 73212402 " Argonne National Laboratory, 1988.

[49] N. Epstein, "Thinking about heat transfer fouling: A 5×5 matrix," *Heat Transfer Eng.*, vol. 4, pp. 43-56, 1983.

[50] J. Taborek, T. Aoki, R. B. Ritter, J. W. Palen, and J. G. Knudsen, "Predictive methods for fouling behavior," *Chem. Eng. Prog.*, vol. 68(7), pp. 69-78, 1972.

[51] E. M. Ishiyama, F. Coletti, S. Macchietto, W. R. Paterson, and D. I. Wilson, "Impact of deposit ageing on thermal fouling: Lumped parameter model," *AIChE J*, vol. 56, pp. 531-545, 2010.

[52] F. Coletti, E. M. Ishiyama, W. R. Paterson, D. I. Wilson, and S. Macchietto, "Impact of deposit aging and surface roughness on thermal fouling: Distributed model," *AIChE J*, vol. 56, pp. 3257-3273, 2010.

[53] A. P. Watkinson and N. Epstein, "Gas oil fouling in sensible heat exchanger," in *C.E.P, Symp. Ser.* vol. 65(92), 1969, pp. 84-90.

[54] N. Epstein, "General thermal fouling models," in *Fouling Science and Technology* vol. 145, L. F. Melo, T. R. Bott, and C. A. Bernardo, Eds.: Kluwer, Academic publishers, 1988, pp. 15-30.

[55] W. L. Nelson, *Petroleum refinery engineering*: McGraw Hill Company, 1969.

[56] W. R. Paterson and P. J. Fryer, "A reaction engineering approach to the analysis of fouling," *Chem. Eng. Sci.*, vol. 43, pp. 1714-1717, 1988.

[57] G. Dickakian and T. Kingwood, "Method for determining crude oil fouling by high performance liquid chromatography." vol. 4,671,103, U. S. Patent, Ed. USA, 1987.

[58] D. I. Wilson and G. T. Polley, "Mitigation of refinery preheat train fouling by nested optimization," in *Advances in Refinery Fouling Mitigation Session, 46, AIChE* Houston, 2001, pp. 287-294.

[59] I. A. Wiehe, R. J. Kennedy, and G. Dickakian, "Fouling of nearly incompatible oils," *Energy and Fuels,* vol. 15, pp. 1057-1059, 2001.

[60] Z. S. Saleh, R. Sheikholeslami, and A. P. Watkinson, "Blending effect on fouling of four crude oils," in *E.C.I Symp. Ser., vol. RP2, In Proc. of 6th Int. Conf. on Heat Exchanger Fouling and Cleaning - Challenges and Opportunities*, H. Müller-Steinhagen, M. R. Malayeri, and A. P. Watkinson, Eds. Kloster Irsee, Germany, 2005b, pp. 37-46.

[61] D. Q. Kern and R. E. Seaton, "A theoretical analysis of thermal surface fouling," *Brit. Chem. Eng.,* vol. 4 No.5, pp. 258-262, 1959.

[62] G. T. Atkins, "What to do about high coking rates," *Petro/Chem Engr,* vol. 34(4), pp. 20-25, 1962.

[63] R. Nijsing, "Diffusional and kinetic phenomena associated with fouling," Euratom, Eur. 543e. European Atomic Energy Community, 1964.

[64] A. Jackman and R. Aris, "Optimal control for pyrolytic reactors," in *Proc. 4th Euro Symp. on Chem. Reaction Eng.* Pergamon, Oxford, 1971, pp. 411-419.

[65] J. M. Fernandez-Baujin and S. M. Soloman, "Industrial application of pyrolysis technology: Lummus SRT III module in industrial and laboratory pyrolyses," in *ACS Symp. Ser*. vol. 32, L. F. Albright and B. L. Crynes, Eds., 1976, pp. 345-372.

[66] K. M. Sundaram and G. F. Froment, "Kinetics of coke deposition in the thermal cracking of propane," *Chem. Eng. Sci.*, vol. 34, pp. 635-644, 1979.

[67] B. D. Crittenden and S. T. Kolaczkowski, "Mass transfer and chemical kinetics in hydrocarbon fouling," in *Proc. Conf. Fouling – Science or Art? Inst. Cor. Sci. Tech. and I. Chem. E* University of Surrey, Guildford, 1979, pp. 169-187.

[68] B. D. Crittenden, S. T. Kolaczkowski, and S. A. Hout, "Modeling hydrocarbon fouling," *Chem. Eng. Res. Des,* vol. 65, pp. 171-179, 1987a.

[69] N. Epstein, "A model of the initial chemical reaction fouling rate for flow within a heated tube and its verification," in *Proc. 10th Int. Heat Trans. Conf. Inst. of Chem. Engrs*. vol. 4 Rugby, 1994, pp. 225-229.

[70] B. L. Yeap, D. I. Wilson, G. T. Polley, and S. J. Pugh, "Retrofitting crude oil refinery heat exchanger networks to minimize fouling while maximizing heat recovery," *Heat Trans. Eng.,* vol. 26, pp. 23-34, 2005.

[71] A. S. Kovo, "Mathematical modeling and simulation of fouling of Nigerian crude oil equipment installations," *Leonardo Journal of Sci.,* vol. 9, pp. 111-124, 2006.

[72] Z. Fan, P. Rahimi, R. McGee, Q. Wen, and T. Alem, "Investigation of Fouling Mechanisms of a Light Crude Oil Using an Alcor Hot Liquid Process Simulator," *Energy and Fuels,* vol. 24, pp. 6110-6118, 2010.

[73] G. T. Polley, "Review of the development of models for the prediction of fouling in heat exchangers heating crude oil," in *11th Intl. Conf. on Petroleum Phase Behaviour and Fouling. Petrophase-2010* NJ, USA, 2010.

[74] D. I. Wilson, G. T. Polley, and S. J. Pugh, "Ten years of Ebert, Pamchal and the threshold fouling concept," in *ECI Symp. Ser., vol. RP2, In Proc. of 6th Intl. Conf. on Heat Exchanger Fouling and Cleaning - Challenges and Opportunities,* H. Muller-Steinhagen, M. R. Malayeri, and A. P. Watkinson, Eds. Kloster Irsee, Germany, 2005, pp. 25-36.

[75] M. Bories and T. Patureaux, "Preheat train crude distillation fouling propensity evaluation by the Ebert and Panchal model," in *E.C.I conf. on Heat Exchanger Fouling and Cleaning: Fundamentals and applications,* P. Watkinson, H. Muller-Steinhagen, and M. R. Malayeri, Eds. New Mexico, USA, 2004, pp. 200-210.

[76] F. Coletti and S. Macchietto, "Refinery preheat train network simulation undergoing fouling: Assessment of energy efficiency and carbon emissions," in *Proc. of Intl. Conf. on Heat Exchanger Fouling and Cleaning VIII (Peer-reviewed),* H. Muller-Steinhagen, Ed. Schladming, Austria, 2009, pp. 61-68.

[77] W. C. Kuru, C. B. Panchal, C. F. Liao, J. W. Palen, and W. A. Ebert, "Development of high temperature, high pressure fouling unit," in *Proc. of Understanding Heat Exchanger Fouling and its Mitigation, Eng., Foundation Conf.* Lucca, Italy, 1997.

[78] M. Yang, A. Young, A. Niyetkaliyev, and B. D. Crittenden, "Modelling the fouling induction period," in *Proceedings of International Conference on Heat Exchanger Fouling and Cleaning VIII - 2009 (Peer-reviewed),* H. Muller-Steinhagen, M. R. Malayeri, and A. P. Watkinson, Eds. Schladming, Austria, 2009, pp. 69-75.

[79] D. H. Troup and J. A. Richardson, "Scale nucleation on a heat transfer surface and its prevention," *Chem. Eng. Commun.* , vol. 2, pp. 167-180, 1978.

[80] M. Srinivasan, "Heat exchanger fouling of some Canadian crude oils." vol. M.Sc Canada: University of British Columbia, 2008.

[81] B. D. Crittenden, S. A. Hout, and N. J. Alderman, "Model experiments of chemical reaction fouling " *Trans IChemE Part A*, vol. 65, pp. 165-170, 1987b.

[82] B. D. Crittenden and E. M. H. Khater, "Fouling in a hydrocarbon vaporiser," in *Institution of Chem. Engrs. Symp. Ser.* vol. 86, 1984, pp. 165-170.

[83] E. A. D. Saunders, "Heat exchangers selection, design and construction," *Longman Scientific and Technical*, 1988.

PUBLICATIONS

1. "Procedure for experiments in a laboratory unit for crude oil fouling in refinery preheat exchangers" PETRONAS Trade Secret document filed.

2. Deshannavar, U.B., M.S. Rafeen, M. Ramasamy and D. Subbarao, 2010. Crude oil fouling: A Review. J. Applied Sci., 10:3167-3174.

3. Deshannavar, U.B., Rafeen, M.S., Johari, M., Ramasamy, M., Subbarao, D., "Effect of blending on fouling characteristics of crude oil and condensate", The Proc. of 3rd Int. Conf. on Chemical & Bioprocess Eng., Sabah (2009).

4. Deshannavar, U.B., Rafeen, M.S., Ramasamy, M., Subbarao, D., "Crude oil fouling - A Review," 24th Symp. of Malaysian Chem. Engineers / 1st Int. Conf. on Process Eng. and Advanced Materials - 1st Int. Conf. on Process Eng. and Advanced Materials, Kuala Lumpur (2010).